

SURFACE CONTACT WEAR AND ABRASIVE WEAR
IN LUBRICATED SLIDING MECHANISMS

By

RIICHI INOUE

Bachelor of Agriculture
Kobe University
Kobe, Japan
1971

Master of Science
Oklahoma State University
Stillwater, Oklahoma
1978

Submitted to the faculty of the Graduate College
of the Oklahoma State University
in partial fulfillment of the requirements
for the degree of
DOCTOR OF PHILOSOPHY
December, 1982

Thesis
1982D
I58s
cop. 2



Copyright by

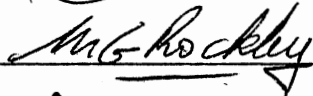
Richi Inoue

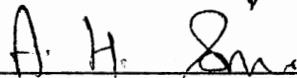
1982

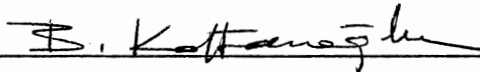
SURFACE CONTACT WEAR AND ABRASIVE WEAR
IN LUBRICATED SLIDING MECHANISMS

Thesis Approved:



Thesis Adviser










Dean of the Graduate College

PREFACE

I would like to express my sincere appreciation and thanks to the people who have encouraged and supported my doctoral program.

I am extremely grateful to Dr. E. C. Fitch, my major adviser and graduate committee chairman, whose personal efforts made this study and indeed my formal education feasible. His contagious enthusiasm for engineering endeavors, guidance based on his rich engineering experience, and support throughout my formal studies are greatly appreciated.

To the other member of my graduate committee, Dr. A. H. Soni, Dr. B. Kaftanoglu, Dr. K. E. Case, and Dr. M. G. Rockley, I extend my thanks for their guidance, critiques, and patience during my doctoral program.

To my colleagues at the Fluid Power Research Center, Ralph Shields, Tokunosuke Ito, Khalil Nafissah, Yiyu Wang, Bassel Abdulhamid, Z. Y. Li and Gabriel Silva, I extend my thanks for their help in fabricating test facilities and conducting experimental tests. Thanks are also in order for Patty Laramore and Robert Hagar for their professional assistance in providing the drafting and artwork for this thesis.

I would like to thank Bonnie Salim for her editing of this dissertation. To Velda Davis, I extend my appreciation for her expert assistance in preparing the final manuscript of this thesis.

Most of all I thank my wife, Nobuko, and children, Takashi and Rick, for their sacrifices, encouragement, and understanding during my graduate study.

TABLE OF CONTENTS

| Chapter | Page |
|--|------|
| I. INTRODUCTION. | 1 |
| II. PREVIOUS INVESTIGATIONS | 4 |
| III. DEVELOPMENT OF THEORETICAL MODELS | 11 |
| Surface Contact Wear Model | 11 |
| Abrasive Wear Model. | 19 |
| IV. VERIFICATION OF SURFACE CONTACT WEAR MODEL. | 40 |
| Experimental Considerations. | 41 |
| Development of Experimental Facility | 42 |
| Repeatability of Experimental Facility | 48 |
| Analysis of Test Wear Mechanism. | 71 |
| Experimental Method. | 87 |
| Experimental Tests and Analysis. | 90 |
| Static Asperity Deformation Tests and Analysis | 97 |
| Dynamic Asperity Deformation Tests and Analysis. | 127 |
| V. VERIFICATION OF ABRASIVE WEAR MODEL | 151 |
| Experimental Considerations. | 151 |
| Development of Experimental Facility | 156 |
| Experimental Tests. | 157 |
| Analysis of Test Results | 169 |
| Abrasive Tests on Fluid Power Pumps. | 173 |
| Pump Test Results and Analysis | 176 |
| VI. SUMMARY AND CONCLUSIONS | 180 |
| Summary. | 180 |
| Conclusions. | 181 |
| BIBLIOGRAPHY | 187 |
| APPENDIX | 190 |

LIST OF TABLES

| Table | Page |
|---|------|
| I. Indentation Parameters for Different Coefficients of Friction | 34 |
| II. Available Wear Test Methods. | 43 |
| III. Gamma Falex Repeatability Test Data with MIL-H-5606. | 52 |
| IV. Incubation Periods of MIL-H-5606 for Statistical Analysis. . | 54 |
| V. Gamma Falex Repeatability Test Data with MIL-L-2104. | 59 |
| VI. Scar Widths for Different Wear Readings. | 76 |
| VII. Gamma Slopes and Values of $(s^{1.5}/W)$ for Nineteen Test Fluids | 91 |
| VIII. Test Results of Two Fluids Tested on Different Materials . . | 95 |
| IX. Test Fluids and Test Materials | 103 |
| X. Deformed Area Corrected for 3000 psi Based on The Area Size Measurement | 111 |
| XI. Deformed Area Corrected for 3000 psi Based on the Lost Length of the Cone | 112 |
| XII. Coefficients of Friction with Different Test Fluids. | 120 |
| XIII. Theoretical and Actual Volume Rates of Plastic Deformation . | 123 |
| XIV. Results of Dynamic Asperity Deformation Tests. | 130 |
| XV. Imprint Regions and Corresponding Sliding Velocities | 144 |
| XVI. Estimated Flash Temperatures for Soft and Hard Materials . . | 150 |
| XVII. Equilibrium Forces for Cutting and Indentation | 153 |
| XVIII. Cutting Depth and Indentation Depth in Abrasive Wear | 155 |

| Table | Page |
|---|------|
| XIX. Rotating Speeds of the Journal and Corresponding Sliding Velocities | 161 |
| XX. Abrasive Wear Test Results on the Variable Speed Gamma Falex System | 167 |

LIST OF FIGURES

| Figure | Page |
|--|------|
| 1. Rate of Wear as a Function of Apparent Contact Pressure | 5 |
| 2. Conical Shape Surface Asperity. | 12 |
| 3. Asperity Deformation Under Sliding Condition. | 14 |
| 4. Friction Coefficient Versus Stress Ratio. | 16 |
| 5. Formation of Wear Fragment. | 18 |
| 6. Shape of Abrasive Particle by Inoue | 20 |
| 7. Some Shapes Observed for ACFTD (Silica) Particles by Ferrography | 22 |
| 8. Shape of Abrasive Particle Defined by Kroeker | 23 |
| 9. Assumed Smooth Surfaces and Abrasive Particles. | 24 |
| 10. Surface Asperities and Abrasive Particles | 25 |
| 11. Abrasive Particle Shape Assumed | 27 |
| 12. Cutting Model for Surface Abrasion. | 28 |
| 13. Minimum Shear Yield Strength Required for Abrasive Particle in Cutting. | 31 |
| 14. Indentation Model for Surface Abrasion | 32 |
| 15. Minimum Shear Yield Strength Required for Abrasive Particle in Indentation. | 35 |
| 16. Illustration of Three-Body Abrasion Mechanism | 36 |
| 17. Illustration of Surface Contact Wear Theory | 41 |
| 18. Falex Wear Tester | 44 |
| 19. Test Specimens of Falex Wear Tester | 46 |
| 20. Schematic of the Gamma Falex System | 47 |

| Figure | Page |
|--|------|
| 21. Hardness of Journal and V-Block | 49 |
| 22. Geometry of Journal and V-Block (mm). | 50 |
| 23. A Typical Result of Gamma Falex Test. | 51 |
| 24. MIL-H-5606 Gamma Falex Test Data, Incubation Period Distribution. | 55 |
| 25. MIL-H-5606 Gamma Falex Test Data, Gamma Slope Distribution. . . | 56 |
| 26. MIL-H-5606 Gamma Slopes Plotted in Chronological Order. | 57 |
| 27. MIL-L-2104 Gamma Falex Test Data, Incubation Period Distribution. | 60 |
| 28. MIL-L-2104 Gamma Falex Test Data, Gamma Slope Distribution. . . | 61 |
| 29. MIL-L-2104 Gamma Slopes Plotted in Chronological Order. | 62 |
| 30. Mineral Oil A Gamma Slope Distribution. | 63 |
| 31. Mineral Oil B Gamma Slope Distribution. | 64 |
| 32. Major and Minor Normal Distributions Considered for the Gamma Slope of MIL-H-5606 | 66 |
| 33. Mean and Standard Deviation of Major Normal Distributions for Four Test Fluids with Minor Data Points | 68 |
| 34. Wear Surfaces on V-Block. | 71 |
| 35. Loading System of the Gamma Falex System. | 73 |
| 36. Wear Geometry of Test Specimens | 74 |
| 37. Wear Reading Versus Unit Load on Wear Surface | 79 |
| 38. Geometry of Wear Progressing in a Finite Period of Time | 80 |
| 39. Theoretical Plotting of Wear Reading on the Gamma Falex System. | 83 |
| 40. A Gamma Falex Test Result with Incubation Period of 10 min. . . | 84 |
| 41. Saturation of Wear Observed in a Gamma Falex Test | 86 |
| 42. Effects of Load, Material and Lubricant on Surface Contact Wear. | 89 |
| 43. Values of $(s^{1.5}/W)$ for Nineteen Test Fluids | 93 |

| Figure | Page |
|--|------|
| 44. Material Effects on Surface Contact Wear. | 96 |
| 45. Test Equipment for Static Asperity Deformation. | 98 |
| 46. Plate Dimensions. | 99 |
| 47. Cone Dimensions | 101 |
| 48. Deformed Soft Cone. | 104 |
| 49. Plate Surface Slided with Soft Cone | 104 |
| 50. Deformed Hard Cone. | 106 |
| 51. Plate Surface Slided with Hard Cone | 107 |
| 52. Measured Data of Test No. 10, Soft Cone with Re-refined Motor Oil | 108 |
| 53. Measured Data of Test No. 11, Hard Cone with Re-refined Motor Oil | 109 |
| 54. Deformed Areas of Soft Cones and Hard Cones | 113 |
| 55. Force Elements without Frictions. | 115 |
| 56. Force Elements with Frictions | 117 |
| 57. Vertical and Horizontal Force Elements. | 118 |
| 58. Coefficients of Friction with Different Test Fluids | 121 |
| 59. Theoretical and Actual Volume Rates of Deformation. | 124 |
| 60. Difference of Conical Shape Expansion Between Ductile and Brittle Materials | 125 |
| 61. Test Equipment for Dynamic Asperity Deformation | 128 |
| 62. Lost Lengths of Test Cones. | 132 |
| 63. Deformed Surface of Soft Cone | 133 |
| 64. Plate Surface Imprint Made by Soft Cone | 134 |
| 65. Deformed Surface of Hard Cone | 135 |
| 66. Plate Surface Imprint Made by Hard Cone | 136 |
| 67. General Pattern of Plate Surface Imprint. | 138 |
| 68. Velocity Profile with Soft Cone | 141 |

| Figure | Page |
|---|------|
| 69. Velocity Profile with Hard Cone | 143 |
| 70. Flash Temperature Chart for Soft Cone | 147 |
| 71. Flash Temperature Chart for Hard Cone | 149 |
| 72. Variable Speed Gamma Falex System | 158 |
| 73. Initial Clean Test with MIL-L-2104. | 159 |
| 74. 0-5 Micrometres Abrasive Test and Clean Test with MIL-L-2104. . | 163 |
| 75. 0-10 Micrometres Abrasive Test and Clean Test with MIL-L-2104 . | 165 |
| 76. Pump Abrasive Wear Test Circuit | 174 |
| 77. Gear Pump Abrasive Wear Test Results. | 177 |
| 78. Particle Distributions of Classified AC Fine Test Dust. | 196 |
| 79. Particle Distributions Controlled by Beta Ten Filters | 198 |

NOMENCLATURE

| | |
|---------------|--|
| n_s | number of surface asperities in contact |
| d | diameter of top surface of asperity squashed by flat surface |
| W | applied load |
| σ | flow pressure of material |
| σ_{ij} | principal stress ($i = x, y, z, j = x, y, z$) |
| σ | normal stress |
| σ | shear stress on particle due to cutting |
| V_1 | deformed volume per asperity |
| V_2 | total volume of deformation due to sliding distance d |
| V_3 | volume rate of deformation per unit sliding distance |
| V_4 | volume rate of surface wear |
| V_r | volume rate of surface contact wear per unit time |
| V | volume rate of abrasive wear per particle |
| v | sliding velocity |
| v_f | final velocity |
| v_0 | initial velocity of combined mass M_1 and M_2 |
| x | wear scar depth on V-block |
| r | journal diameter |
| b | scar width |
| N | wear reading (number of ratchet wheel gear teeth advanced) |
| h | distance from top surface to the bottom of lower surface |
| T_y | material yield strength in tension |
| T | diagonal of a particle |

| | |
|---------------|---|
| T | wear life of sliding mechanism |
| T_f | flash temperature |
| t_1 | cutting depth |
| t_2 | indentation depth |
| t | test time |
| t_0 | incubation period |
| m | height of asperity |
| m | constant |
| m_1 | mass of weight M_1 |
| m_2 | mass of weight M_2 |
| A | deformed surface area of asperity |
| A | area of one contact surface |
| a | width of contact area |
| τ | shear stress |
| μ | coefficient of friction |
| μ_1 | coefficient of friction between slider A and cone |
| μ_2 | coefficient of friction between slider A and the slide base |
| θ_s | base angle of surface asperity |
| θ | angle of slider A |
| K | coefficient of wear fragment formation |
| k | shear yield strength of surface material |
| k_1 | shear yield strength of the cut surface |
| k_2 | shear yield strength of the indented surface |
| k_1 & k_2 | thermal conductivities of two contacting materials |
| F_c | cutting force |
| F_i | force element ($i = 1, 2, 3, \dots$) |
| F_c | contact force |

| | |
|-----------|--|
| s | Gamma slope |
| c | constant |
| γ | angle between $-F_1$ and F_6 |
| p | indentation pressure |
| ψ | indentation parameter |
| λ | indentation parameter |
| α | particle angle relative to sliding surface |
| d | particle size |
| l | length of contact area |
| P | unit load of contact surface |
| g | acceleration |
| L | height of weight M_1 for free fall |
| E | surface energy |
| J | mechanical equivalent of heat |

CHAPTER I

INTRODUCTION

In most mechanical systems, there are elements that slide against each other. When two surfaces are in sliding contact, removal of surface materials is generally observed, which is referred to as surface contact wear. To eliminate or minimize the removal of materials, a lubricant is applied between the sliding surfaces; however, the lubricant film cannot avoid direct contact of surface asperities under boundary lubrication conditions. Protection of the sliding surfaces under boundary lubrication conditions relies on the interaction between the lubricant and the surface materials.

An adhesive wear theory developed by Holm (1) has been used to describe surface contact wear. Holm's adhesive wear theory considers the hardness of the surface material, but it does not incorporate the effect of the lubricant. A recent study on surface contact wear revealed that there are two important phenomena involved in surface contact wear other than adhesion--deformation and delamination of surface materials. Thus, Holm's adhesive wear theory is insufficient to properly describe surface contact wear in lubricated mechanical systems.

Direct contact of the surfaces can be eliminated by increasing lubricant film thickness, which may be achieved by either high sliding velocity or static pressure. When the protective lubricant film is formed by a high sliding velocity, it is called hydrodynamic

lubrication; whereas, when the lubricant film is formed by static pressure, it is called hydrostatic lubrication.

The protection of the sliding surfaces under hydrodynamic lubrication relies merely on fluid viscosity. The higher fluid viscosity, the thicker fluid film that can be obtained and the better the protection of the sliding surface.

No wear generation is expected under hydrodynamic lubrication because sliding surfaces are completely separated from each other, and no direct contact of the surfaces occurs. However, abrasive particles usually exist in lubricated systems that migrate into the clearance between the sliding surfaces and cause abrasive wear. Abrasive wear often jeopardizes the performance of mechanical systems that are lubricated with proper hydrodynamic lubrication.

Abrasive wear theory has been studied by many researchers; however, the research activities were focused upon two-body abrasion with no lubricant applied between the two sliding surfaces. Abrasive wear under three-body abrasion where lubricant and abrasive particles are involved has not been properly studied in spite of its importance to mechanical systems.

Surface contact wear and abrasive wear are two major wear modes for sliding surfaces that lead to failures of the mechanical system. Despite the importance of these wear modes, feasible theories are not available to properly describe these situations.

This dissertation presents the development of theories for surface contact wear and abrasive wear in lubricated sliding mechanisms. Numerous experimental tests have been conducted to validate the developed theories that are presented, and the test results are

analyzed. The effects of lubricants to protect sliding surfaces from wear are theoretically discussed and validated by the analysis of experimental test results.

CHAPTER II

PREVIOUS INVESTIGATIONS

Surface contact wear occurs when surfaces slide against each other, and the pressure between the contacting asperities is high enough to cause local plastic deformation and adhesion. Since it is widely known that wear debris is formed due to adhesion of surface materials, this wear mode is often called adhesive wear.

Holm (1) developed a model for adhesive wear which states that the total volume of material removed due to adhesion is proportional to both the applied normal load and the sliding distance, and it is inversely proportional to the flow pressure of the material. Burwell and Strange (2) have examined Holm's model by running conical brass and steel pins on steel disks under dry conditions. As a result of their work, it was found that the adhesive wear rate is proportional to the apparent normal contact pressure up to a value that equals the tensile strength in tension of the pin material, Fig. 1. The rate of wear is expressed by h/PS , where h is a height lost by the pin due to wear, P is contact pressure, and S is a sliding distance. Beyond the tensile strength, Holm's model is not applicable and the wear rate increases drastically. Their work is important because the limitations of the Holm's model were experimentally determined.

Archard (3) assumed hemispherical asperities and incorporated a shape factor into the adhesive wear model. Yoshimoto and Tsukizoe (4)

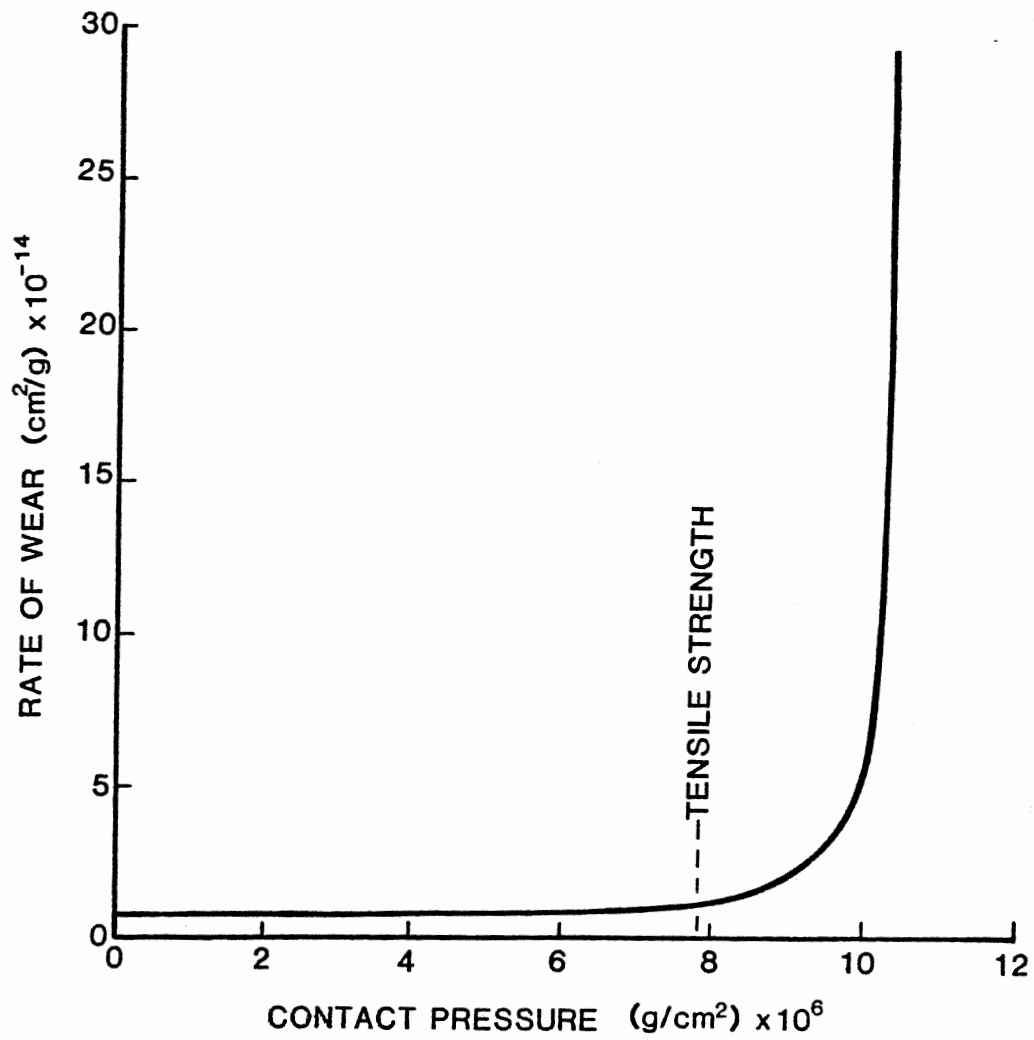


Fig. 1. Rate of Wear as a Function of Apparent Contact Pressure

suggested that real surfaces are not a regular array of hemispherical projections but have shapes between a cone and a hemisphere. They proposed conical asperities and incorporated sharpness of asperity into the wear model as one of the parameters.

A new theory for sliding surface wear of metals was proposed by Suh (5). The theory, called the delamination theory, is based on the behavior of dislocations at the surface, subsurface crack and void formation, and subsequent joining of cracks by shear deformation of the surface. He proposed a simplified wear equation to show that the theory is consistent with phenomenological wear behavior. The equation states that the wear rate is proportional to the normal load and the sliding distance. The above statement agrees with Archard's wear equation; however, the equation differs from Archard's because it does not depend directly on hardness. He concluded that the so-called "adhesive," fretting, and fatigue wear are all caused by the same mechanisms.

Rigney and Glaeser (6) studied the dislocation wear process, which is similar to Suh's delamination wear theory. The wear process, in which flake-like debris are developed and removed from the surface of metals in sliding contact, is the direct result of heavy plastic deformation of a thin surface layer. The repeated ploughing of asperity contacts over a mating surface can produce high dislocation densities and eventual change in the microstructure to a cell-type structure found in heavily deformed metals.

Using the dislocation theory, Kuhlmann-Wilsdorf (7) developed a number of qualitative and quantitative relationships in the area of friction and wear. Recent study by Suh and Sin (8) revealed that the coefficient of friction is composed of three components that are due to

the deforming asperities, to plowing by wear particles entrapped between sliding surfaces and hard surface asperities, and to adhesion. The overall coefficient of friction contributed by plowing and asperity deformation can be greater than that by adhesion.

Although Holm's adhesive wear theory has been widely quoted for many years, it completely ignores the physics of metal deformation. Suh's delamination theory includes a plastic deformation of the material; however, his theory was verified by experimental test only at a very low sliding velocity (0.5 cm/sec) (5). The sliding speed for most mechanical applications is at least one order of magnitude higher than that.

If the basic wear concept developed by Holm is coupled with the plastic material deformation, a new wear theory must be considered that is applicable to most mechanical sliding contact elements.

Abrasive wear occurs when hard particles or asperities penetrate a surface and displace material in the form of elongated chips. A situation where hard surface asperities plow a series of grooves in the soft surface is called two-body abrasion; whereas, when loose hard particles entering the sliding interface act as grits, the process of material removal by these particles is termed three-body abrasion. Wear in fluid power systems due to contaminant is the second type. Most investigators used two-body geometry (9, 10, 11) to study abrasive wear, but three-body abrasion has also been studied (12, 13).

Kruschov (14) stated that abrasive wear resistance is inversely proportional to material hardness. Richardson (15) showed in his work that the hardness of the surface resisting abrasive wear must be greater than half the hardness of the abrasive if any real improvement in wear

resistance is to be achieved. However, it is unnecessary to increase the hardness of the material beyond 1.3 times that of the abrasive because no further significant improvement will be obtained.

Rabinowicz and Mutis (16) derived an abrasive wear model assuming that the part of one abrasive particle which contacts the surface has a cone shape. The model simply considers the measured angle of the cone as a shape factor and the hardness of the abraded surface; however, it does not include the hardness of abrasives. This model has been widely used to represent both two-body and three-body abrasions (17).

Rabinowicz and Mutis made two important statements--one is that an important variable that affects wear rate is the size of the abrasive particles. As the abrasive size increases, starting from a very small value, there is an initial increase in the wear rate until a certain characteristic value of the abrasive size is reached. Above that value, the wear rate is independent of abrasive size. This is referred to as the critical size effect. The best explanation they could give for this was that there may be interference between the abrasive wear process and adhesive wear, which is continuous. Thus, if the abrasive particles are small, two abrading bodies may contact, and an adhesive particle may be formed. If the adhesive particles are large, they will prevent abrasive action, either completely or partially. The critical size effect with and without lubricant was experimentally verified. The second important statement is that lubricants reduce the size of adhesive wear particles and thus allow abrasion to occur with small grit sizes.

Rabinowicz (18) also stated that the effect of lubrication on abrasive wear appears to be that of flushing wear debris from the system

more completely. Thus, the effectiveness of the abrading action is increased.

Nathan and Jones (19) developed a model including the hardness of both surface material and abrasive particles by experimentation. However, their tests were conducted using two-body abrasion with the absence of lubricant.

Sin, Saka and Suh (20) carefully studied abrasive wear mechanisms and the grit size effect based on an extensive review of previous works and developed a more accurate empirical model for three-body abrasion. Their experimental tests were conducted under a no lubricant three-body abrasion condition.

In a practical study of abrasive wear, Roach (21) reported that the wear of oil-film bearings is proportional to the abrasive concentration in the lubricant. Scott (22) studied Roach's work and emphasized that abrasive particles smaller than the minimum oil film thickness have no serious effect on bearing performance. This may then be considered the desired limit of filtration. Scott also stated that, for conditions of abrasive wear where a lubricant is present (such as in hydraulic systems), the evidence suggests that the quantity of wear is increased in comparison to the dry conditions; however, the source of this statement was not clarified in his report.

With the presence of lubricant, adhesive wear can take place only under boundary lubrication and mixed lubrication conditions. Adhesive wear can be avoided by increasing the lubricant film thickness and eliminating surface asperity contacts. The film thickness can be increased by three conditions: i.e., hydrodynamic, hydrostatic and elastohydrodynamic lubricating conditions. Scott pointed out that the minimum film

thickness corresponds to the minimum size of abrasives that may be harmful to the system.

Tao and Appeldoorn (23) proposed a concept developed from the results of their experiments that antiwear additives prevent three-body abrasion by preventing the particles from adhering to one of the moving surfaces where they can act like small cutting tools. The effect of antiwear additives on abrasive wear proposed by Tao and Appeldoorn can be correct based on the abrasive wear mechanism explained by Burwell (2) and Rabinowicz (19); i.e., an abrasive grain adheres temporarily to one of the sliding surfaces, or is embedded in it and plows a groove in the other. However, Tao's statement is contradictory with the positive effects of lubricants on abrasive wear suggested by Rabinowicz and Mutis.

To summarize the previous studies on abrasive wear presented above, the following comments are made. Abrasive wear from sliding surfaces in the presence of a lubricant was studied by Rabinowicz, Mutis, Roach, Tao and Appeldoorn. Roach and Tao showed only the experimental test results and made observations and discussions. Rabinowicz and Mutis developed a model; however, their model was developed assuming dry conditions. Therefore, no parameters that represent the effect of a lubricant are included in the model.

CHAPTER III

DEVELOPMENT OF THEORETICAL MODELS

Surface Contact Wear Model

Assume that an interface exists where the top surface is flat, but the bottom surface is undulated with asperities of conical shape that are randomly distributed with a base angle θ_s shown in Fig. 2.

When the load is applied, the tips of the asperities are squashed until the flow pressure of the material times total contact area becomes equal to the applied load. Hence,

$$n_s \frac{\pi d^2}{4} = \frac{W}{\sigma} \quad (1)$$

where

n_s = number of surface asperities in contact

d = diameter of top surface of asperity squashed by flat surface

W = applied load

σ = flow pressure of material

Due to the squashing action, the volume of one asperity deformed is calculated by :

$$V_1 = \frac{1}{3} \pi \frac{d^2}{4} (m - h) \quad (2)$$

where

V_1 = deformed volume per asperity

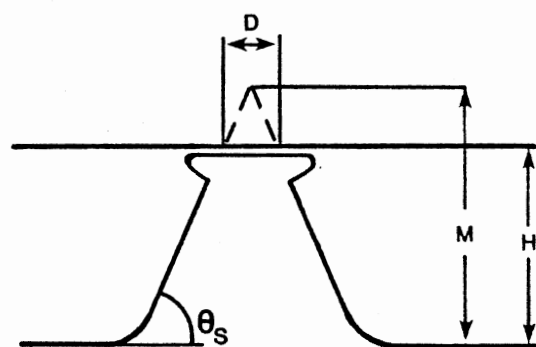


Fig. 2. Conical Shape Surface
Asperity

m = height of asperity

h = distance from top surface to the bottom of lower surface

Since the surfaces slide against each other, shear stress is acting on the asperity in addition to the normal load as illustrated in Fig.

3. In this case, the deformation of the asperity is considered with the yield criterion of metal (24). A yield criterion is a hypothesis concerning the limit of elasticity under any possible combination of stresses. According to the Von Mises yield criterion,

$$(\sigma_{xx} - \sigma_{yy})^2 + (\sigma_{yy} - \sigma_{zz})^2 + (\sigma_{zz} - \sigma_{xx})^2 + 6(\sigma_{xy}^2 + \sigma_{yz}^2 + \sigma_{zx}^2) = 2T_y^2 \quad (3)$$

where

σ_{ij} = principal stress

T_y = material yield strength in tension.

In this case,

$$\sigma_{xx} = \sigma_{zz} = \sigma_{yz} = \sigma_{zx} = 0 \quad (4)$$

$$\sigma_{yy} = \sigma = \frac{W}{A} \quad (5)$$

and

$$\sigma_{xy} = \tau = \frac{W\mu}{A} \quad (6)$$

where

σ = normal stress

A = deformed surface area of asperity

τ = shear stress

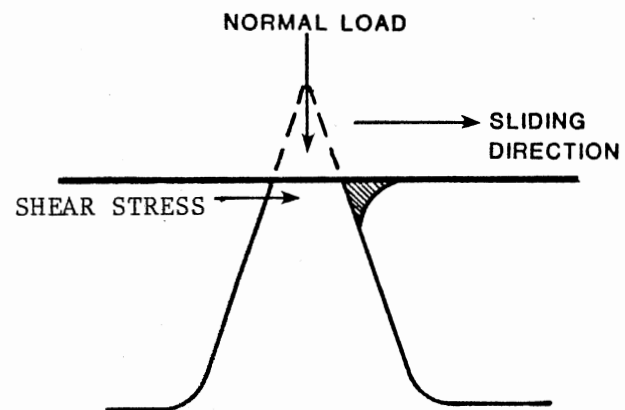


Fig. 3. Asperity Deformation Under Sliding Condition

μ = coefficient of friction

Hence,

$$\sigma^2 + 3\sigma^2\mu^2 = T_y^2 \quad (7)$$

or

$$\frac{\sigma}{T_y} = \frac{1}{\sqrt{1 + 3\mu^2}} \quad (8)$$

Eq. (8) states that the plastic deformation of the asperity occurs when normal stress is less than the yield strength of the material because the friction coefficient is always greater than zero. If no sliding action exists, the plastic deformation starts when the normal stress equal to the yield strength. Eq. (8) is plotted for various values of the friction coefficient in Fig. 4.

Applicable range of the friction coefficient in Fig. 4 is limited up to 0.577 because the asperity material starts to flow toward a direction of shear stress when the friction coefficient exceeds 0.577. This limitation is derived from the Von Mises criterion.

Assuming that all the asperities in contact have a height m , the total volume of deformation due to a sliding distance d is expressed by:

$$V_2 = n_s V_1 = \frac{\pi}{12} n_s d^2 (m - h) \quad (9)$$

where

V_2 = total volume of deformation due to sliding distance d .

The volume rate of deformation per unit sliding distance is derived by simply dividing the total volume by the sliding distance d ,

$$V_3 = \frac{V_2}{d} = \frac{\pi}{12} n_s d(m - h) \quad (10)$$

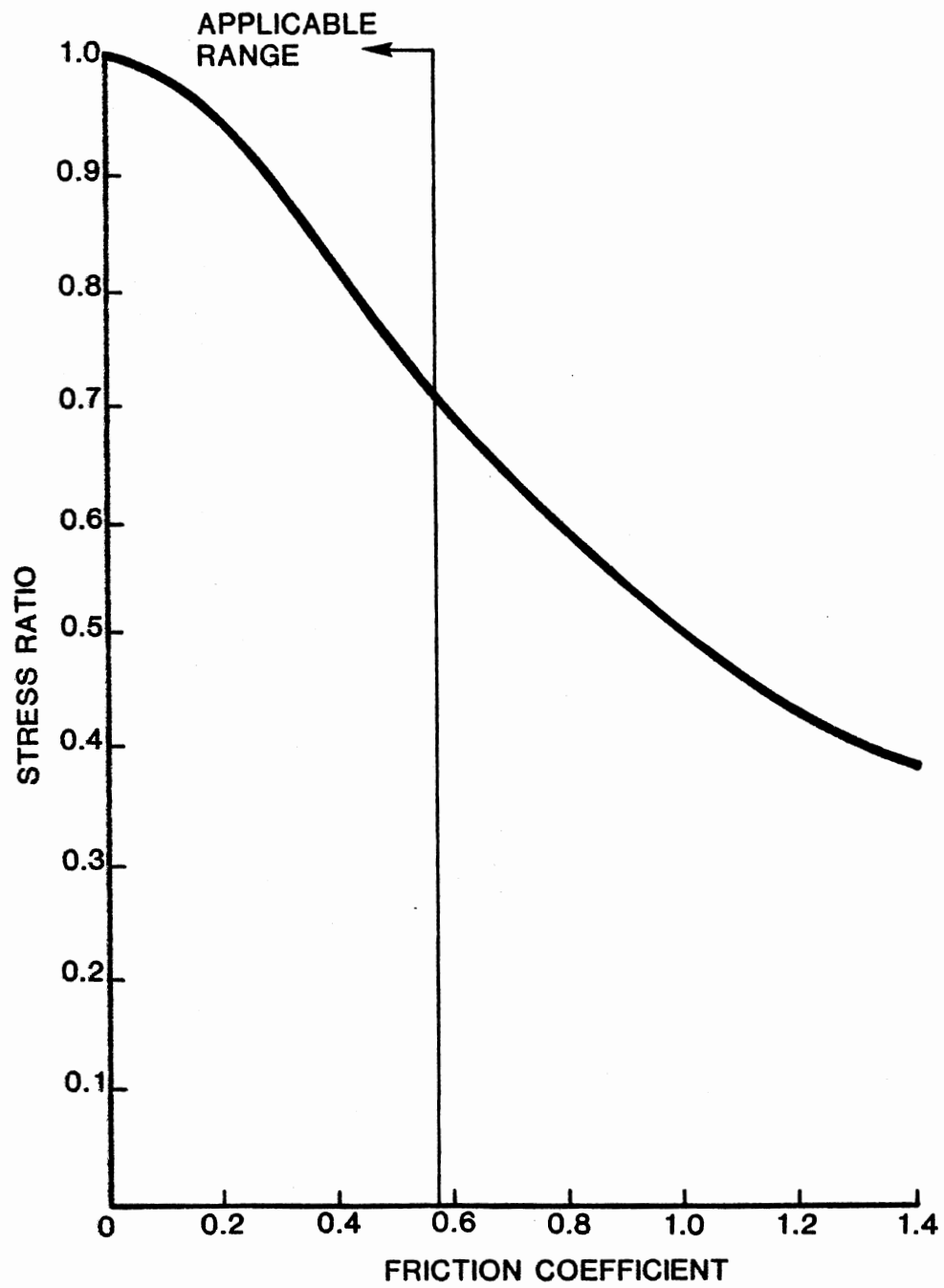


Fig. 4. Friction Coefficient Versus Stress Ratio

where

V_3 = volume rate of deformation per unit sliding distance.

We have

$$d = 2(m - h) \cot \theta_s \quad (11)$$

where

θ_s = base angle of surface asperity

Substituting Eq. (11) into Eq. (10) yields:

$$V_3 = \frac{\pi}{6} n_s (m - h)^2 \cot \theta_s \quad (12)$$

Substituting Eqs. (8) and (11) into Eq. (1) yields:

$$\pi n_s (m - h)^2 \cot \theta_s = \frac{W \sqrt{1 + 3\mu^2}}{T_y} \tan \theta_s \quad (13)$$

Substituting Eq. (13) into (12) yields:

$$V_3 = \frac{W \sqrt{1 + 3\mu^2}}{6T_y} \tan \theta_s \quad (14)$$

In the process of asperity deformation, part of the deformed material breaks off and forms a wear fragment when deformation exceeds the elongation limit, Fig. 5. The volume of wear fragments is considered to be proportional to the volume of deformation. Then, the volume rate of surface contact wear is given by:

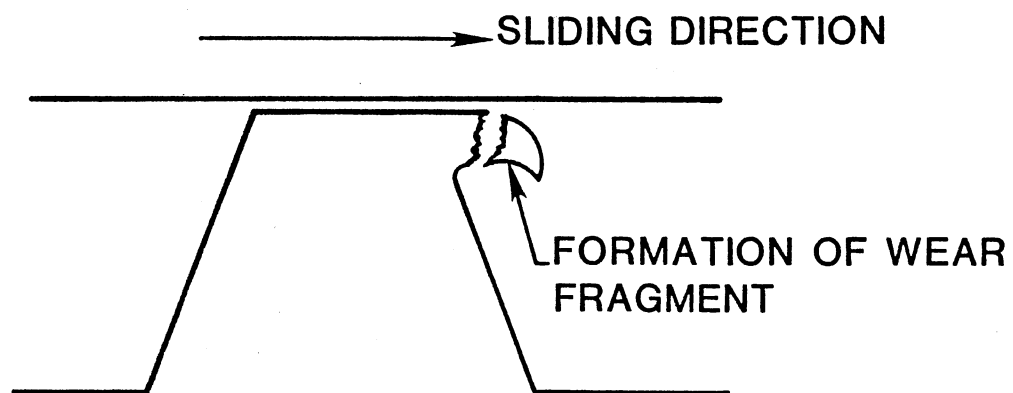


Fig. 5. Formation of Wear Fragment

$$V_4 = KW \frac{\sqrt{1 + 3\mu^2}}{6T_y} \tan \theta_s \quad (15)$$

where

V_4 = volume rate of surface contact wear

K = coefficient of wear fragment formation.

Abrasive Wear Model

Most of the previous investigators assumed that the abrasive particle has a conical edge that plows the surface material to produce abrasive wear (16). The shape of the other end of the abrasive particle was undefined and not considered because the two-body abrasion model was extended and applied to three-body abrasion where abrasive particles are involved.

For two-body abrasion, the other end of the conical abrading edge is attached to the surface. But the abrasive particle in three-body abrasion is independent of the two sliding surfaces.

Inoue (25) first defined the complete shape of the abrasive particle in three-body abrasion. The shape of the abrasive particle defined by Inoue has a conical edge and a flat top as shown in Fig. 6.

A further study on the shape of abrasive particles revealed that the shape defined by Inoue does not accurately describe the actual abrasive particles. In general, the abrasive particles found in hydraulic systems and lubricating systems have irregular shapes. They have edges that indent one surface and plow the other. Because of these edges, the particles are abrasive in the system. The shape of the abrasive particle is often called an "angular shape."

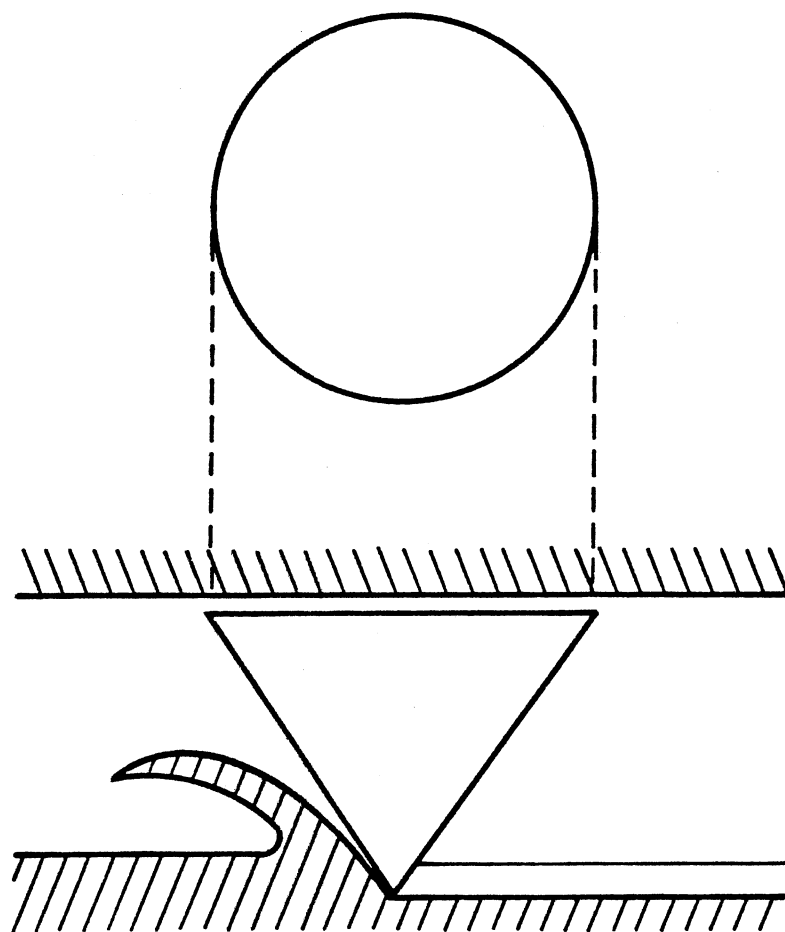


Fig. 6. Shape of Abrasive Particle by
Inoue

Several shapes such as a sphere, ellipsoid, spheroid, cylinder, cube, square, prism, pyramid, and paraboloid have been proposed for the shape model of the abrasive particle (26, 27, 28). The author actually took abrasive particles (AC Fine Test Dust--silica particles) and observed their shapes by ferrography (29). Some of the shapes observed are shown in Fig. 7. Notice from this figure that it is difficult to determine a model which represents all these abrasive particles. But it is definitely necessary to determine an appropriate shape model for the abrasive particles to develop an abrasive wear theory.

Kroeker (30) assumed a square prism shape for AC Fine Test Dust which is one of the most common abrasive test particles. The shape of a square prism is considered appropriate for the study of abrasive wear because analysis of the abrading process can be reasonably simple with a square prism particle. A square prism may also represent satisfactorily most of the abrasive particles observed in Fig. 7.

The shape of a square prism assumed by Kroeker is used to develop an abrasive wear theory. Fig. 8 depicts the shape of the abrasive particle defined by Kroeker.

Three-body abrasion is a process of indenting and cutting of sliding surfaces by abrasive particles. If perfectly smooth surfaces are considered with a lubricant film thickness h , only particles with minimum lengths less than or equal to a clearance h can migrate into the clearance as shown in Fig. 9. Since perfectly smooth surfaces are assumed, no wear can occur in this case. But actual sliding surfaces are not perfectly smooth. Microscopic observation of the actual sliding surfaces revealed many surface asperities as shown in Fig. 10 (31). From the microscopic observation of the sliding surfaces, it is clear

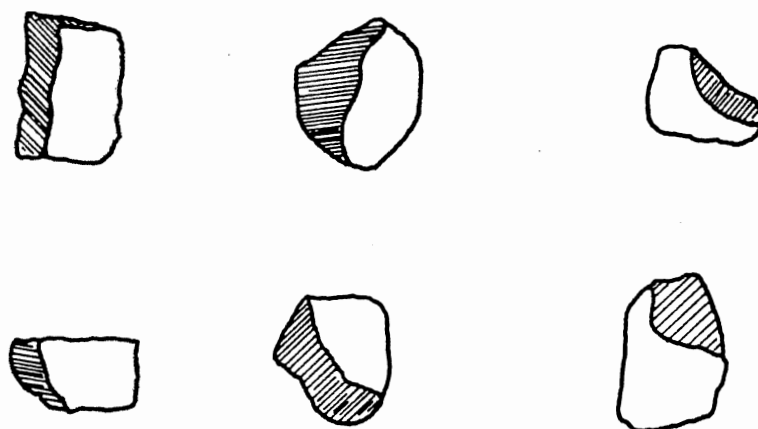


Fig. 7. Some Shapes Observed for ACFTD
(Silica) Particles by
Ferrography

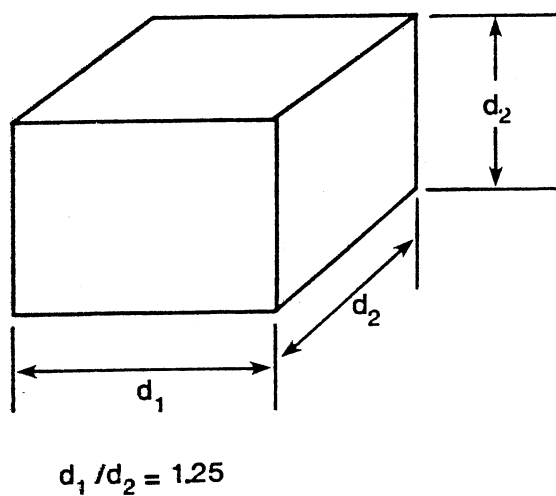


Fig. 8. Shape of Abrasive Particle
Defined by Kroeker

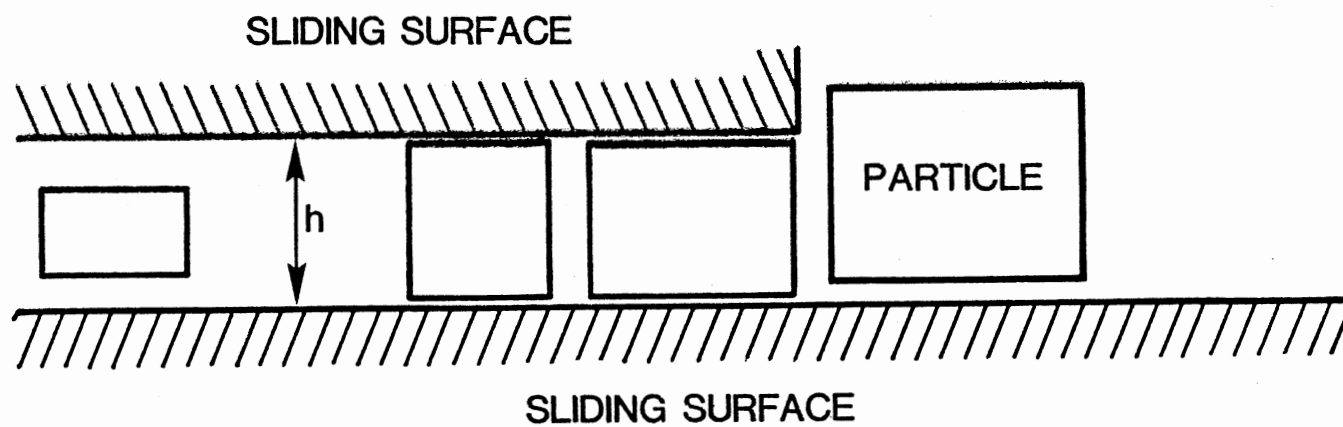


Fig. 9. Assumed Smooth Surfaces and Abrasive Particles

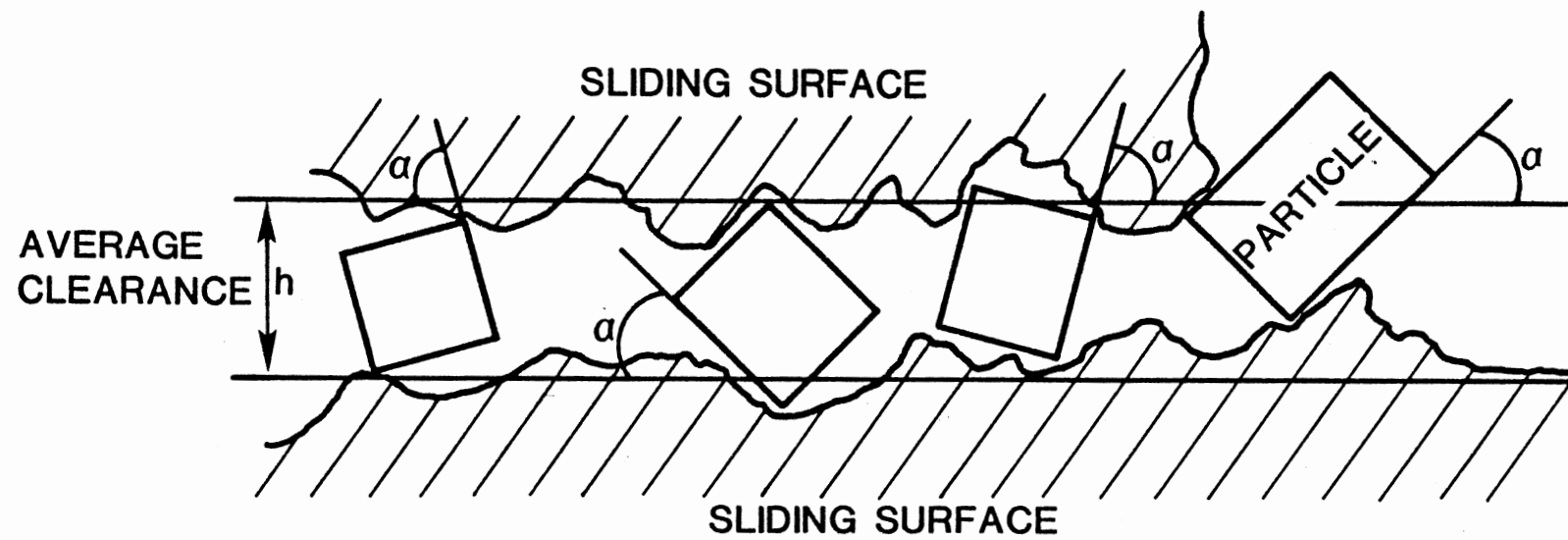


Fig. 10. Surface Asperities and Abrasive Particles

that the clearance between the two surfaces varies from one place to another. The assigned value for the clearance is an average of clearances between two rough surfaces. Abrasive particles that are slightly larger or slightly smaller than the clearance can be trapped in the clearance and cause abrasion. The particles are trapped between the two surfaces at various angles because of surface roughness. The size range of abrasive particles trapped in the clearance and the variation of the particle angle relative to the surfaces depend on the surface roughness. The rougher the surfaces, the wider the particle size range that can be trapped. The rougher surfaces are also associated with a larger variation of the angle between the particles and the surfaces.

In general, the particle size is designated by the length of the longest edge of the particle (30). Hence, a particle of 100 micrometres assuming a square prism shape has a longer edge of 100 micrometres, a shorter edge of 80 micrometres, and a diagonal of 128 micrometres as illustrated in Fig. 11.

As mentioned above, abrasive wear is a process of indentating and cutting the sliding surfaces by abrasive particles. The indented surface supports the abrasive particle while the other edge of the particle is cutting the other sliding surface. Both indentation and cutting mechanisms need to be studied to develop an abrasive wear theory.

First, the cutting mechanism in the abrading process is investigated. Fig. 12 delineates the cutting model of surface abrasion by an abrasive particle. Orthogonal cutting is assumed in which the cutting face is perpendicular to the surface, and the rake angle is null. Then, the force required to achieve cutting is:

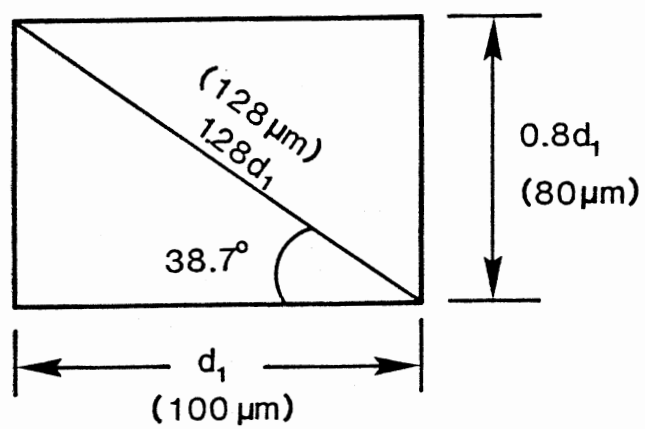


Fig. 11. Abrasive Particle Shape Assumed

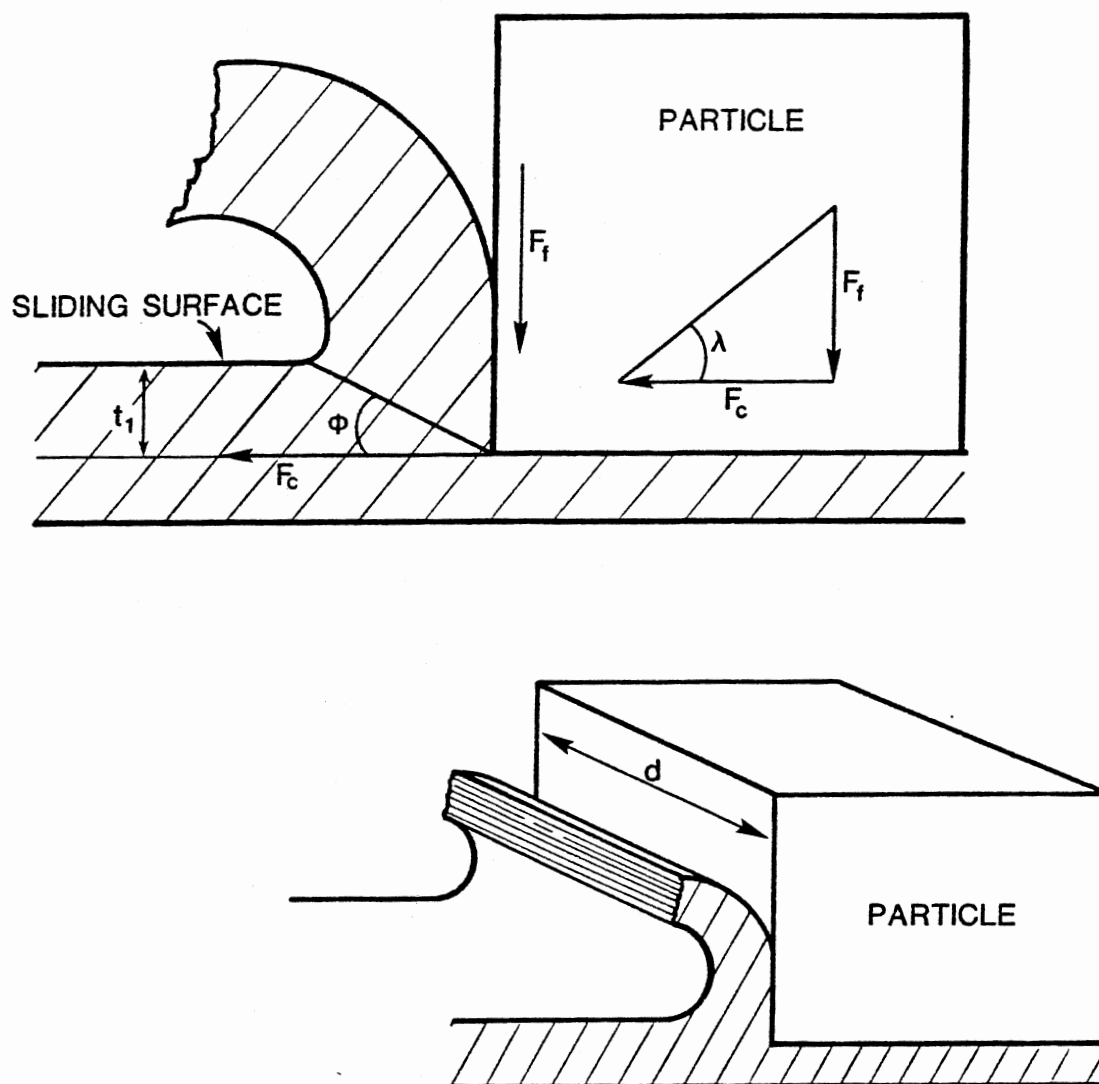


Fig. 12. Cutting Model for Surface Abrasion

$$F_c = 2 k t_1 d \cot(45^\circ - \frac{\arctan \mu}{2}) \quad (16)$$

where

F_c = cutting force

k = shear yield strength of surface material

t_1 = cutting depth

d = particle size

μ = coefficient of friction

The volume rate of abrasive wear produced by particle is expressed by:

$$V = t_1 d v \quad (17)$$

where

V = volume rate of abrasive wear per particle

v = sliding velocity

Since the effective area of the particle for cutting is $t_1 d$, stress induced on the effective cutting area of the particle is:

$$\sigma = 2 k \cot(45^\circ - \frac{\arctan \mu}{2}) \quad (18)$$

where

σ = shear stress on particle due to cutting.

Eq. (18) is useful for determining whether cutting actually occurs.

When cutting stress calculated by Eq. (18) exceeds the shear yield strength of the abrasive particle, cutting does not occur. Instead, the particle is sheared off.

The shear yield strengths of sliding surfaces and abrasive particles are usually known in mechanical systems. The coefficient of friction is the factor altered by different lubricants and, consequently, determines the occurrence of abrasive wear. Fig. 13 shows that the minimum shear yield strength of abrasive particles causes abrasive wear to be a function of the coefficient of friction. In Fig. 13, the minimum shear yield strength of abrasive particles is expressed relative to the shear yield strength of the surface material.

This discussion is also valid when the material hardness is replaced by the material shear yield strength because the shear yield strength is usually proportional to the hardness of material. When the coefficient of friction is zero, the abrasive particle should be at least twice as hard as the surface material to achieve cutting. However, when the coefficient of friction is 0.5, the abrasive particle should be more than 3.24 times as hard as the surface material. This implies that with better fluid lubricity, it is easier for the abrasive particle to cut the surface material. On the other hand, when the fluid lubricity is worse, there is the higher probability for abrasive particles to be sheared off by the surfaces instead of cutting the surfaces.

The second abrading process to be investigated is the indentation mechanism. Fig. 14 shows the indentation model for surface abrasion. Grunzweig and others (32), measured experimentally the amount of indentation and the force required for indentation with various wedge angles and friction coefficients. The stress on the wedge surface to achieve indentation is calculated by:

$$p = k (1 + 2\psi + \sin 2\lambda) \quad (19)$$

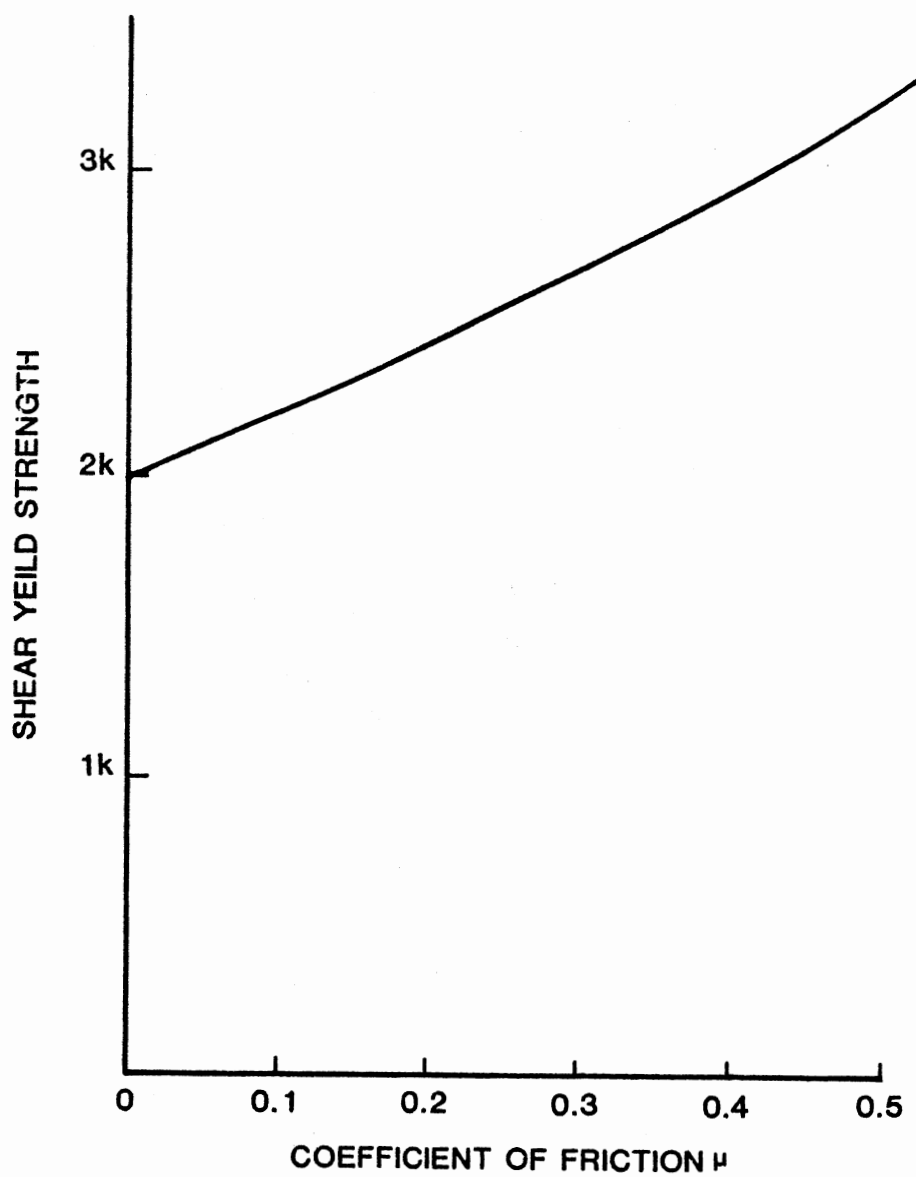


Fig. 13. Minimum Shear Yield Strength Required for Abrasive Particle in Cutting

where

p = indentation pressure

ψ and λ = indentation parameters (angles)

The abrasive particle model defined in this study has a wedge angle of 45 deg. The parameters determined experimentally by Grunzweig and others for a wedge angle of 45 deg are tabulated in Table 1 for various friction coefficients. With the parameters tabulated in Table 1, the stress on the indenting edge of the particle is calculated and plotted as a function of the coefficient of friction in Fig. 15. When no friction is considered, the abrasive particle should be more than 3.15 times as hard as the surface material to indent it; however, the particle should be more than 3.81 times as hard as the surface material when the coefficient of friction is 0.2. The coefficient of friction plays an important role in indentation process of the abrasive wear just as in the cutting process.

With knowledge of the cutting and indentation mechanisms in abrading process, an abrasive wear theory can be developed. An abrasive particle that migrates into the clearance between two sliding surfaces with an angle α indents one surface and cuts the other surface as shown in Fig. 16. Indentation and cutting of the surfaces occurs in the equilibrium state where the force required for cutting is equal to the force necessary to indent the other surface. If one of the stresses on the particle due to cutting or indentation exceeds the shear yield strength of the particle, the particle is sheared off instead of indenting or cutting the surface, and no abrasive wear occurs.

From the way that the particle angle is defined with the sliding surfaces in Fig. 16, a particle angle of 38.7 deg is the minimum

TABLE I

INDENTATION PARAMETERS FOR DIFFERENT
COEFFICIENTS OF FRICTION

| COEFFICIENT OF FRICTION | λ | ψ |
|----------------------------|------------|---------------|
| 0 | 45° | 33.06° |
| 0.05 | 40.18 | 39.16 |
| 0.10 | 34.66 | 45.73 |
| 0.15 | 28.19 | 53.18 |
| 0.20 | 20.12 | 62.02 |

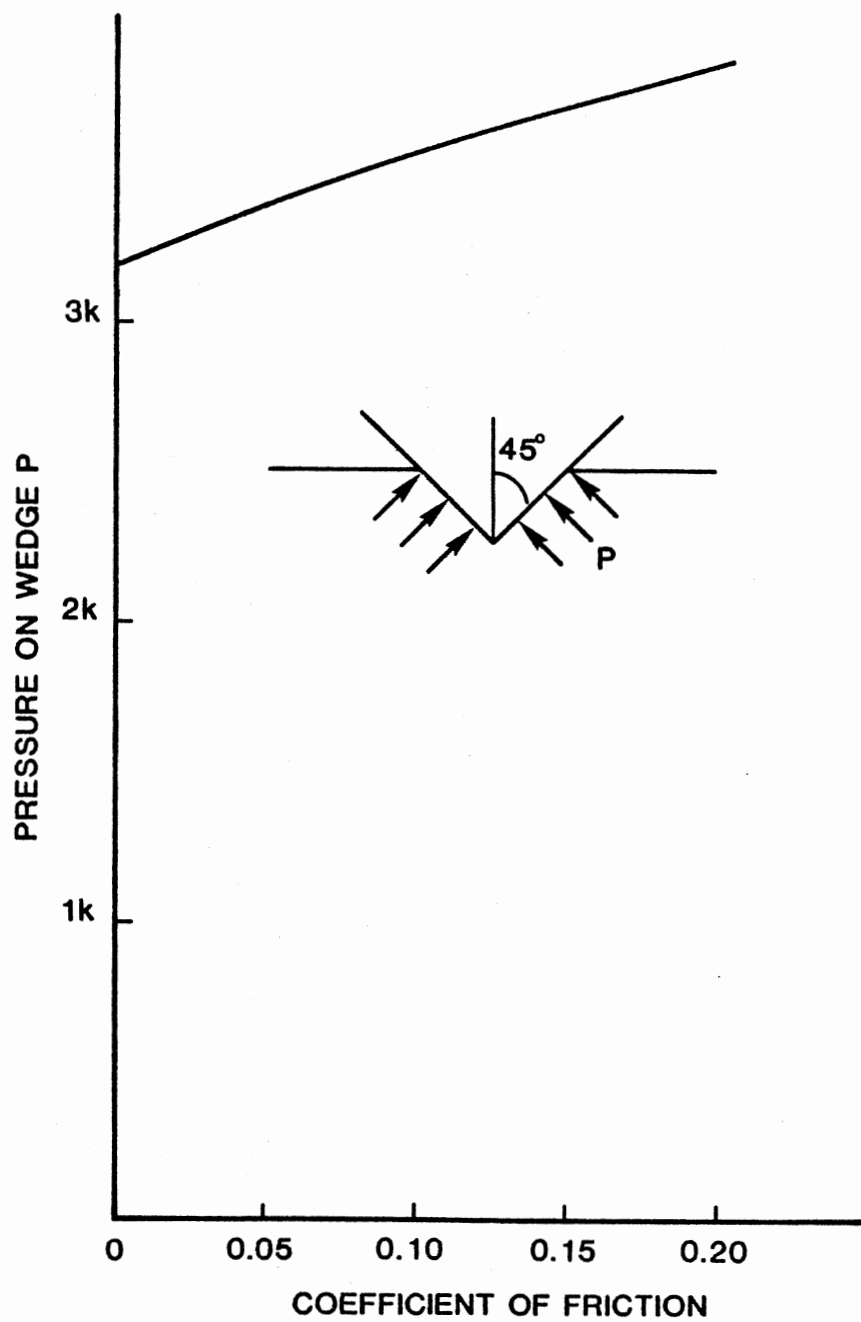


Fig. 15. Minimum Shear Yield Strength Required for Abrasive Particle in Indentation

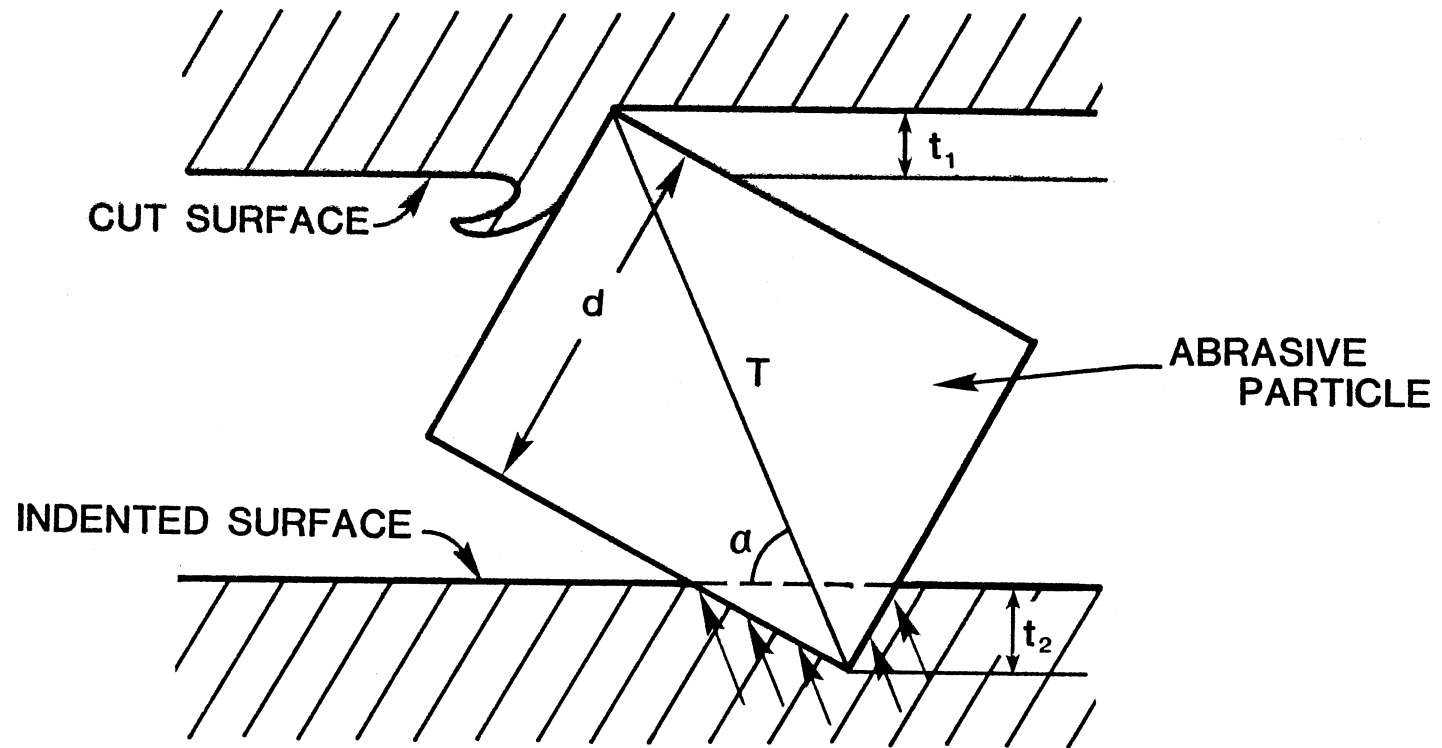


Fig. 16. Illustration of Three-Body Abrasion Mechanism

angle. Theoretically, no wear is generated at this angle. Abrasive particles of the size smaller than the clearance can generate abrasive wear because of rough surfaces; however, smaller size particles generate less wear. When the size of abrasive particles decreases there is a lower size limit where abrasive wear no longer occurs. The lower limit of the particle size for abrasive wear depends on the clearance size and the surface roughness. For the upper size limit, the same concept is applied.

To develop an abrasive wear model, the most critical particle size is the particle whose shorter length is the same as the clearance. When an angle of the particle relative to the surface becomes larger than 38.7 deg., cutting and indentation start. The rake angle of the particle cutting face becomes slightly negative when the particle angle gets larger; however, orthogonal cutting is always assumed.

The cutting force required is calculated by Eq. (16). The angle of the indenting wedge is always 45 deg by definition of the particle shape. The indenting pressure is calculated by Eq. (19).

Cutting and indentation first occur simultaneously and reach an equilibrium state where the cutting force and the indenting force are the same. At the equilibrium state, indentation stops, the indented surface supports the particle, and only cutting continues until the equilibrium state breaks due to some disturbances such as a sudden change of the surface geometry, vibration, or discontinuity of the sliding surface.

In the equilibrium state in Fig. 16, the cutting force and the indenting force are balanced along the diagonal. Hence, the force balance at the equilibrium state is expressed by:

$$F_c \sec \alpha = p t_2 d [\csc(\alpha - 38.7^\circ) \sin 38.7^\circ + \sec(\alpha - 38.7^\circ) \cos 38.7^\circ] \quad (20)$$

where

α = particle angle relative to sliding surface

t_2 = indentation depth

Since the clearance was assumed to be the same as the shorter length of the particle, the sum of cutting depth and indentation depth is:

$$t_1 + t_2 = T \sin \alpha - d \quad (21)$$

where

T = diagonal of a particle.

From the geometry of the particle, the diagonal T is equivalent to $1.6d$, and therefore,

$$t_2 = d (1.6 \sin \alpha - 1) - t_1 \quad (22)$$

Substituting Eqs. (16) and (22) into Eq. (20) yields an equation that expresses the cutting depth t_1 as a function of the coefficient of friction; however, the parameters ψ and λ are given only in Table I for several friction coefficients.

Using the third order polynomial approximation technique (the special Chebyshev polynomial for discrete intervals is used), the indenting pressure p may be expressed as a function of the coefficient of friction as:

$$p = [3.154 + 4.051\mu - 1.457\mu^2 - 12\mu^3] k \quad (23)$$

In the sliding mechanism, the shear yield strength of the surface that is cut by the abrasive particle may be different from that of the

indented surface. Hence, the shear yield strength of the cut surface is designated k_1 and that of the indented surface is k_2 . Let

$$f(\mu) = 2 \cot(45^\circ - \frac{\arctan \mu}{2}) \quad (24)$$

and

$$g(\mu) = 3.154 + 4.051\mu - 1.457\mu^2 - 12\mu^3 \quad (25)$$

Using the above, the cutting stress and the indenting stress on the abrasive particle are expressed by:

$$\sigma = k_1 f(\mu) \quad (26)$$

and

$$p = k_2 g(\mu) \quad (27)$$

From Eqs. (16), (18), (20), (22), (26) and (27), the equation to derive the cutting depth t_1 for a given coefficient of friction is:

$$k_1 t_1 f(\mu) \sec \alpha = k_2 g(\mu) [d (1.6 \sin \alpha - 1) - t_1] [\csc(\alpha - 38.7^\circ) \sin 38.7^\circ + \sec(\alpha - 38.7^\circ) \cos 38.7^\circ] \quad (28)$$

CHAPTER IV

VERIFICATION OF SURFACE CONTACT WEAR MODEL

Experimental Considerations

The methodology to experimentally verify the developed theory of surface contact wear is discussed in this section. The surface contact wear equation, Eq. (15), can be rewritten as:

$$\frac{6V_4}{KW} = \left(\sqrt{1 + 3\mu^2} \right) \frac{\tan \theta_s}{T_y} \quad (29)$$

Eq. (29) describes the relationship among the applied load, the friction coefficient, material properties, and surface contact wear as shown in Fig. 17.

If the same material with the same surface finish is used for a series of tests, a value on the X-axis which is a function of material properties is fixed. In this condition, the figure indicates that a change of the applied load does not alter a value on the Y-axis as long as the friction coefficient remains the same. The wear volume is supposed to change in proportion to the applied load to maintain the same value on the Y-axis.

The data points moves along the Y-axis only when the friction coefficient changes. Since the material properties are the same in this case, the change of the friction coefficient can be only achieved by

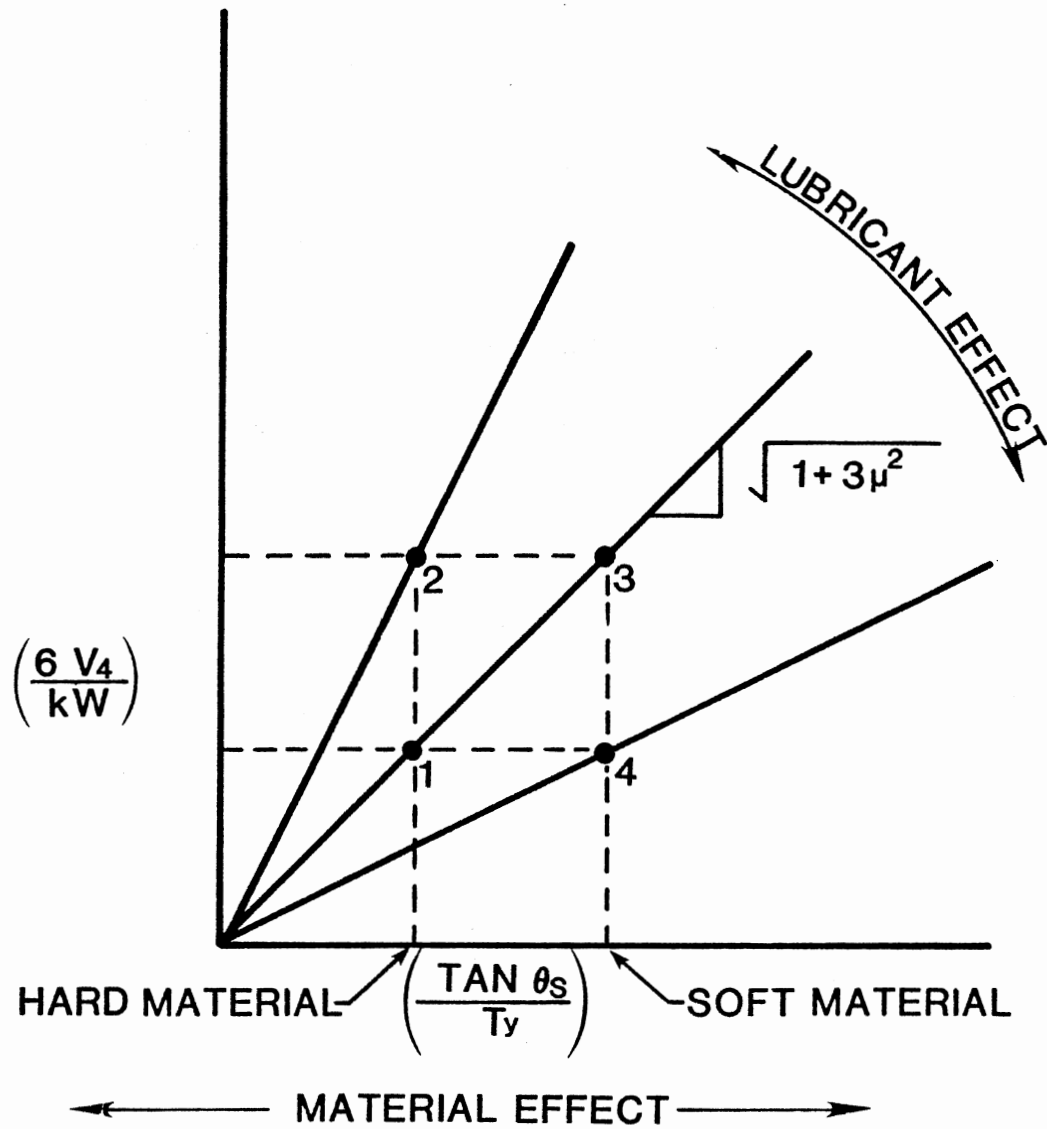


Fig. 17. Illustration of Surface Contact Wear Theory

applying different lubricating conditions. When the friction coefficient is constant and the material is changed, the data point moves along a specific slope devoted to a given friction coefficient.

With the foregoing knowledge, the theory can be verified by a simple experimental test. Two kinds of materials, one soft and the other hard, with the same surface finish are considered. Thus, the asperity angle is the same for both materials, but the yield strengths are different. A value of $(\tan \theta_s / T_y)$ for the soft material is larger than that for the hard material, Fig. 17; therefore, two values are assigned on the X-axis.

Suppose that data point 1 in Fig. 17 is given for the hard material and a certain lubricant is applied to the contacting surfaces. Keeping the material and the applied load constant, the data point moves from 1 to 2 when the lubricating condition is worse. The actual change observed in this case is an increase of the wear volume such that the value of $(6V_4/KW)$ increases from point 1 to point 2. From point 2, the data can be moved to point 3 by changing the material to a soft one and by improving lubrication. From point 3, the data can be shifted down to point 4 by further improving the lubricating condition with the same soft material.

By examining how close the actual data points follow the theoretical points 1, 2, 3, and 4 with changes in the appropriate parameters, the validity of the theory can be proven.

Development of Experimental Facility

There are many wear test methods available, as summarized in Table II. The Falex test method, Fig. 18, was selected to conduct the test

TABLE II
AVAILABLE WEAR TEST METHODS

| PROCEDURE | STANDARD NO. | EQUIPMENT |
|---|--|-----------------------------------|
| MEASURING WEAR PROPERTIES OF FLUID LUBRICANTS (falex method) | ANSI/ASTM D 2670-67 (reapproved 1977) | FALEX |
| MEASUREMENT OF EXTREME PRESSURE PROPERTIES OF FLUID LUBRICANTS (falex method) | ANSI/ASTM D 3233-73 (reapproved 1978) | FALEX |
| WEAR PREVENTIVE CHARACTERISTICS OF LUBRICATING GREASE (four-ball method) | ANSI/ASTM D 2266-67 (reapproved 1977) | FOUR-BALL |
| MEASUREMENT OF EXTREME PRESSURE PROPERTIES OF LUBRICATING FLUIDS (four-ball method) | ANSI/ASTM D 2783-71 (reapproved 1976) | FOUR-BALL |
| MEASUREMENT OF EXTREME PRESSURE PROPERTIES OF LUBRICATING FLUIDS (Timken method) | ANSI/ASTM D 2782-77 | TIMKEN TESTER |
| CALIBRATION AND OPERATION OF THE ALPHA MODEL LFW-1 FRICTION AND WEAR TESTING MACHINE | ANSI/ASTM D 2714-68 (reapproved 1978) | ALPHA LFW-1 |
| WEAR PREVENTIVE PROPERTIES OF LUBRICATING GREASES USING THE (Falex) RING AND BLOCK TEST MACHINE IN OSCILLATING MOTION | ANSI/ASTM D 3704-78 | FALEX RING AND BLOCK TEST MACHINE |
| PRELIMINARY EXAMINATION OF HYDRAULIC FLUIDS (wear test) | ANSI/ASTM D 2271-66 (reapproved 1976) | BASIC HYDRAULIC TEST SYSTEM |
| VANE PUMP TESTING OF PETROLEUM HYDRAULIC FLUIDS | ANSI/ASTM D 2882-74 | VANE PUMP |

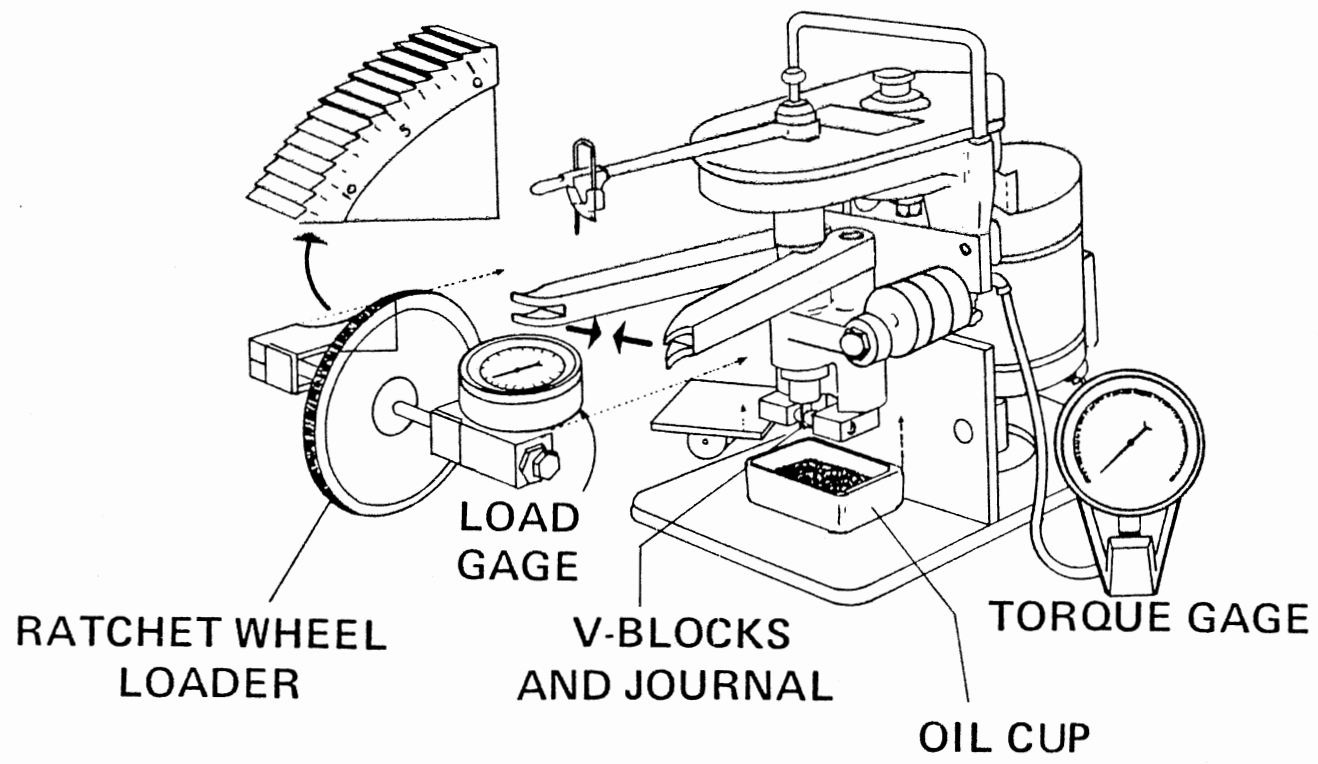


Fig. 18. Falax Wear Tester

for verifying the surface contact wear theory because the wear mechanism of the Falex tester, Fig. 19, maintains boundary lubrication at a journal rotating speed of 290 rpm. The Falex method measures wear by means of the gear teeth differential between the initial and final ratchet wheel readings.

It was found that the Falex test, standardized by ASTM procedures, needs major improvements for two reasons:

1. Since the Falex tester uses a small fluid container, the fluid temperature increases quickly as wear takes place. The increase of temperature is steep for severe wear. Thus, appropriate temperature control is unobtainable.
2. Wear debris generated from contact surfaces are accumulated in the small fluid container and its density increases significantly as the test proceeds. The effect of the generated wear debris on the contact surfaces soon reaches much more severe levels than would occur under actual field situations.

Because of these two faulty test conditions, seizure of the test specimens takes place frequently.

Major improvements made on the Falex tester were to:

1. Provide a fluid circulation system.
2. Provide a temperature controller to maintain constant temperature.
3. Install a filter circuit to control contamination level.

The improved Falex tester with the attached fluid circulation system is designated as the "Gamma Falex system." The Gamma Falex system is illustrated in Fig. 20.

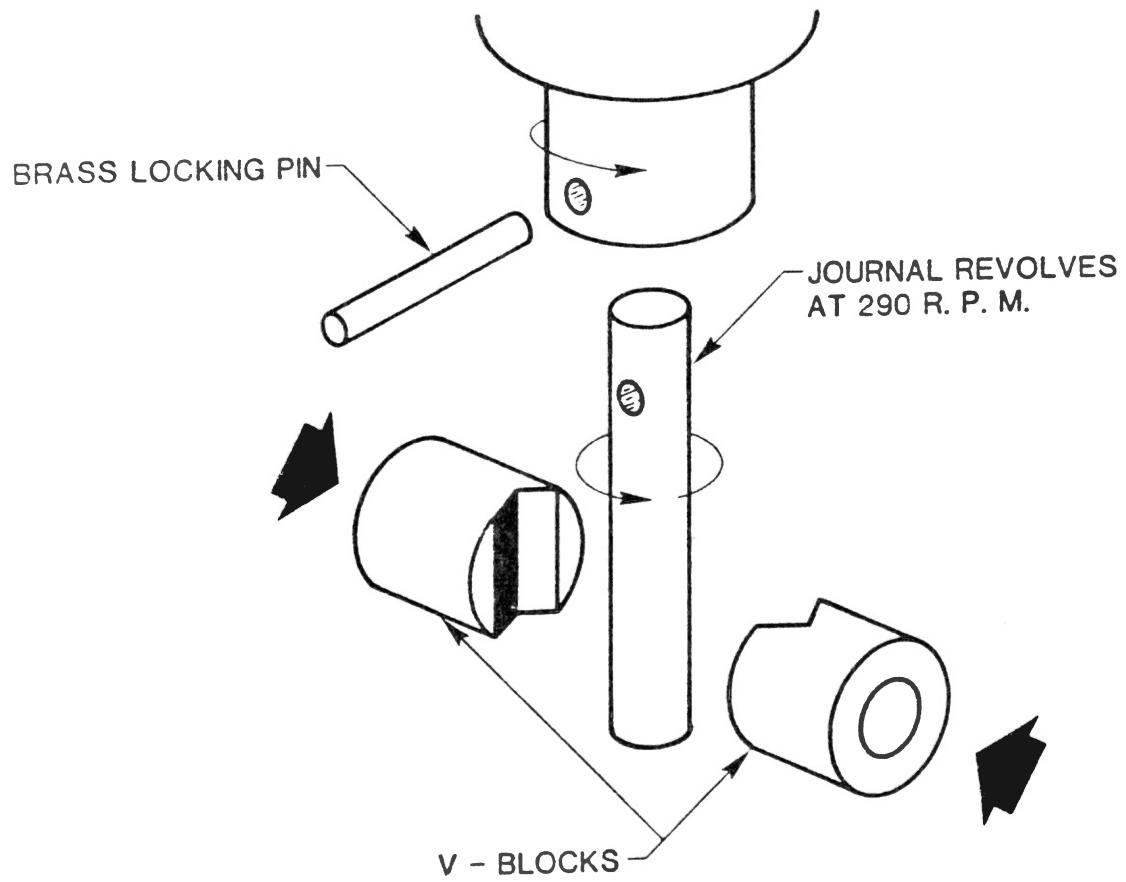


Fig. 19. Test Specimens of Falex Wear Tester

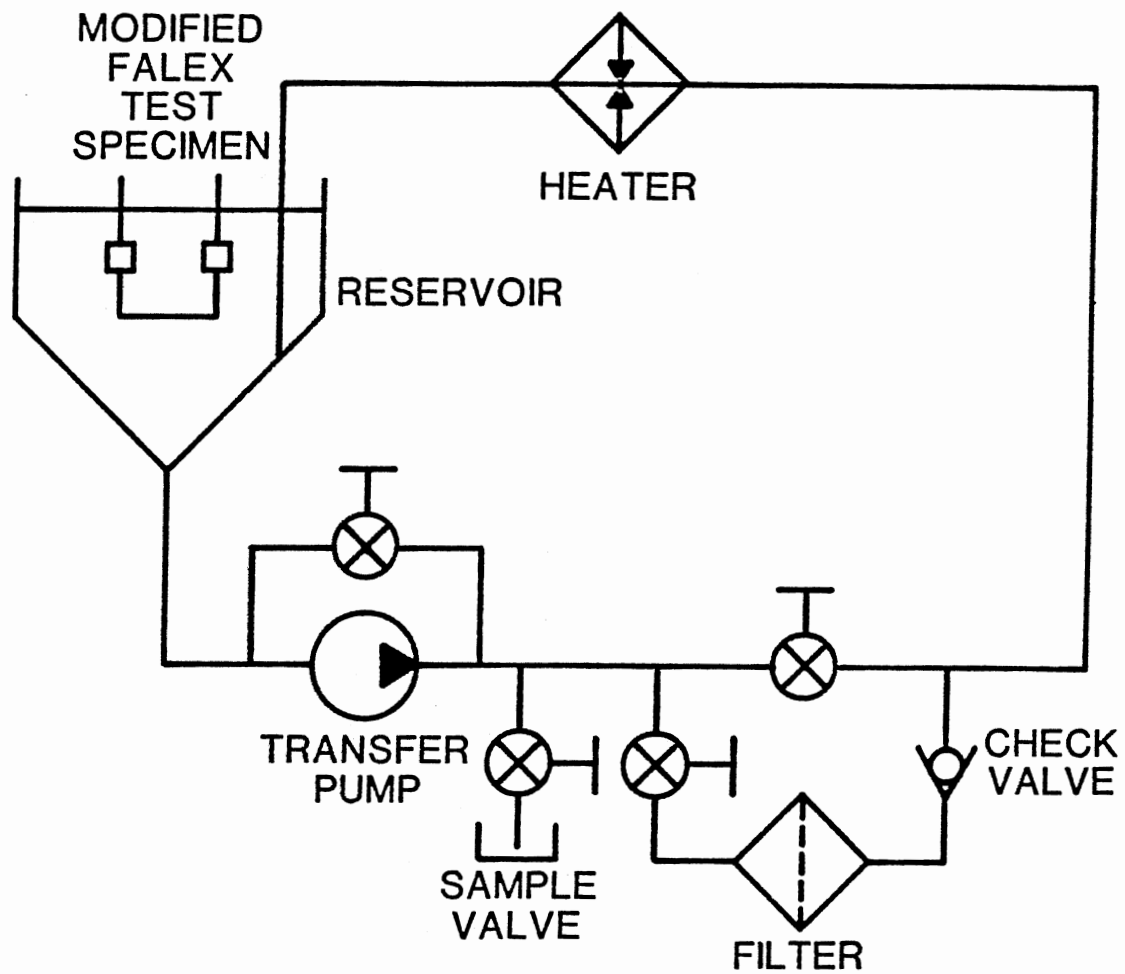


Fig. 20. Schematic of the Gamma Falex System

The standard material of the V-block used on the Gamma Falex system is AISI C-1137 steel, Rockwell hardness number 20 to 24 on the C-scale with a surface finish of 5 to 10 microinches (1.3×10^{-7} to 2.5×10^{-7} m) rms. The standard journal is AISI 3135 steel, Rockwell hardness number 87 to 91 on the B-scale. The journal has the same surface finish as the V-block. Fig. 21 shows a comparison of the hardness of the journal and V-block, which reveals that the standard V-block is harder than the standard journal.

Geometries of the journal and V-blocks during the wear test are illustrated in Fig. 22. Experimental tests revealed that wear on the journal is negligibly small; whereas, the wear scar on the V-block increases as the test proceeds. The unit load on the wear surface decreases as the contact surface area increases when a constant load is applied to the V-blocks.

A typical result of the Gamma Falex test conducted with MIL-L-2104 at a 100-lb. load is shown in Fig. 23. Notice in Fig. 23 that the wear data from the Gamma Falex system have straight-line characteristics.

Repeatability of Experimental Facility

Fifteen identical tests were conducted with mineral base fluid MIL-H-5606. The data are shown in Table III. Since the wear data from the Gamma Falex system have straight-line characteristics, a best-fit straight line was calculated by the least squares method for each set of the test data. The incubation period, the slope, and the correlation coefficient of a best-fit straight line were calculated for each set of the test data and also tabulated in Table III. A slope of the best-fit straight line of the data is designated as the "Gamma slope" which

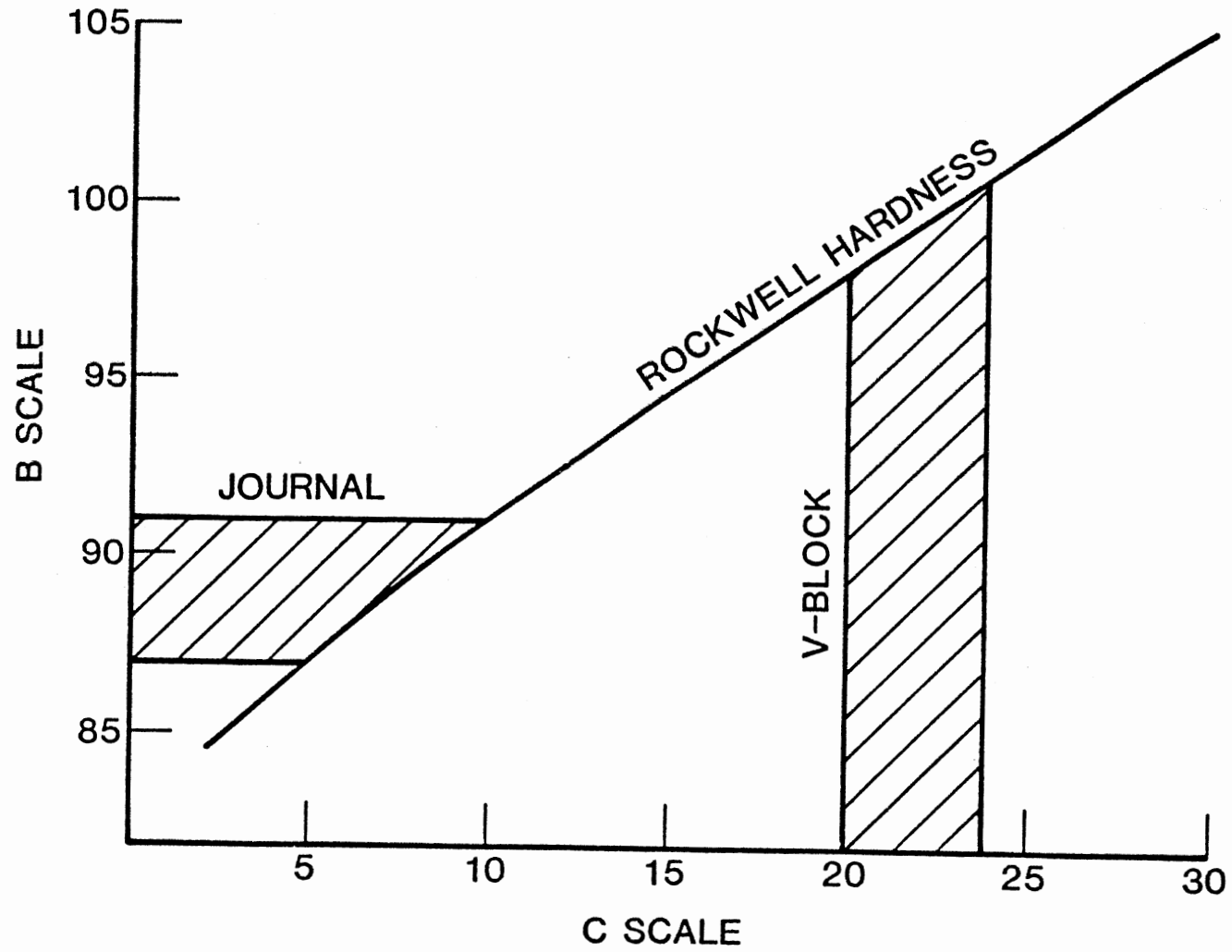


Fig. 21. Hardness of Journal and V-Block

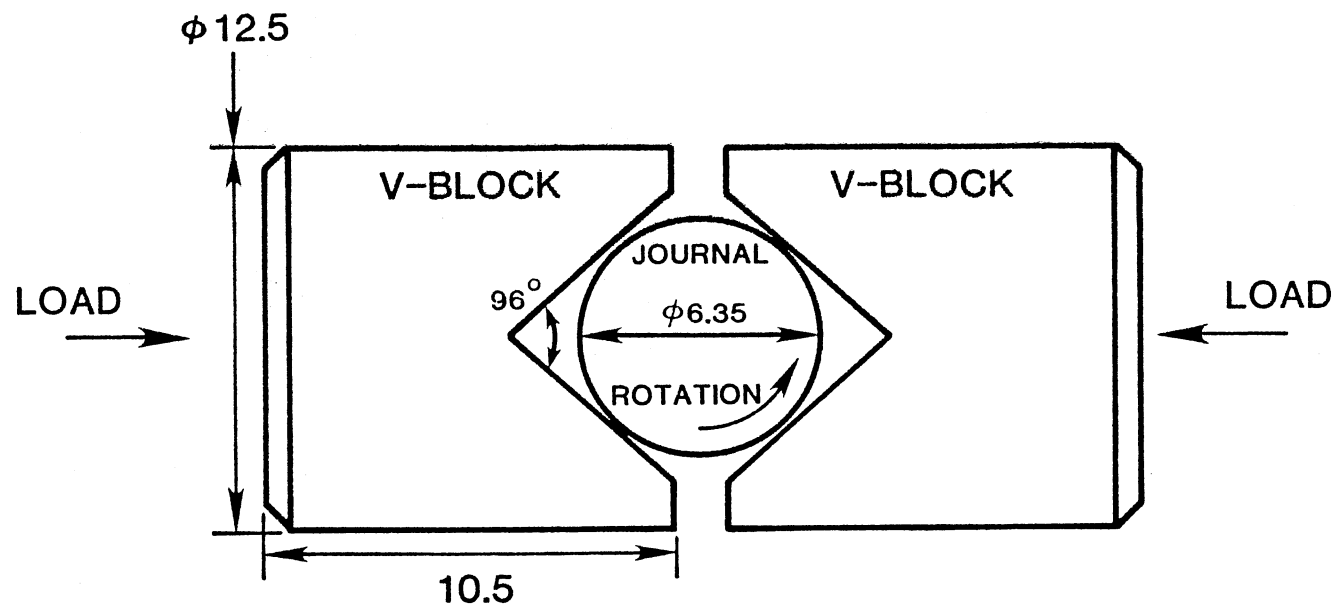


Fig. 22. Geometry of Journal and V-Block (mm)

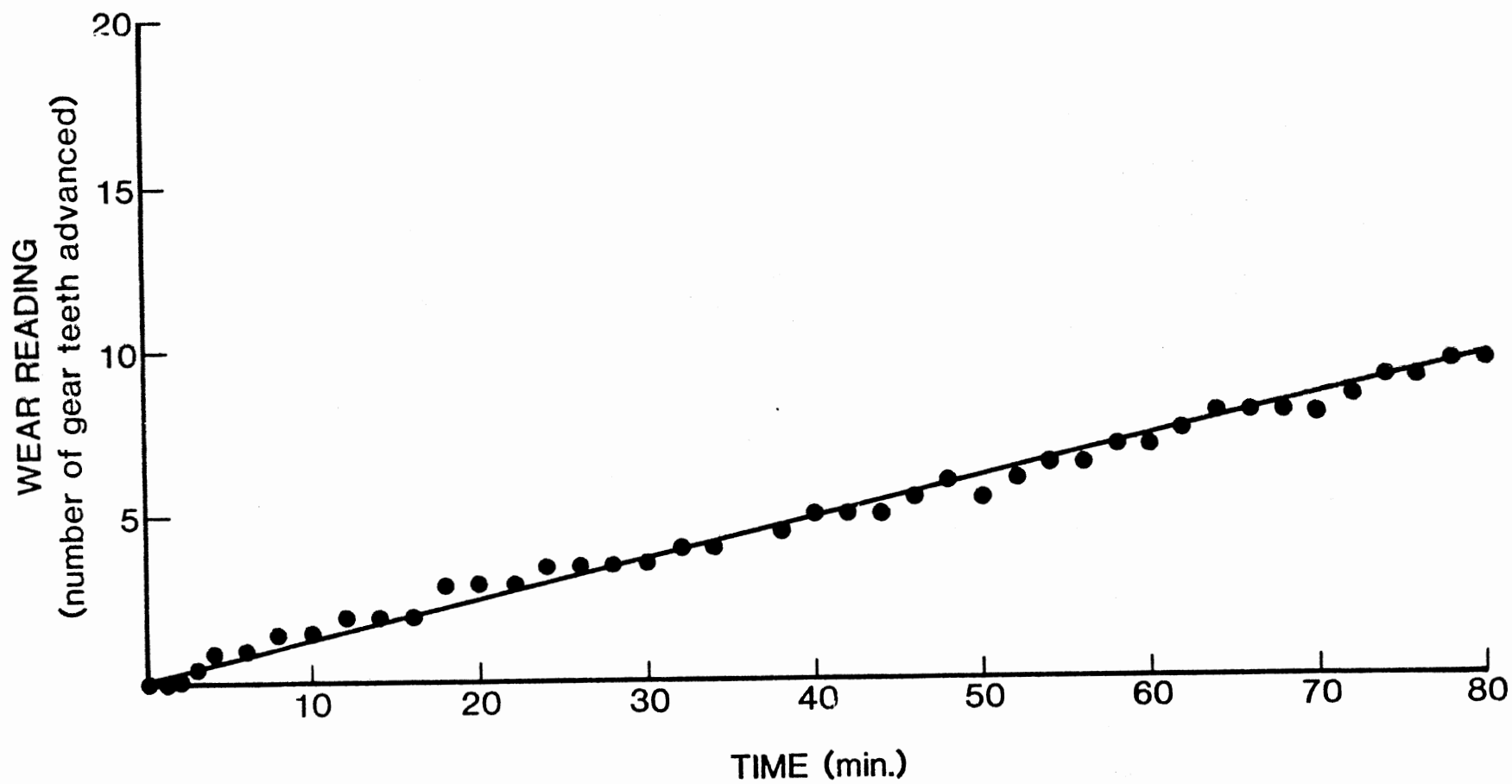


Fig. 23. A Typical Result of Gamma Falex Test

TABLE III

GAMMA FALEX REPEATABILITY TEST DATA WITH MIL-H-5606

| TEST NO. | WEAR READING | | | | | | INCUBATION PERIOD (min.) | GAMMA SLOPE | CORRELATION COEFFICIENT |
|----------|--------------|---------|---------|---------|---------|---------|-----------------------------|----------------|----------------------------|
| | 5 min. | 10 min. | 15 min. | 20 min. | 25 min. | 30 min. | | | |
| 80-1 | 0 | 1 | 4 | 7 | 10 | 13 | 6.76 | 0.543 | 0.993 |
| 80-2 | 1 | 4 | 7 | 10 | 14 | 18 | 4.15 | 0.674 | 0.997 |
| 80-3 | 0 | 0 | 2 | 3 | 6 | 9 | 8.39 | 0.366 | 0.961 |
| 80-4 | 0 | 0 | 3 | 6 | 9 | 12 | 7.78 | 0.514 | 0.982 |
| 80-5 | 0 | 0 | 3 | 6 | 9 | 12 | 7.78 | 0.514 | 0.982 |
| 80-6 | 0 | 1 | 4 | 5 | 6 | 6 | 3.55 | 0.263 | 0.952 |
| 80-7 | 0 | 2 | 5 | 7 | 8 | 9 | 3.58 | 0.371 | 0.980 |
| 80-8 | 0 | 0 | 1 | 3 | 4 | 6 | 8.25 | 0.251 | 0.971 |
| 80-9 | 0 | 1 | 2 | 4 | 5 | 6 | 5.58 | 0.251 | 0.994 |
| 80-10 | 0 | 0 | 1 | 3 | 5 | 6 | 8.18 | 0.269 | 0.971 |
| 80-11 | 0 | 0 | 2 | 3 | 4 | 6 | 7.32 | 0.246 | 0.980 |
| 80-12 | 0 | 1 | 3 | 4 | 6 | 7 | 5.50 | 0.291 | 0.995 |
| 80-13 | 0 | 1 | 2 | 4 | 5 | 6 | 5.58 | 0.251 | 0.994 |
| 80-14 | 0 | 1 | 2 | 3 | 4 | 5 | 5.00 | 0.200 | 1.000 |
| 80-15 | 0 | 1 | 3 | 4 | 5 | 7 | 5.36 | 0.274 | 0.994 |

which indicates a wear rate per unit time. The straight line characteristics of the Gamma Falex data are assured by the fact that all the correlation coefficient values are close to one (1.000).

A suitable statistical distribution for the variation of the incubation period was studied. The data was arranged for a statistical analysis as shown in Table IV. For such a data set from the wear test, the normal distribution is the most reasonable model to try first. The arranged data in Table IV were plotted on the normal probability paper, Fig. 24. Observe in Fig. 24 that the straight line which fits the data points indicates the data fit well to the normal distribution. In other words, the incubation period of MIL-H-5606 distributes normally, the mean of the incubation period is 6.2 minutes, and the standard deviation is 1.5 minutes, both of which can be obtained from Fig. 24.

Data of the Gamma slope were also arranged in the same manner as in Table IV and plotted on normal probability paper, Fig. 25. It is obvious in Fig. 25 that some of the data points do not fit a straight line; however, a majority of the data points closely fit a straight line. To investigate the discrepancy observed in Fig. 25, the values of the Gamma slope are plotted in chronological order in Fig. 26. Fig. 26 indicates that the Gamma slope decreased as the test proceeded and reached a steady state during the sixth test. Reasons suspected for this are:

1. The test engineer was not familiar with the test equipment and the test procedure. He gradually became familiar with them as the test proceeded and finally reached the point where he could obtain consistent data.
2. Contaminants remained in the system in the initial period

TABLE IV
 INCUBATION PERIODS OF MIL-H-5606
 FOR STATISTICAL ANALYSIS

| X_o | i | X_o ORDERED | $100i/(n + 1)$ PLOTING PERCENTAGE |
|-------|----|---------------|---|
| 6.76 | 1 | 3.55 | 6.3 |
| 4.15 | 2 | 3.58 | 12.5 |
| 8.39 | 3 | 4.15 | 18.8 |
| 7.78 | 4 | 5.00 | 25 |
| 7.78 | 5 | 5.36 | 31.3 |
| 3.55 | 6 | 5.50 | 37.5 |
| 3.58 | 7 | 5.58 | 43.8 |
| 8.25 | 8 | 5.58 | 50 |
| 5.58 | 9 | 6.76 | 56.3 |
| 8.18 | 10 | 7.32 | 62.5 |
| 7.32 | 11 | 7.78 | 68.8 |
| 5.50 | 12 | 7.78 | 75 |
| 5.58 | 13 | 8.18 | 81.3 |
| 5.00 | 14 | 8.25 | 87.5 |
| 5.36 | 15 | 8.39 | 93.8 |

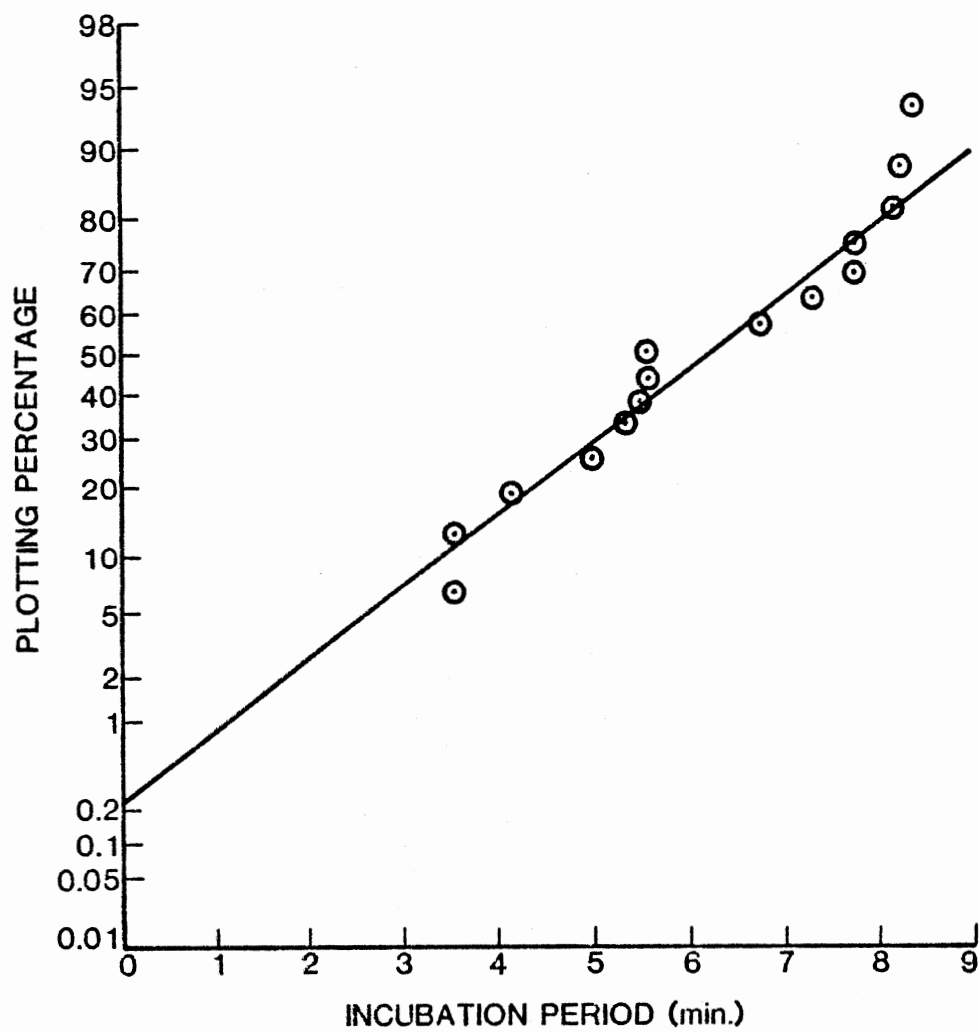


Fig. 24. MIL-H-5606 Gamma Falex Test Data, Incubation Period Distribution

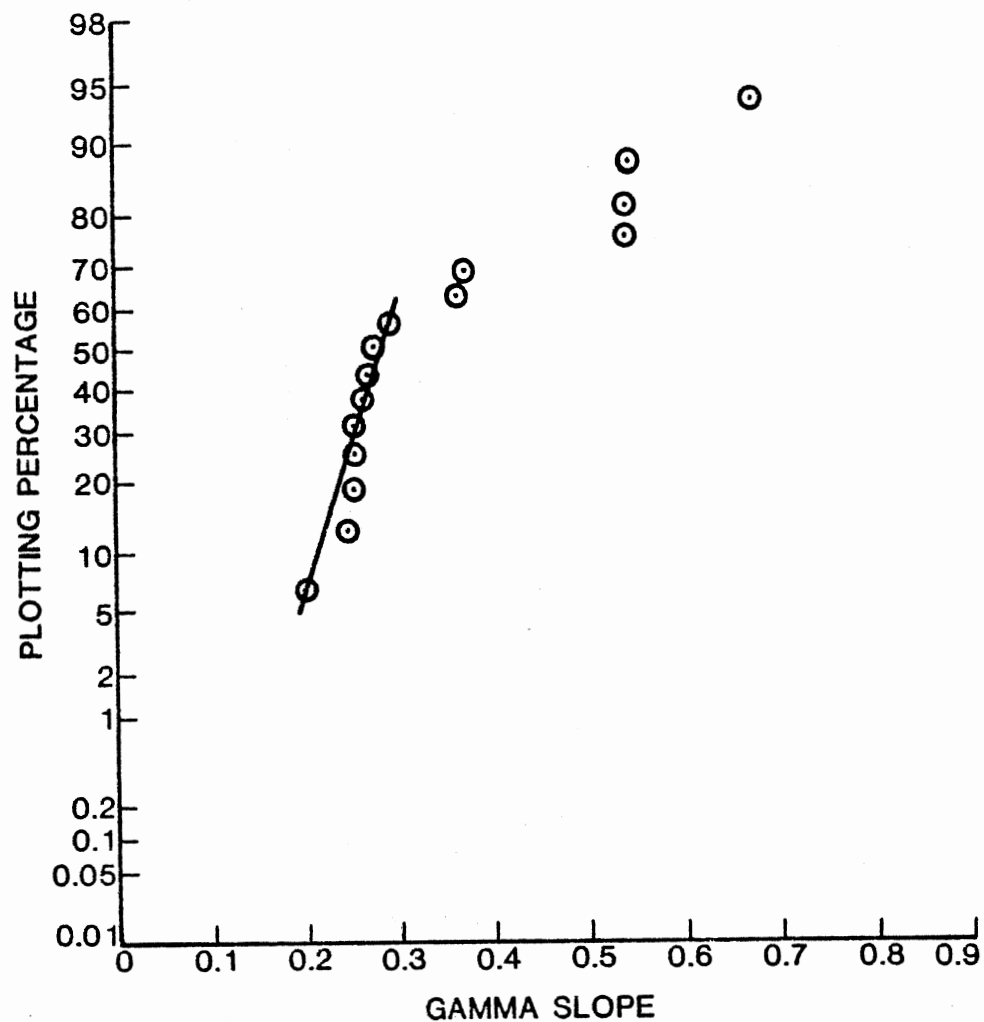


Fig. 25. MIL-H-5605 Gamma Falex Test Data, Gamma Slope Distribution

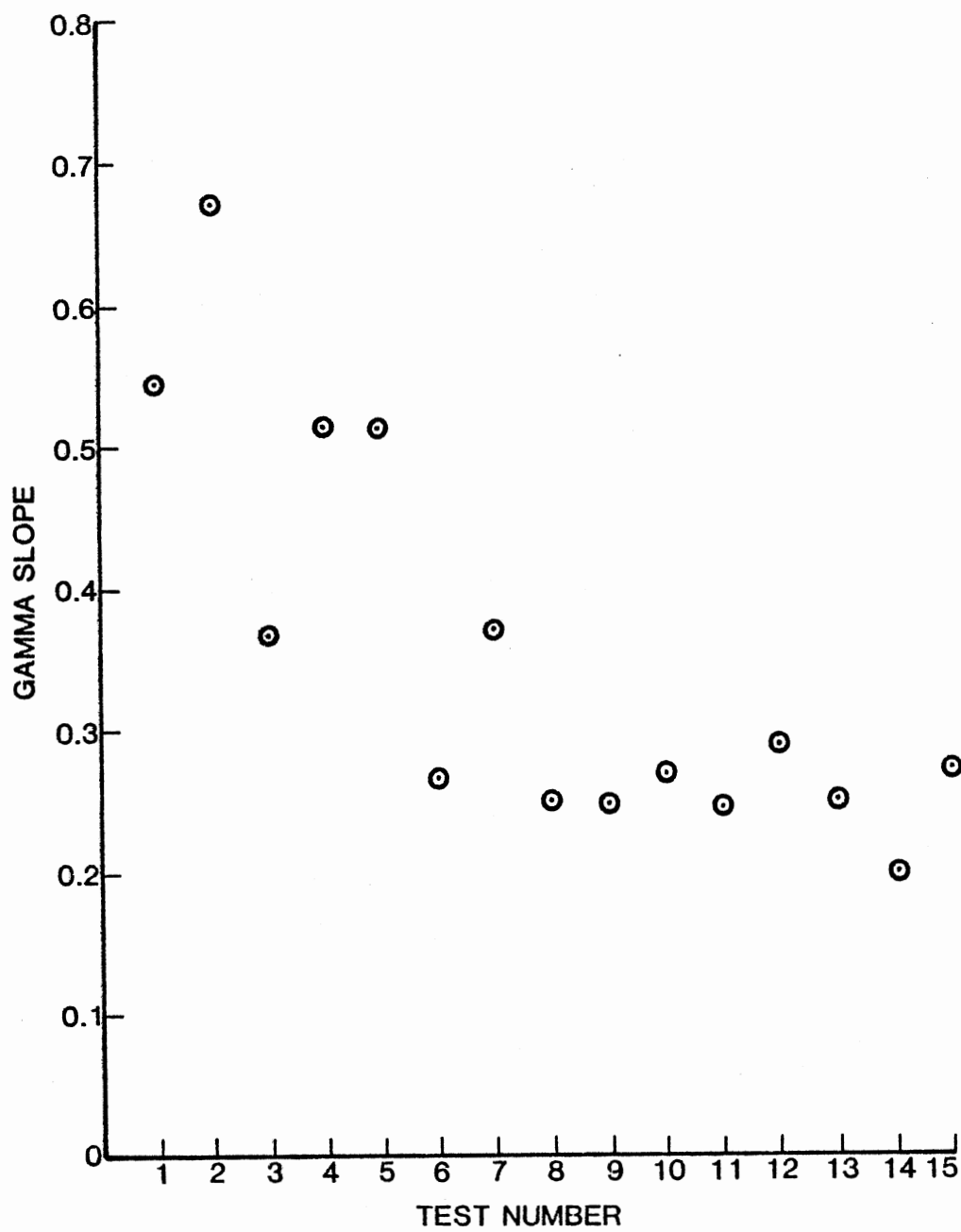


Fig. 26. MIL-H-5606 Gamma Slopes Plotted in Chronological Order

despite cleaning and filtration; however, the residue of contaminants was gradually washed away as the test proceeded and reached steady state or was finally eliminated completely.

A second set of repeatability tests was conducted with mineral base fluid MIL-L-2104. The test data were interpreted for the incubation period, the Gamma slope, and the correlation coefficient, all of which are tabulated in Table V. Values of the correlation coefficient in Table V assure the straight-line characteristics of the data.

Values for the incubation period of MIL-L-2104 were plotted on normal probability paper, Fig. 27, which proves that it distributes normally. The mean value is 2.5 minutes, and the standard deviation is 2.3 minutes.

Values of the Gamma slope were also plotted on normal probability paper, Fig. 28, which shows the same discrepancy as observed with MIL-H-5606. All the data points fit a straight line except one data point as shows in Fig. 28. The values of the Gamma slope are now plotted in chronological order in Fig. 29 to discuss the discrepancy. Fig. 29 shows consistent data points except for a point from seventh test. Skills of the test engineer and the contamination control of the system were considered satisfactory in this case.

Two more sets of repeatability tests were conducted with mineral base fluid A and mineral base fluid B to further study the distribution of the Gamma slope. Fig. 30 and Fig. 31 are normal probability plottings of the Gamma slope for mineral base fluid A and mineral base fluid B, respectively. Mineral base fluid A, Fig. 30 shows the same discrepancy as seen in the foregoing analyses. Only two data points are

TABLE V

GAMMA FALEX REPEATABILITY TEST DATA WITH MIL-L-2104

| TEST NO. | WEAR READING | | | | | | INCUBATION PERIOD (min.) | GAMMA SLOPE | CORRELATION COEFFICIENT |
|----------|--------------|---------|---------|---------|---------|---------|--------------------------|-------------|-------------------------|
| | 5 min. | 10 min. | 15 min. | 20 min. | 25 min. | 30 min. | | | |
| 80-25 | 0 | 1 | 1 | 2 | 2 | 3 | 3.67 | 0.109 | 0.968 |
| 80-26 | 0 | 0.5 | 1.5 | 2 | 2.5 | 3.5 | 5.35 | 0.137 | 0.994 |
| 80-27 | 0 | 1 | 1.5 | 2 | 2.5 | 3 | 2.92 | 0.114 | 0.990 |
| 80-28 | 0.5 | 1 | 1.5 | 2 | 2.5 | 3 | 0 | 0.1 | 1.000 |
| 80-31 | 0.5 | 1 | 1.5 | 2 | 2.5 | 3 | 0 | 0.1 | 1.000 |
| 80-40 | 1 | 1.5 | 2 | 2.5 | 3 | 3.5 | 0 | 0.1 | 1.000 |
| 80-41 | 0.5 | 1.5 | 3 | 3.5 | 5.5 | 6.5 | 3.43 | 0.243 | 0.992 |
| 80-42 | 0.5 | 1 | 1.5 | 2 | 3 | 3.5 | 1.89 | 0.123 | 0.992 |
| 80-50 | 0.5 | 1 | 1.5 | 2 | 2.5 | 3 | 0 | 0.1 | 1.000 |
| 80-59 | 0.5 | 1 | 1.5 | 2 | 2.5 | 3 | 0 | 0.1 | 1.000 |
| 80-56 | 0 | 0 | 1 | 2.5 | 2.5 | 2.5 | 5.96 | 0.123 | 0.926 |
| 80-57 | 0 | 0.5 | 0.5 | 1 | 2.5 | 2.5 | 6.72 | 0.109 | 0.940 |
| 80-58 | 0 | 0 | 0 | 1.5 | 1.5 | 2.0 | 8.39 | 0.0914 | 0.919 |

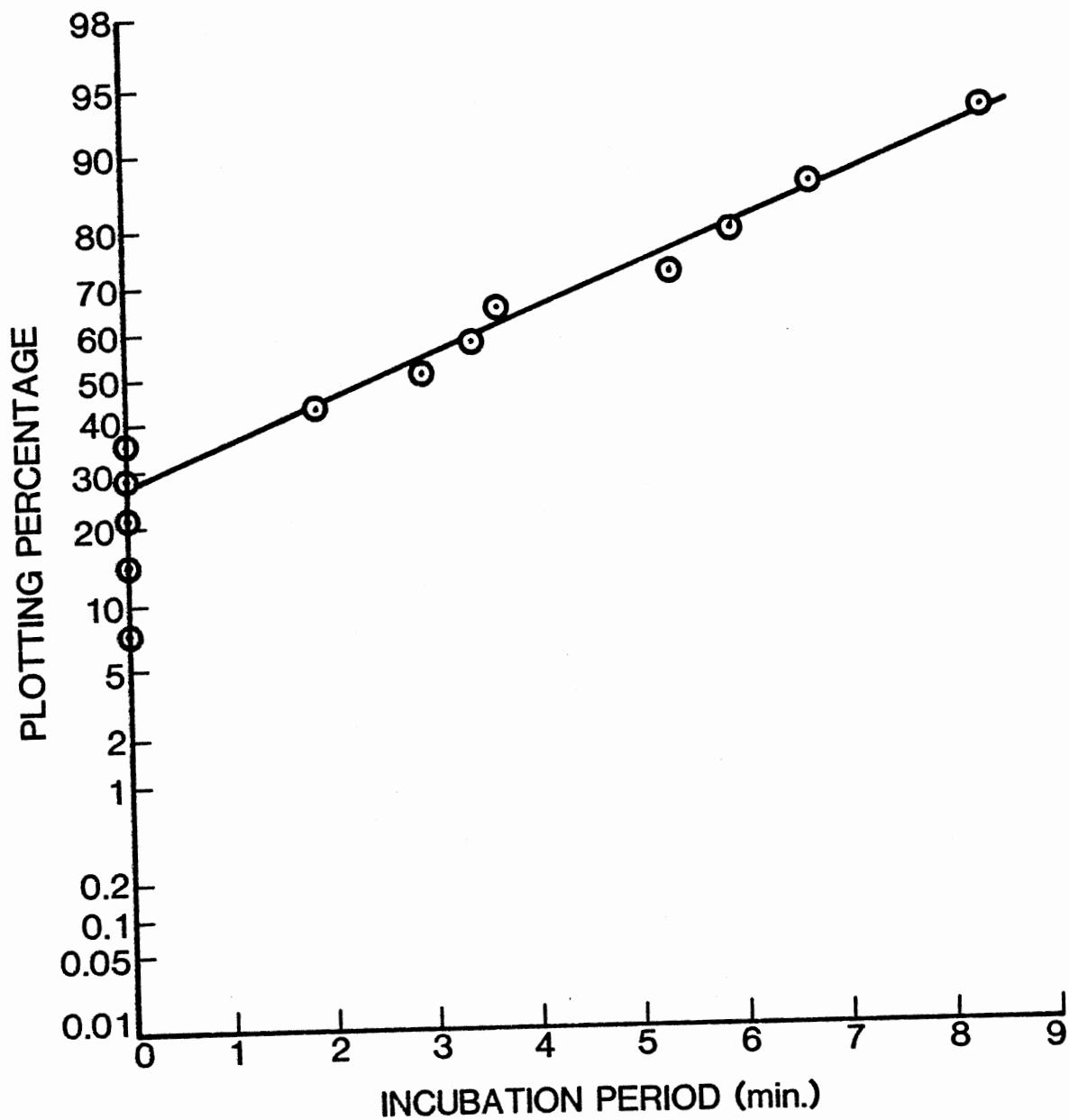


Fig. 27. MIL-L-2104 Gamma Falex Test Data, Incubation Period Distribution

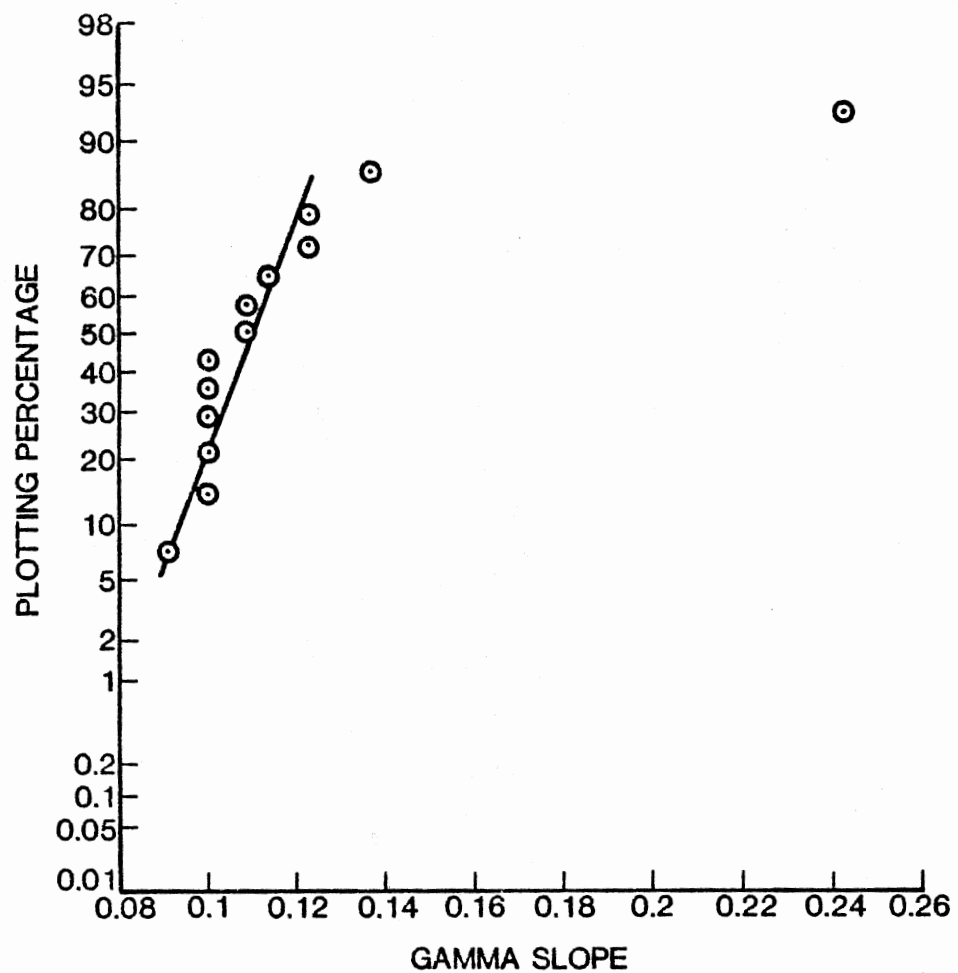


Fig. 28. MIL-L-2104 Gamma Falex Test Data, Gamma Slope Distribution

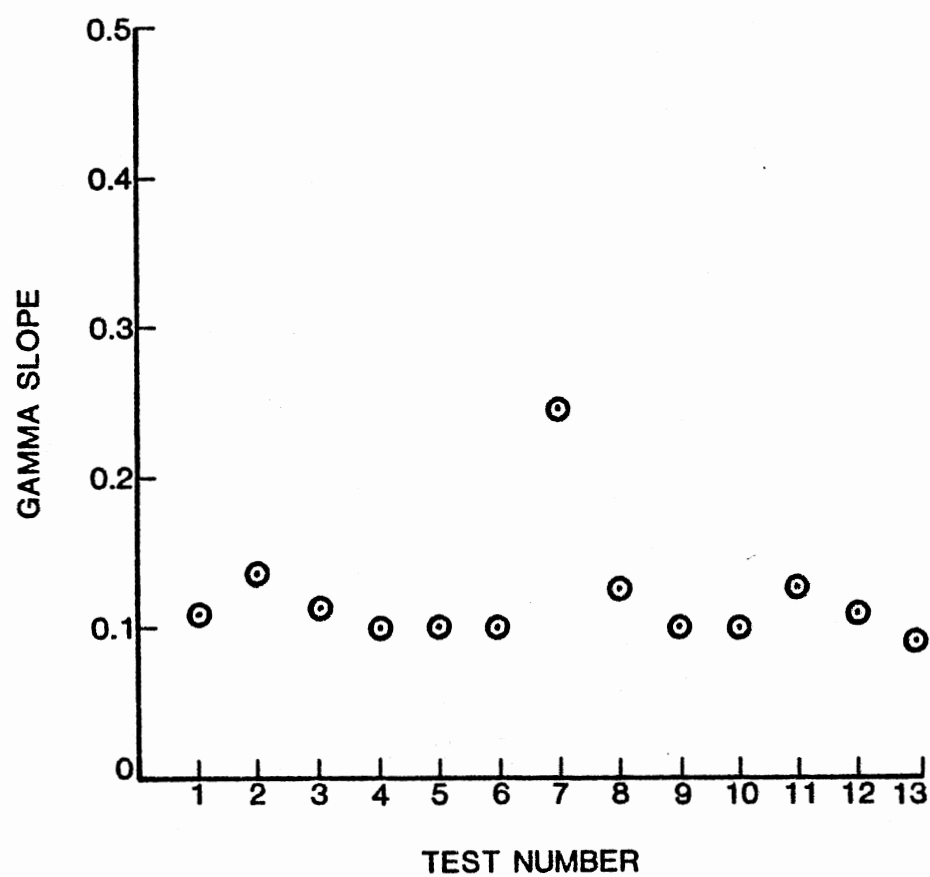


Fig. 29. MIL-L-2104 Gamma Slopes Plotted in Chronological Order

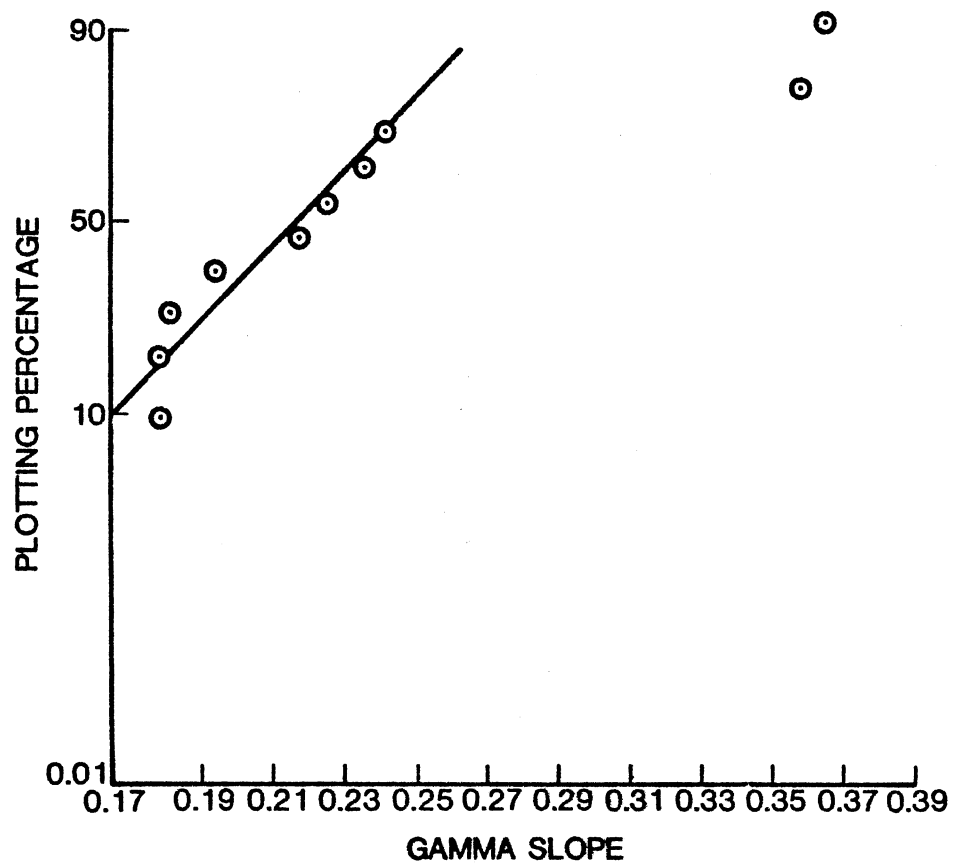


Fig. 30. Mineral Oil A Gamma Slope Distribution

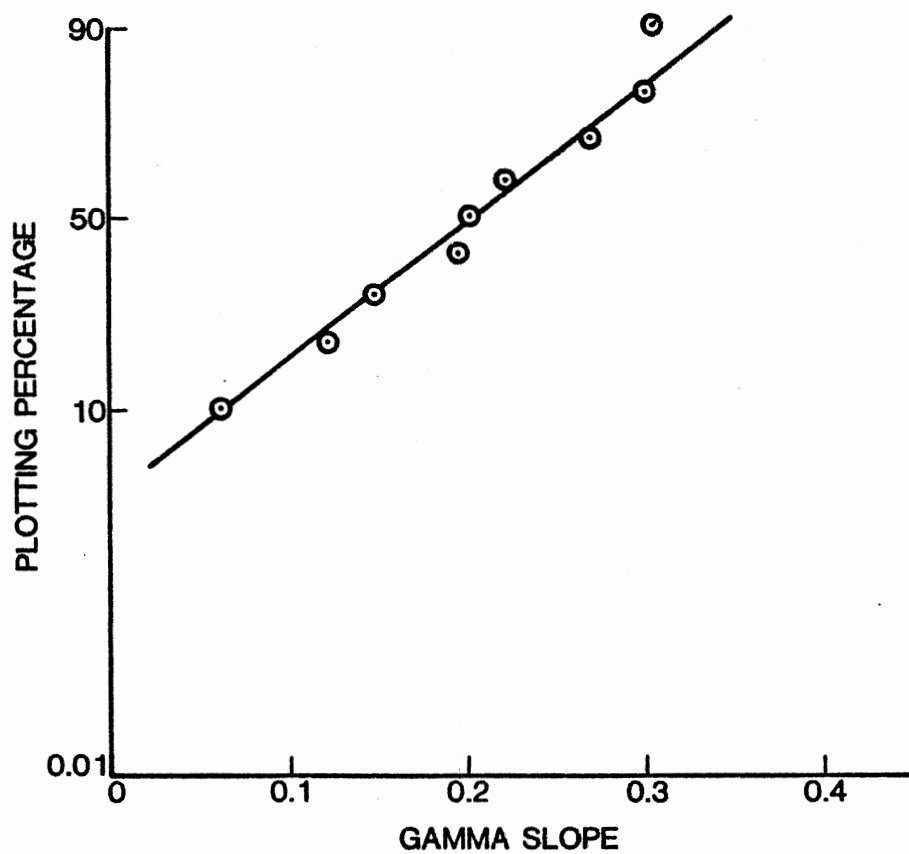


Fig. 31. Mineral Oil B Gamma Slope Distribution

off from a best-fit straight line, and the rest of the data are closely fit by the straight line, Fig. 30.

Mineral base fluid B, Fig. 31, shows a good straight-line fit of all the data points, which means that all the data fall within the normal distribution.

It was verified in the foregoing analysis that the incubation period of the Gamma Falex test has a normal distribution; whereas, the Gamma slope, which is a measure of the fluid lubricity, showed some inconsistency. Three data sets out of four showed discrepancies in the normal distribution analysis of the Gamma slope. In all three cases, the majority of the data points followed a normal distribution; however, a few points are outside the distribution.

Such a phenomenon may be observed sometimes in the measurement of machine tool vibration. The vibration usually stays within a certain range, and the variation within the range distributes normally. Occasionally, the vibration level suddenly changes its range and stays in a new range. While the vibration level stays in the new range, it also distributes normally. Later, the vibration level returns to the previous range and stays in that range with a normally distributed variation again. The sudden range change of the vibration distribution may be due to many parameters, such as operating and environmental conditions. This example illustrates a condition where two or more distinct distributions exist for one set of measurements.

For the Gamma slope data, one major distribution and one minor distribution are considered, which is illustrated in Fig. 32 for the Gamma slope of MIL-H-5606. The major distribution was formed from eleven test data; whereas, the minor distribution was formed from only four test

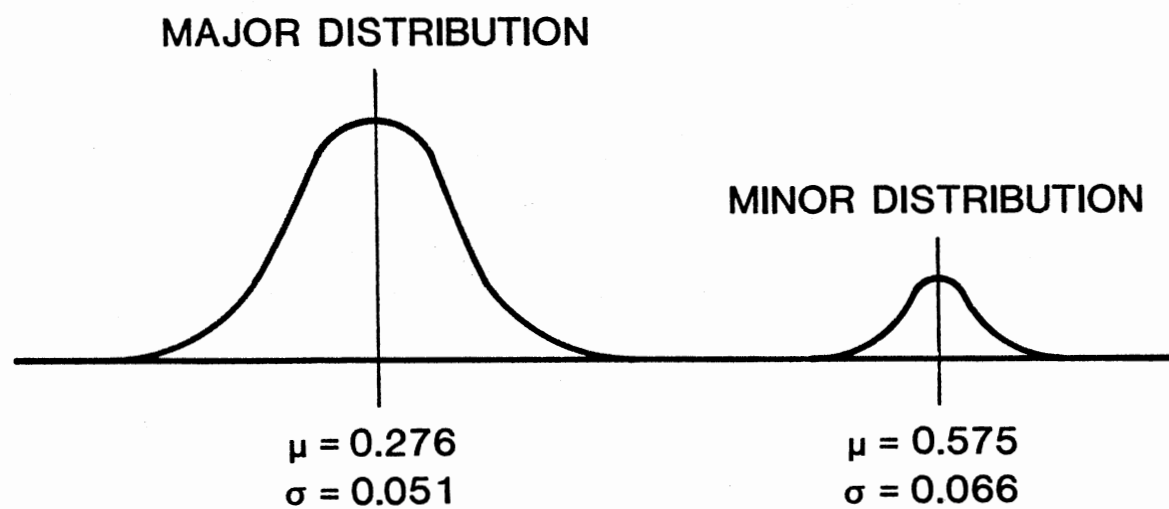


Fig. 32. Major and Minor Normal Distribution Considered for the Gamma Slope of MIL-H-5606

data. Accordingly, it is reasonable to consider that the major distribution represents the true Gamma slope of MIL-H-5606. In the same manner, the major distribution is considered to represent the true Gamma slope for MIL-L-2104 and mineral base fluid A. For mineral base fluid B, only the major distribution is known from the measurements.

The mean value and standard deviation of the major distribution were calculated for each test fluid and are illustrated with minor data points in Fig. 33. The white circle indicates a mean value of the major distribution, and bars extending up and down from the white circle indicate magnitudes of plus and minus one standard deviation, respectively. Figures beside the white circles show the number of test data from which a mean and standard deviation were calculated.

The number of data points forming the major distribution was sufficient to calculate a mean value and standard deviation of the normal distribution for each test fluid; however, the number of minor data points was insufficient to calculate any distribution parameters. Hence, all the minor data points are plotted in Fig. 33. Fig. 33 illustrates the accuracy and repeatability of the Gamma Falex test.

Fifteen tests were conducted with MIL-H-5606. Eleven test data among the fifteen fall within the normal distribution with a mean value of 0.276 and a standard deviation of 0.051. The remaining four are minor data points that do not follow the major normal distribution. Therefore, 27 percent of the test data, in this case, are outside the major distribution, and 73 percent of the data fall within the major distribution.

Thirteen tests were conducted for MIL-L-2104, and twelve test data

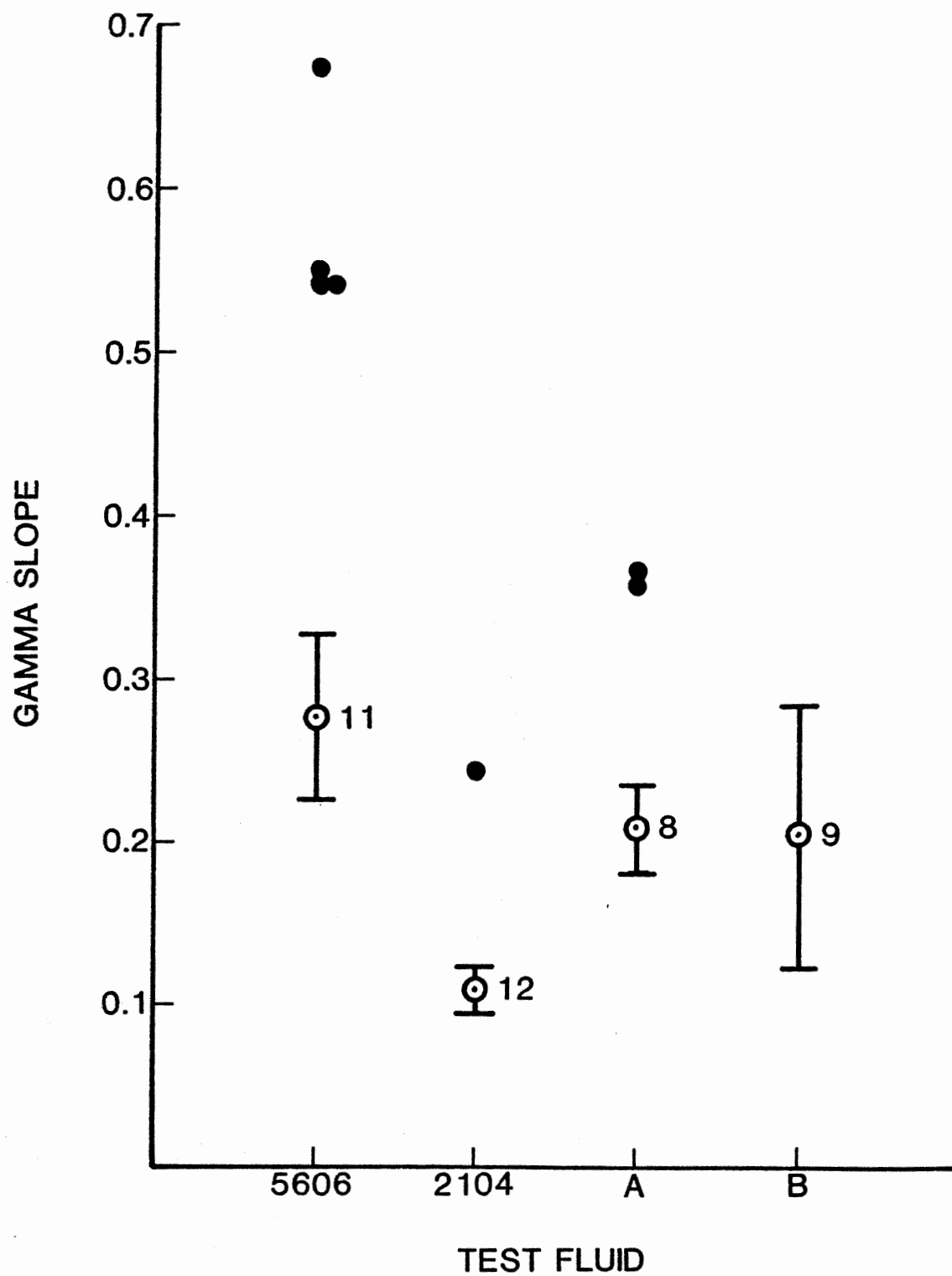


Fig. 33. Mean and Standard Deviation of Major Normal Distributions for Four Test Fluids with Minor Data Points

among them fall within the major distribution. The mean value is 0.109, and the standard deviation is 0.013. Only one test among the thirteen tests did not follow the major normal distribution. In this case, therefore, 8 percent of the tests is outside the major distribution, and 92 percent is within the major distribution.

Ten tests were conducted for mineral base fluid A. Eight tests among them fall in the major distribution with a mean value of 0.207 and a standard deviation of 0.027. Accordingly, 20 percent of the tests is outside the major normal distribution, and 80 percent is within the major normal distribution.

In the case of mineral base fluid B, nine tests were conducted. All of the tests fall in the major normal distribution with a mean of 0.203 and a standard deviation of 0.082. Hence, 100 percent of the test falls within the major normal distribution and none is outside the major normal distribution.

From the above analysis of the percentage of minor test data, the following information is now available:

| <u>Test Fluid</u> | <u>Ratio of Minor Test Data</u> |
|----------------------|---------------------------------|
| MIL-H-5606 | 27% |
| MIL-L-2104 | 8% |
| Mineral Base Fluid A | 20% |
| Mineral Base Fluid B | 0% |

A normal distribution analysis was conducted on normal probability paper for these four ratios in the same way as the foregoing analyses. As a result, it was verified that the normal distribution is applicable to these ratios. Thus, the ratio of the minor tests can be represented by a normal distribution with a mean value of 14 percent.

For the values of the standard deviation of the four test fluids, a similar analysis was made to find a mean standard deviation. The values of the standard deviation of the Gamma slope for the four test fluids are:

| <u>Test Fluid</u> | <u>Gamma Slope Standard Deviation</u> |
|----------------------|---------------------------------------|
| MIL-H-5606 | 0.051 |
| MIL-L-2104 | 0.013 |
| Mineral Base Fluid A | 0.027 |
| Mineral Base Fluid B | 0.082 |

The analysis revealed that the normal distribution can fit the variation of the Gamma slope standard deviation with a mean value of 0.043.

From the study of the four fluid test data with a total number of 47 tests, a repeatability model for the test on the Gamma Falex system is constructed. When a multiple number of Gamma Falex tests are conducted under identical test conditions, 86 percent of the tests fall within a major normal distribution with a standard deviation of 0.043. The remaining 14 percent of the tests are outside the major normal distribution.

This repeatability model for the Gamma Falex test is based on the repeatability tests of the four fluids, all of which have relatively good lubricity (estimated Gamma slopes of less than 0.3). The repeatability model has a limit in its application; however, it provides significant guidance for judging the adequacy and confidence level of the Gamma Falex test.

Analysis of Test Wear Mechanism

Fig. 34 illustrates the wear surfaces on the V-block of the

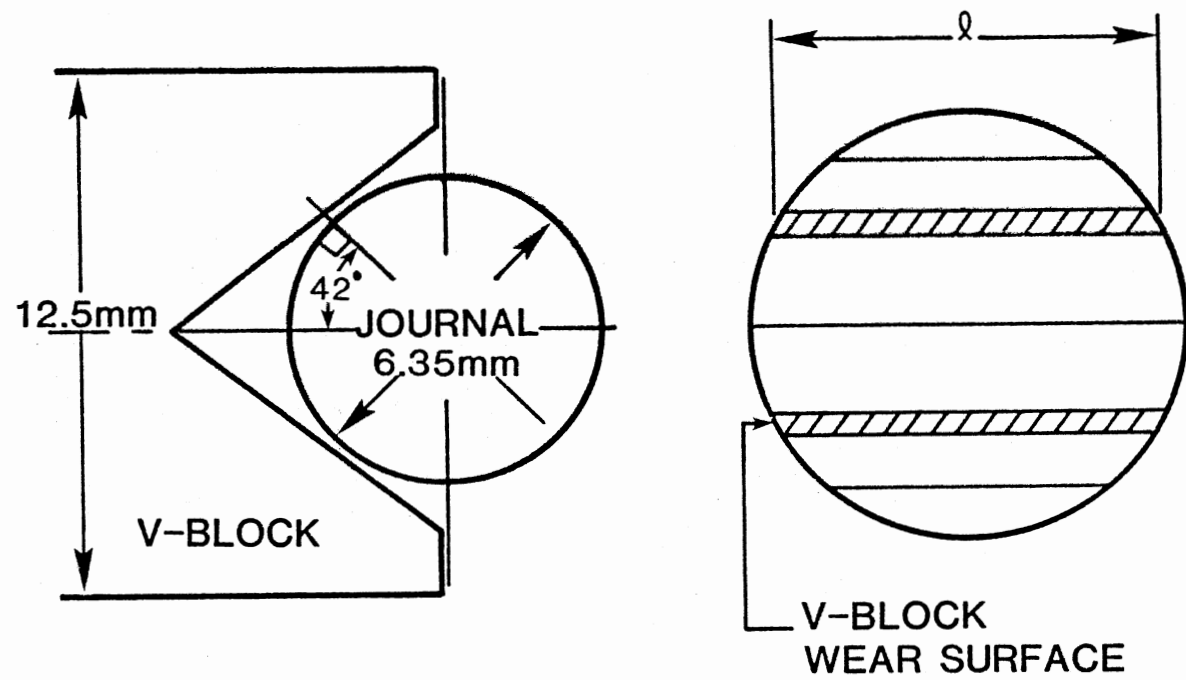


Fig. 34. Wear Surfaces on V-Block

Gamma Falex system. Wear scar depth and width increase as wear progresses. Fig. 35 shows a schematic of the right hand side of the loading system. The left hand side of the loading system is identical to the right hand side. As wear advances, the two V-blocks move toward the journal since a constant load is maintained at both ends of the loading arms by rotating the ratchet wheel. Hence, the movement of the V-block toward the journal due to wear is proportional to the number of the ratchet wheel gear teeth advanced.

Fig. 36 is an enlarged view of the geometry of the wear scar on the V-block. Experimental tests revealed that wear on the journal is negligibly small; whereas, the wear scar on the V-block increases as the test proceeds. This can be explained by the different degrees of wear severity to which the V-block and the journal are exposed.

There are two narrow wear surfaces on the V-block, Fig. 34, which are always subjected to sliding contact with the journal. On the other hand, the journal wear surface is its circumference. Only four small parts of the journal circumference are subjected to sliding contact at a time, and the rest of the surface is free from the contact. Thus, the wear condition of the V-block surface is much more severe than that of the journal.

From the wear geometry shown in Fig. 36, the relationship between the wear scar depth and the scar width is expressed by:

$$x = r \left[1 - \cos \left(\arcsin \frac{b}{2r} \right) \right] \quad (30)$$

where

x = wear scar depth on V-block

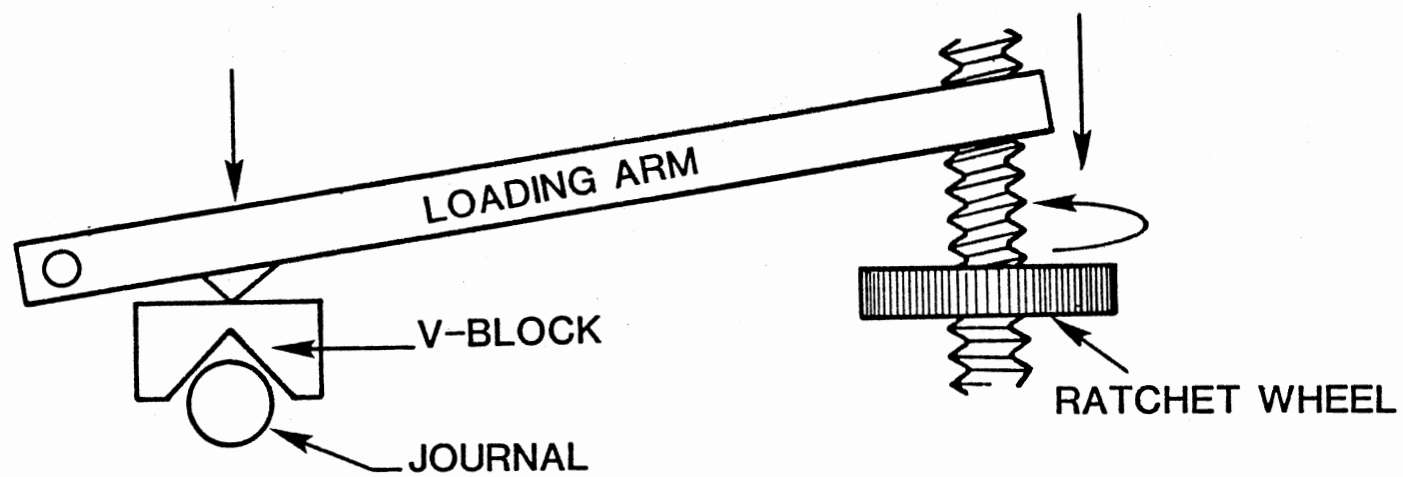


Fig. 35. Loading System of the Gamma Falex System

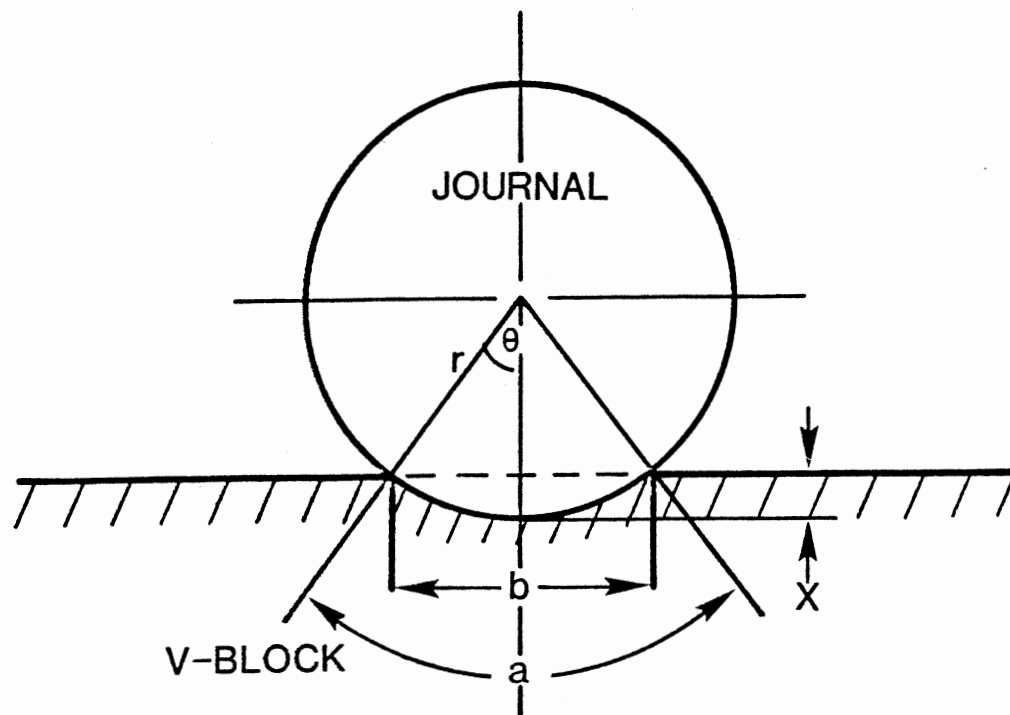


Fig. 36. Wear Geometry of Test Specimens

r = journal diameter

b = scar width

Using Eq. (30) the scar depth can be calculated from the scar width.

Values of the scar width for different wear readings were obtained from experimental tests, Table VI.

Scar widths at null gear teeth are due to stress deformation and may be calculated by the Hertizian stress equation. The scar widths at various gear advancements were measured accurately through a microscope.

From the data in Table VI with the use of Eq. (30), three values of scar depth are obtained with corresponding numbers of gear teeth advanced:

| <u>Gear Teeth Advanced</u> | <u>Scar Depth</u> |
|----------------------------|-------------------|
| 9.5 | 0.02192 mm |
| 9.5 | 0.02232 mm |
| 56.5 | 0.08957 mm |

Since the scar depth is linearly proportional to the number of gear teeth advanced, a best-fit straight line that passes through the origin is obtained. The slope of the line is calculated to be 0.001625 with a correlation coefficient of 0.9684. Hence, the relationship between the scar depth and the wear reading (the number of gear teeth advanced) is given by:

$$x = 1.625 \times 10^{-3} N \quad (31)$$

where

N = wear reading (number of ratchet wheel gear teeth advanced)

TABLE VI

SCAR WIDTHS FOR DIFFERENT WEAR READINGS

| TEST NO. | TEST LOAD | NO. OF GEAR TEETH ADVANCED | SCAR WIDTH |
|----------|-----------|-------------------------------|-----------------------|
| 248 | 50 lb | 0 9.5 | 0.0425 mm 0.746 mm |
| 249 | 100 lb | 0 9.5 | 0.0601 mm 0.754 mm |
| 250 | 200 lb | 0 56.5 | 0.0850 mm 1.50 mm |

The relationship between the wear reading and the unit load on the wear surface can be derived from a force analysis of the Falex wear tester. The contact force on one wear surface of the V-block is given by:

$$F_c = \frac{W}{2 \cos 42^\circ} = 0.6728W \quad (32)$$

where

F_c = contact force

W = applied test load

The area of one contact surface is given by:

$$A = a l \quad (33)$$

where

A = area of one contact surface

a = width of contact area

l = length of contact area

The length of the contact area is calculated to be 11.76 mm. The width of contact area is given by:

$$a = 2r \arccos \left(1 - \frac{x}{r} \right) \quad (34)$$

With $r = 3.175$ mm, the width of contact area is written:

$$a = 6.35 \arccos (1 - 5.118 \times 10^{-4} N) \quad (35)$$

Then, the unit load of the contact surface is given by:

$$P = \frac{F_c}{A} \quad (36)$$

where

P = unit load of contact surface

The derived relationship is shown in Fig. 37. Notice that the relationship between the scar depth and the wear reading is expressed by a straight line on a log-log scale. From Fig. 37, a simplified equation of the relationship can be developed by taking advantage of the straight-line characteristics.

$$\log P = - 1/2 \log N + 4.74 \quad (37)$$

Eq. (37) is a simplified equation for the relationship at a test load of 300 lbs.

According to the surface contact wear theory, the volume rate of surface contact wear per unit time on the Gamma Falex system is given by:

$$V_r = \frac{K v F_c \sqrt{1 + 3\mu^2}}{6T_y} \tan \theta_s \quad (38)$$

where

V_r = volume rate of surface contact wear per unit time

v = sliding velocity

K = coefficient of wear fragment formation

μ = coefficient of friction

T_y = yield strength of surface material

θ_s = base angle of surface asperity

Fig. 38 shows the geometry of wear progressing over a finite period of time on the V-block. From Fig. 38, the volume of wear over a finite period of time on the V-block can be expressed by:

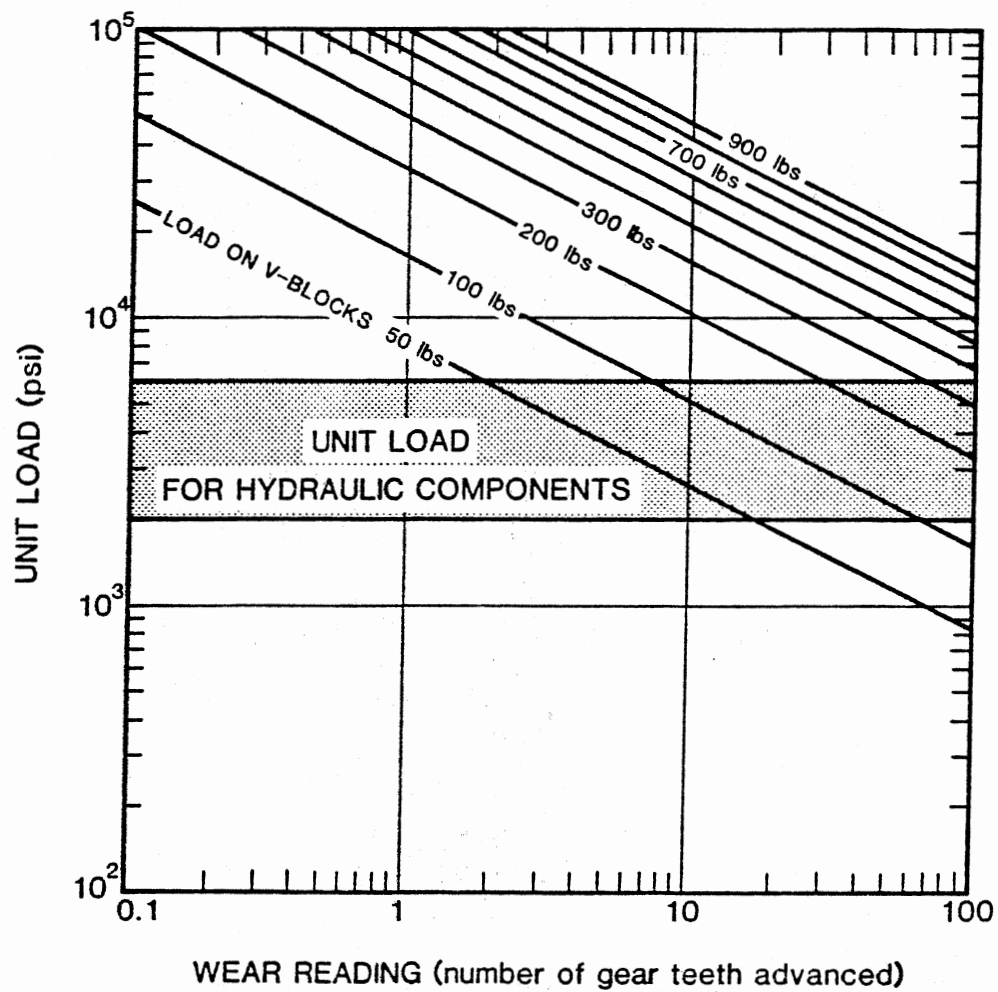


Fig. 37. Wear Reading Versus Unit Load on Wear Surface

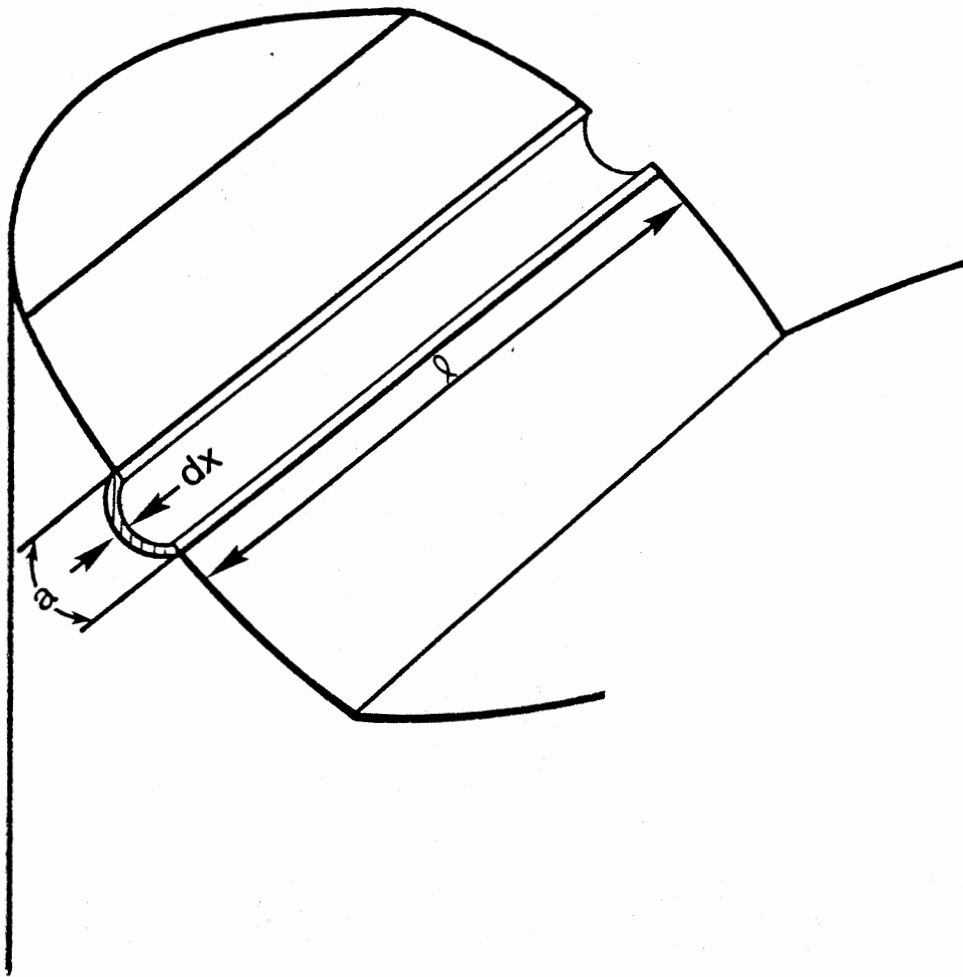


Fig. 38. Geometry of Wear Progressing in a Finite Period of Time

$$V_r dt = a l dx \quad (39)$$

where

dt = finite period of time

dx = finite scar depth advanced during a time period of dt

From the wear geometry of the V-block, the width of contact area a is expressed by:

$$a = \frac{\sqrt{N}}{4.92} \quad (40)$$

Substituting Eqs. (31) and (40) into Eq. (39) yields:

$$V_r dt = 3.884 \times 10^{-3} \sqrt{N} dN \quad (41)$$

where

dN = wear reading during a time period of dt

Substituting Eq. (38) into Eq. (41) and integrating it from time zero to t yields:

$$N = 16.06 \left(\frac{K v F_c \tan \theta}{T_y} \right)^{2/3} (1 + 3\mu^2)^{1/3} t^{2/3} \quad (42)$$

Eq. (42) shows the relationship between the wear reading versus test time on the Gamma Falex system. The wear reading versus test time is expected to show a straight line from the experimental test results; however, Eq. (42) is not a straight line but a power curve with the power of two over three.

To simplify the discussion, Eq. (42) is rewritten as:

$$N = m t^{2/3} \quad (43)$$

where

$$m = \text{constant}$$

Three values, 0.5, 1 and 2 are applied to the constant m in Eq. (43), and wear readings N corresponding to these constant values are plotted as a function of time in Fig. 39. It is obvious in Fig. 39 that a majority of the points fit straight lines. Three sets of data points beyond 10 minutes fit straight lines with a correlation coefficient of 0.999, which indicates an excellent correlation. But some points at the beginning period do not fit the straight line.

Fig. 40 shows the results of Gamma Falex test that has an incubation period of 10 minutes. The incubation period is the name given to a time period at the initiation of the test during which no wear occurs. Unlike the theoretical curve of the wear reading versus test time, no wear is observed during the initial 10 minutes. After that time, wear starts to occur at a constant rate. A best-fit straight line for the data points beyond the 10 minutes was derived with a correlation coefficient of 0.987, which indicates good correlation of the line to the data.

During the initial period of the Gamma Falex test, the journal and the V-block theoretically have line contact; however, the unit load under the line contact is so high that the surfaces are plastically deformed, and the contact surface area increases until the surface area maintains the unit load equivalent to the material yield strength. In this condition, not only the surface asperities but also the entire contact surfaces are compressed to form the so-called "mirror surfaces"

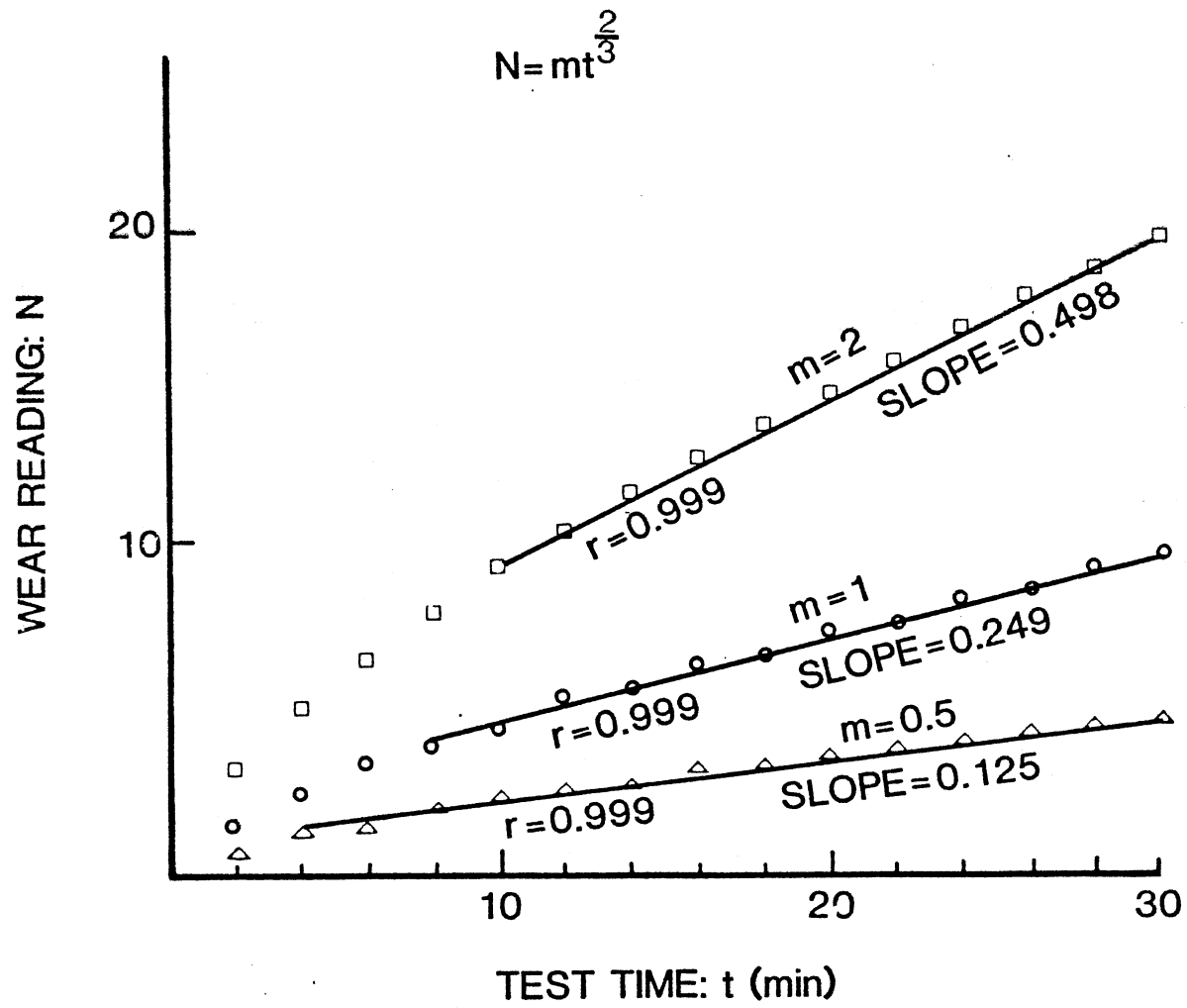


Fig. 39. Theoretical Plotting of Wear Reading on the Gamma Falex System

GAMMA FALEX TEST RESULT

Test No.: _____ Fluid: _____

Test Load: _____

Temperature: _____ Gamma Slope: _____

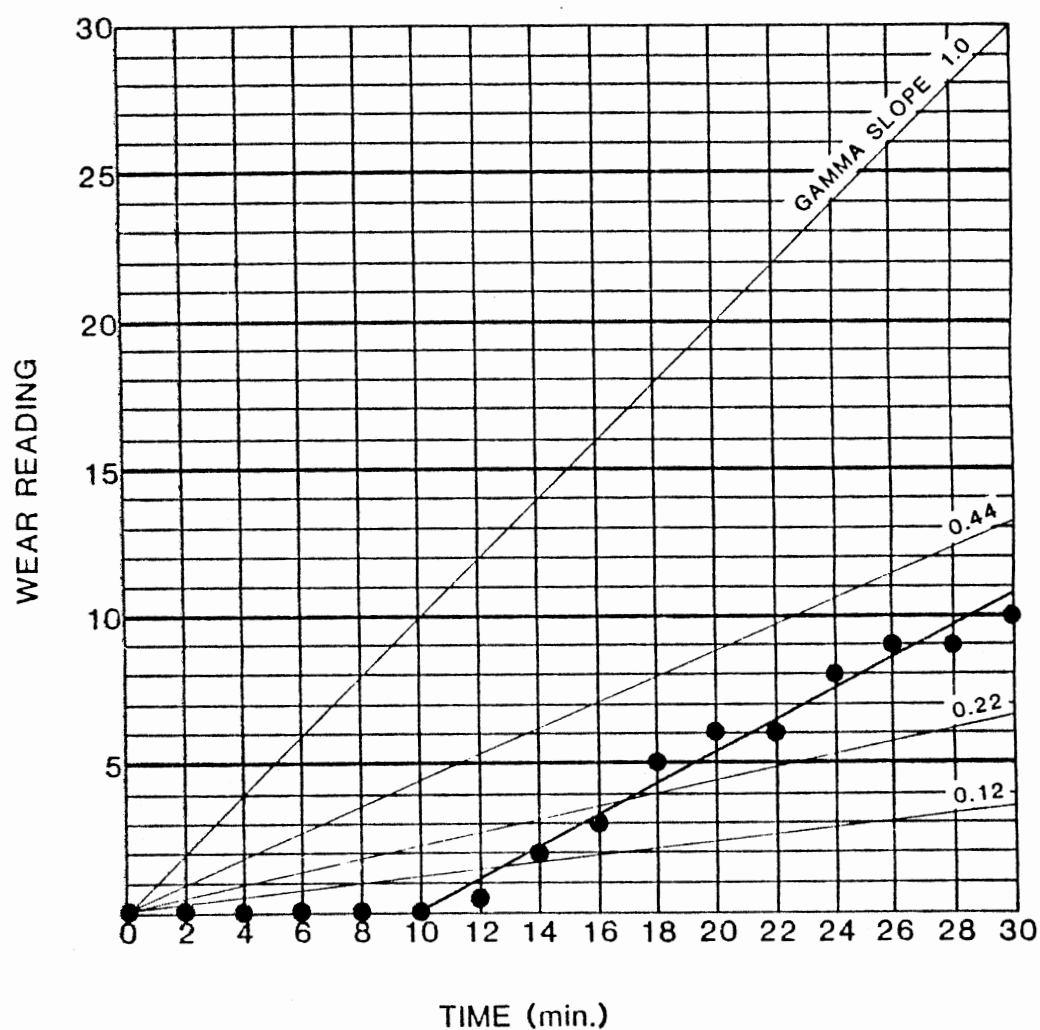


Fig. 40. A Gamma Falex Test Result with Incubation Period of 10 min.

that are work-hardened. If the applied lubricant is capable of protecting the surface from delamination, the work-hardened surface layer can be maintained for a sufficient period of time during which no wear is generated. Thus, a long incubation period is observed in such a case.

When a lubricant is not capable of protecting the surface in this condition, the work-hardened mirror surface layer is soon delaminated due to friction, and wear starts taking place.

As wear on the V-block progresses, the contact surface material is continuously removed due to wear, and the contact surface area increases. Accordingly, the number of surface asperities in contact increases. The force acting on one asperity is inversely proportional to the number of asperities; and, therefore, it constantly decreases as wear progresses. The test condition will reach a point where the force acting on the asperity is so small that deformation of the asperity is minute, and no additional wear fragments are formed. This situation can be reflected by a change of the coefficient K in the theoretical equation, Eq. (42).

As long as wear fragments are formed due to plastic deformation, the value of K stays fairly constant. When the force acting on the asperity becomes sufficiently small, the value of K begins to decrease and approaches zero.

Fig. 41 shows a typical example of the saturation of wear on the Gamma Falex test. After 1.5 hours of test time, the wear rate began to decrease and reached steady state in 2 hours.

From the foregoing analysis, it is concluded that the theoretical Gamma Falex data curve expressed by Eq. (42) is closely fit by:

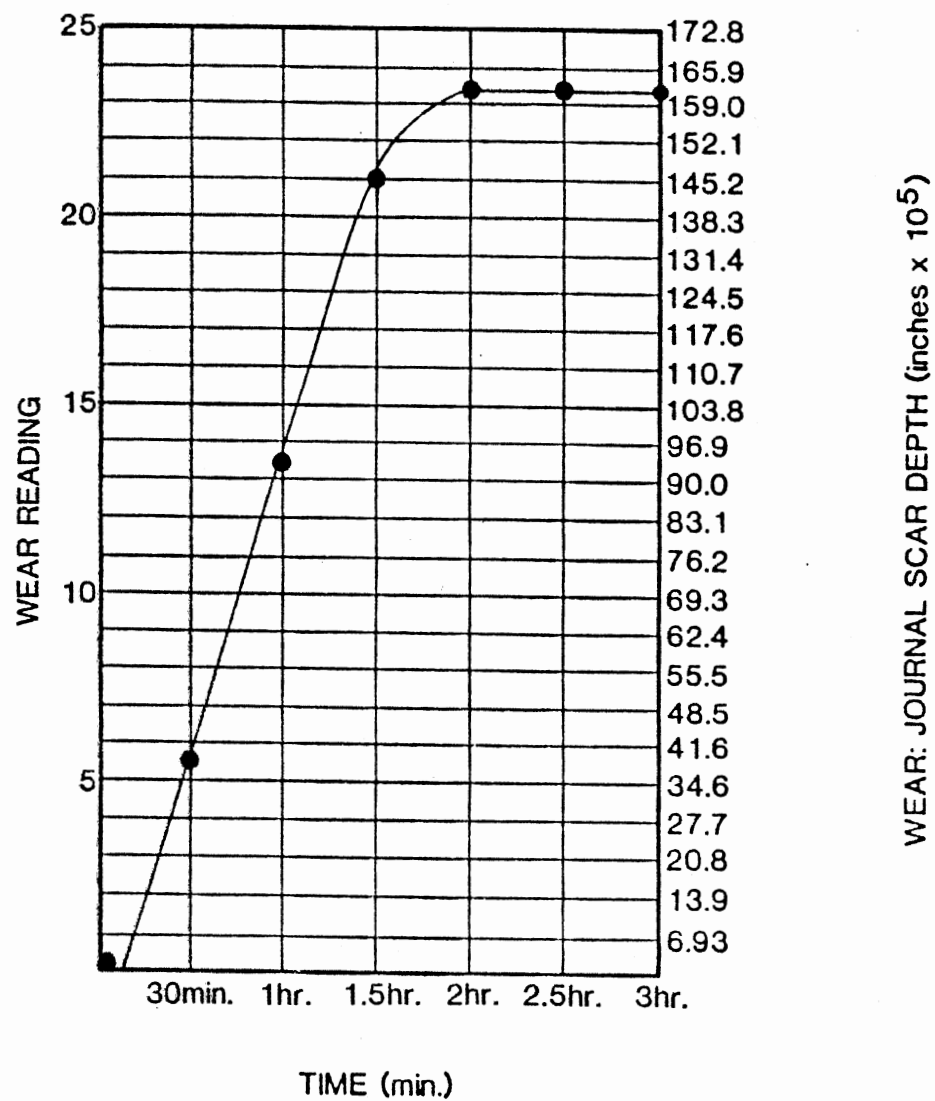


Fig. 41. Saturation of Wear Observed in a Gamma Falex Test

$$N = st + t_0 \quad (44)$$

where

s = Gamma slope (wear rate--wear reading per unit time)

t = test time

t_0 = incubation period

for the test time above 10 minutes. From Eqs. (42) and (44) in reference to Fig. 39, the Gamma slope can be expressed by:

$$s = 4.02 \left(\frac{K v F_c \tan \theta_s}{T_y} \right)^{2/3} (1 + 3\mu^2)^{1/3} \quad (45)$$

Substituting Eq. (32) into Eq. (45) and rearranging it yields:

$$\frac{s}{W}^{1.5} = [5.423v] \left[\frac{K \tan \theta_s}{T_y} \right] [\sqrt{1 + 3\mu^2}] \quad (46)$$

The right hand side of Eq. (46) is grouped into three terms by brackets. The first term is a constant because the Gamma Falex system is operated at a constant rotating speed of 290 rpm, which is translated to a sliding velocity of 9.6 cm/sec. The second term reflects the surface material properties. The third term includes the coefficient of friction between the sliding surfaces that is determined by an applied lubricant.

Experimental Method

Eq. (46) is simplified to:

$$\frac{s^{1.5}}{W} = c \sqrt{1 + 3\mu^2} \left[\frac{K \tan \theta_s}{T_y} \right] \quad (47)$$

where

c = constant

Eq. (47) is illustrated in Fig. 42, which reflects the effect of the applied test load on the Y-axis, the effect of the surface material properties on the X-axis, and the effect of the friction coefficient on the slope of a straight line.

The following three conditions are considered for the experimental test:

1. When the same material with the same surface finish is used with the same friction coefficient on the Gamma Falex system, the right hand side of Eq. (47) becomes constant. Hence, a value of $(s^{1.5}/W)$ is constant regardless of the test load in this condition. In other words, the Gamma slope changes for different test loads in such a way that the value of $(s^{1.5}/W)$ remains constant.
2. When the test material is kept the same but the friction coefficient is changed by applying different lubricants, the value of $(s^{1.5}/W)$ changes.
3. When the friction coefficient is constant and the material yield strength is changed, the value of $(s^{1.5}/W)$ changes along a straight line with a slope of $c(1 + 3\mu^2)^{0.5}$ as shown in Fig. 42.

If the above three conditions are met by the experimental test, the developed surface contact wear model is considered feasible.

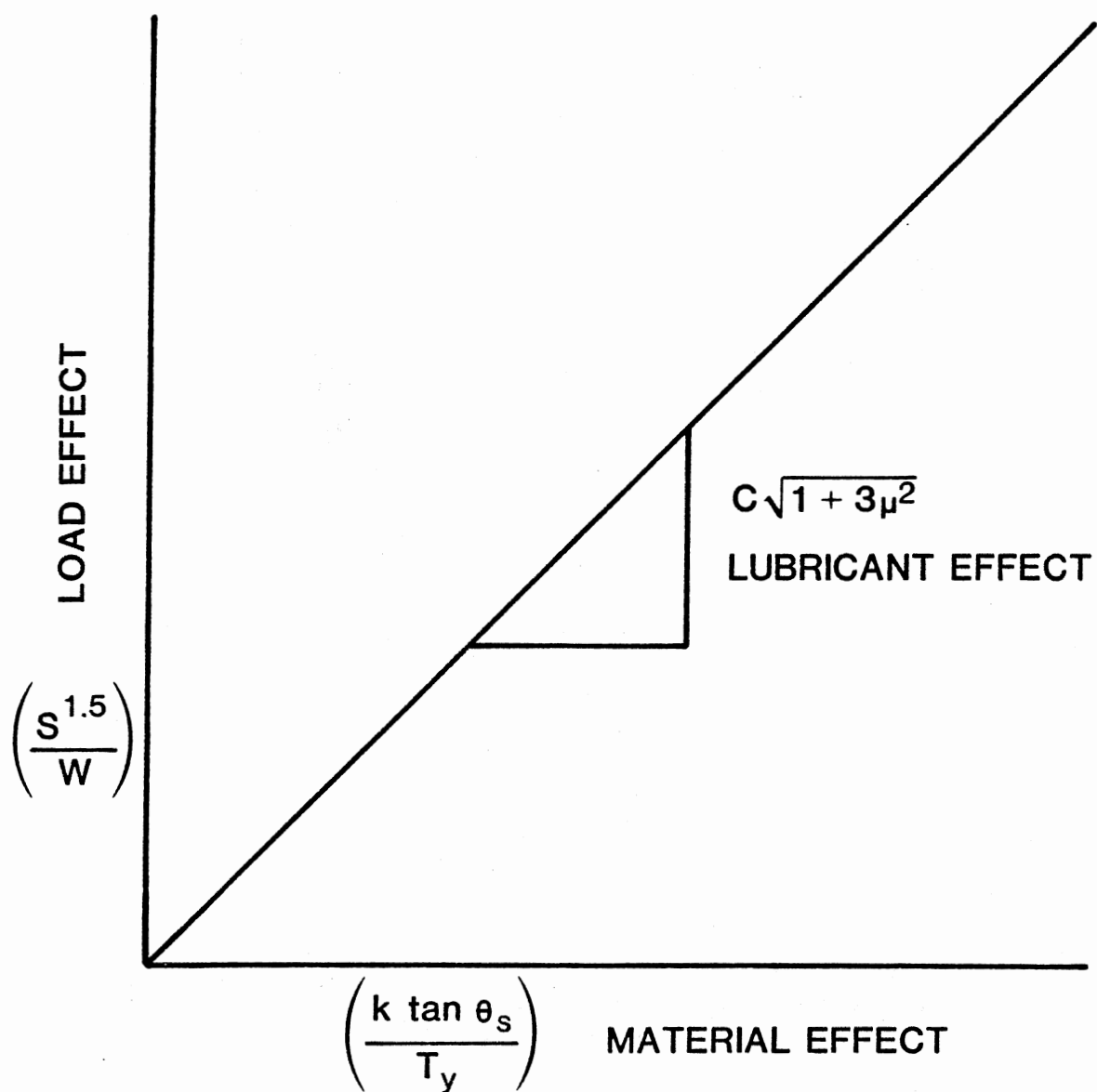


Fig. 42 Effects of Load, Material and Lubricant on Surface Contact Wear

Experimental Tests and Analysis

The standard test specimens, the V-block made of AISI 1137 steel with a yield strength of 91 kpsi and the journal made of AISI 3135 steel with a yield strength of 66 kpsi, were tested with 19 different lubricating fluids on the Gamma Falex system at various test loads. The test fluids include eight mineral base fluids (MBF 1 through 8), eight high water base fluids (HWBF 1 through 8), one water in oil emulsion fluid (WIOE 1), one water glycol fluid (WG 1), and one synthetic fluid (SYN 1). Table VII tabulates the test load, the Gamma slope, and the calculated value of $(s^{1.5}/W)$ for the test fluids.

The data tabulated in Table VII are also plotted in Fig. 43. The white circle dot in Fig. 43 indicates an average value of $(s^{1.5}/W)$ for the lubricant. A bar extending from the white circle dot shows an entire range of variation of $(s^{1.5}/W)$.

Referring to Table VII and Fig. 43, the first condition stated at the beginning of this section is examined. If the coefficient of friction remains the same regardless of the test load when the same lubricant is applied, the value of $(s^{1.5}/W)$ in Table VII is expected to be the same for the same lubricant according to theory. Table VII shows some variations of the value of $(s^{1.5}/W)$ even for the same lubricant when different loads were applied. However, Fig. 43 clearly illustrates the fact that good lubricants showed only small values of $(s^{1.5}/W)$, and poor lubricants showed large values of $(s^{1.5}/W)$ regardless of the test load, although some variations existed. Thus, the first condition is considered met. It also becomes evident that the friction coefficient changes slightly even with the same lubricant when different loads are applied.

TABLE VII
GAMMA SLOPES AND VALUES OF $(s^{1.5}/W)$
FOR NINETEEN TEST FLUIDS

| TEST FLUID | W TEST LOAD (lbs) | S GAMMA SLOPE | $(S^{1.5}/W) \times 10^4$ |
|------------|-------------------------|------------------|---------------------------|
| MBF 1 | 50 | 0.05 | 2.24 |
| | 100 | 0.15 | 5.81 |
| | 200 | 0.23 | 5.52 |
| | 400 | 0.39 | 6.09 |
| | 500 | 0.50 | 7.07 |
| | 800 | 0.80 | 8.94 |
| HWBF 1 | 100 | 0.199 | 8.88 |
| | 300 | 0.322 | 6.09 |
| | 600 | 0.630 | 8.33 |
| HWBF 2 | 100 | 0.266 | 13.72 |
| | 300 | 0.329 | 6.29 |
| | 600 | 0.404 | 4.28 |
| HWBF 3 | 300 | 1.02 | 34.34 |
| | 400 | 1.22 | 33.69 |
| HWBF 4 | 300 | 0.544 | 13.37 |
| | 400 | 0.729 | 15.56 |
| HWBF 5 | 100 | 0.178 | 7.51 |
| | 200 | 0.135 | 2.48 |
| | 300 | 0.124 | 1.46 |
| | 400 | 0.247 | 3.07 |
| HWBF 6 | 100 | 0.21 | 9.62 |
| | 300 | 0.60 | 13.25 |
| HWBF 7 | 100 | 0.75 | 64.95 |
| | 300 | 1.57 | 65.57 |

TABLE VII (Continued)

| | | | |
|--------|-----|--------|-------|
| WIOE 1 | 100 | 0.0915 | 2.77 |
| | 300 | 0.331 | 6.35 |
| MBF 2 | 100 | 0.158 | 6.28 |
| | 300 | 0.190 | 2.76 |
| MBF 3 | 100 | 0.102 | 3.26 |
| | 300 | 0.129 | 1.54 |
| MBF 4 | 100 | 0.251 | 12.58 |
| | 300 | 0.297 | 5.40 |
| MBF 5 | 100 | 0.163 | 6.58 |
| | 300 | 0.524 | 12.64 |
| MBF 6 | 100 | 0.244 | 12.05 |
| | 300 | 0.409 | 8.72 |
| MBF 7 | 100 | 0.139 | 5.18 |
| | 300 | 0.382 | 7.87 |
| WG 1 | 100 | 0.113 | 3.80 |
| | 300 | 0.381 | 7.84 |
| HWBF 8 | 100 | 0.045 | 0.95 |
| | 300 | 0.196 | 2.89 |
| MBF 8 | 100 | 0.069 | 1.81 |
| | 200 | 0.104 | 1.68 |
| | 300 | 0.183 | 2.61 |
| | 400 | 0.228 | 2.72 |
| SYN 1 | 100 | 0.033 | 0.60 |
| | 200 | 0.067 | 0.87 |
| | 300 | 0.083 | 0.80 |
| | 400 | 0.183 | 1.96 |

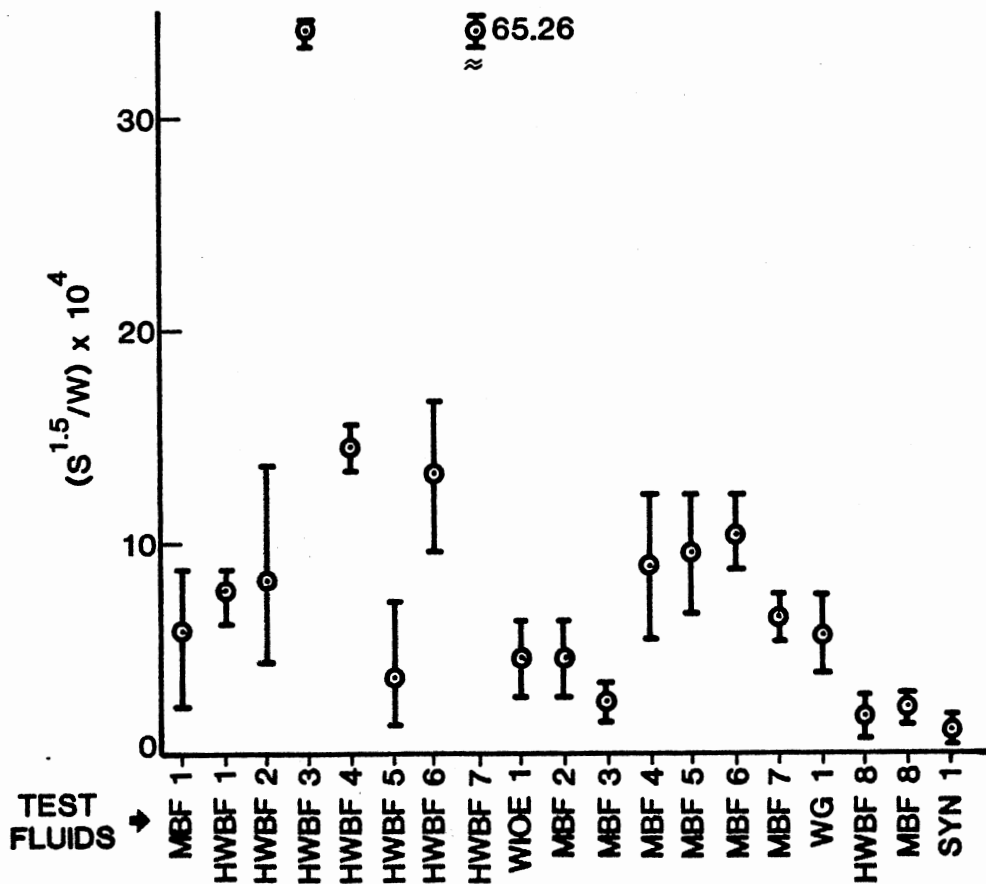


Fig. 43. Values of $(s^{1.5}/W)$ for Nineteen Test Fluids

The second condition is verified clearly by observing different values of $(s^{1.5}/W)$ for different test lubricants at the same test load, Table VII. To verify the third condition, a different material was used for the V-block. Numerous experimental tests revealed that wear on the journal is negligibly small; whereas, wear on the V-block is the major wear recorded. Hence, a different material was substituted only for the V-block; that is, AISI 1020 steel with a yield strength of 39 kpsi and a surface finish like the standard V-block. The V-block made of the standard AISI 1137 steel was designated the "hard" V-block, and the V-block made of AISI 1020 steel was designated the "soft" V-block.

Two mineral base fluids, MBF 9 and MBF 10, were tested on the Gamma Falex system with both soft and hard V-blocks. Test fluid MBF 9 was tested at loads of 300 lb. and 450 lb. with both V-block materials. Test fluid MBF 10 was tested at loads of 300 lb. and 600 lb. with both V-block materials.

Table VIII tabulates the test results and the value of $(s^{1.5}/W)$. Average values of $(s^{1.5}/W)$ with the hard V-block and the soft V-block are plotted in Fig. 44. In Fig. 44, the value of $(K \tan \theta_s)$ was to be assumed the same for both materials, and values of the hard V-block and the soft V-block were assigned on the X-axis. Note that a change of $(s^{1.5}/W)$ can be projected by a straight line for the same lubricant in both cases as stated in the third condition. Thus, the third condition is also verified. Since the three conditions stated at the beginning of this discussion are met, the feasibility of the developed surface contact wear model is validated for the experimental test that are presented.

TABLE VIII

TEST RESULTS OF TWO FLUIDS TESTED
ON DIFFERENT MATERIALS

| TEST FLUID | V-BLOCK MATERIAL & YIELD STRENGTH | W TEST LOAD (lbs.) | S GAMMA SLOPE | $^{1.5}(S/W) \times 10^4$ |
|------------|--|--------------------------|---------------------|---------------------------|
| MBF 9 | HARD 91 kpsi | 300 | 0.132 | 1.60 |
| | | 450 | 0.411 | 5.86 |
| | | AVERAGE | | 3.73 |
| | SOFT 39 kpsi | 300 | 0.375 | 7.66 |
| | | 450 | 0.475 | 7.28 |
| | | AVERAGE | | 7.47 |
| MBF 10 | HARD 91 kpsi | 300 | 0.114 | 1.28 |
| | | 600 | 0.377 | 3.86 |
| | | AVERAGE | | 2.57 |
| | SOFT 39 kpsi | 300 | 0.216 | 3.35 |
| | | 600 | 0.527 | 6.38 |
| | | AVERAGE | | 4.87 |

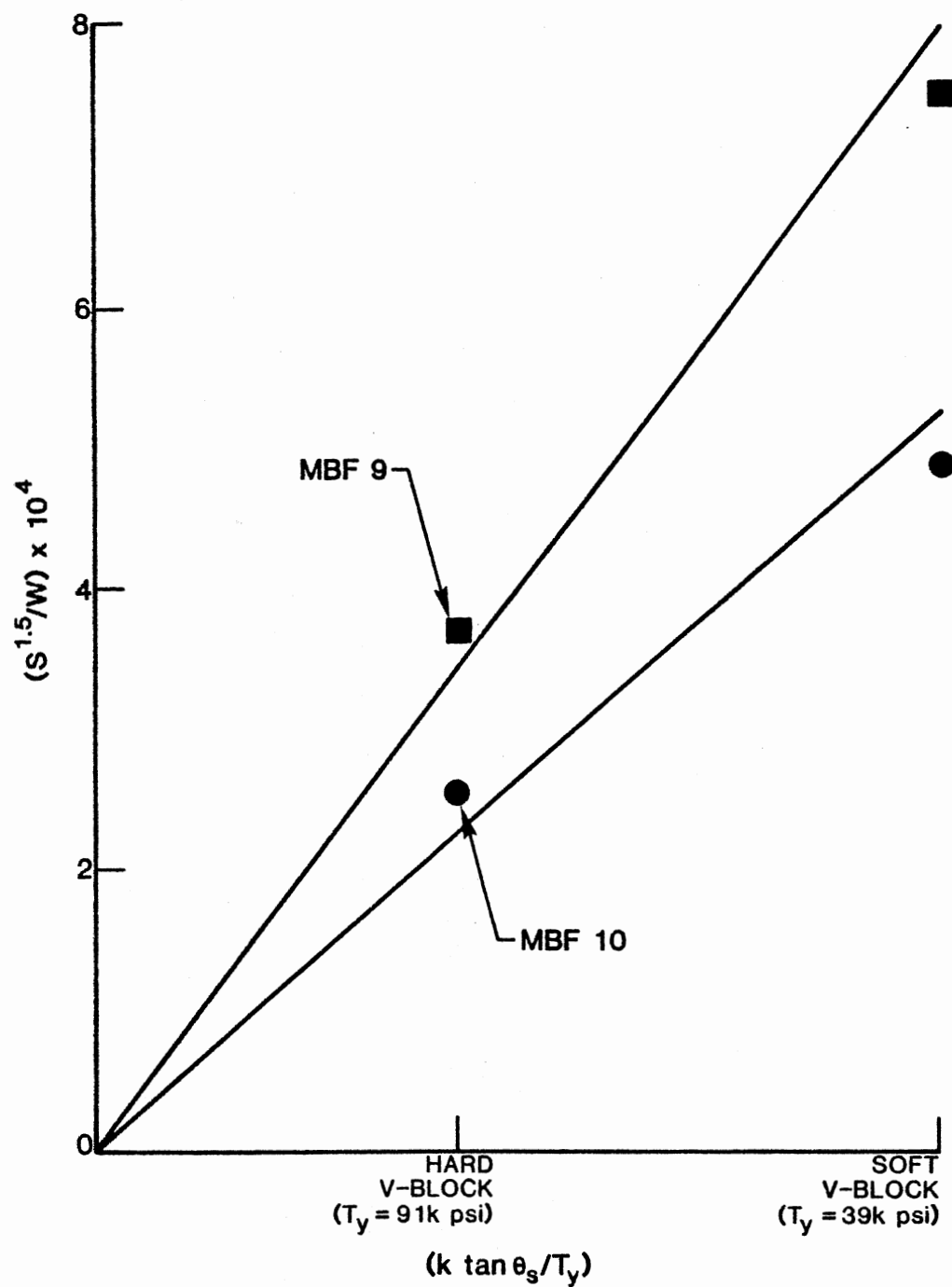


Fig. 44. Material Effects on Surface Contact Wear

Static Asperity Deformation Tests and Analysis

The developed surface contact wear model includes the plastic deformation process of the surface asperities. To investigate the mechanism of the surface asperity plastic deformation, the simulated surface asperity model was made with a base angle of 60 deg and experimental tests were conducted. This section presents the experimental test and analysis of the static plastic deformation of the surface asperity.

Fig. 45 shows the test equipment. The cone with a conically shaped top simulates the surface asperity, and the plate simulates the other surface which compresses the asperity as it slides against the asperity. Slider A has an inclined sliding surface with an angle of 16.7 deg so that it moves down one unit distance while it moves to the left by three-tenths of the unit distance. Slider A is pushed down vertically by a 60-ton hydraulic press via slider B. Slider A can slide relative to slider B to compensate for its lateral movement. The vertical force F_0 applied to push down slider A is monitored by the fluid pressure of the hydraulic press. The force F_1 acting on top of the cone to compress it is monitored by fluid pressure of the cylinder which is connected to the slide base. The surface of the slide base is lubricated by grease so that the friction between slider A and the slide base is small.

Various test lubricants were applied to the surface of the plate by a syringe periodically so that the surface is always wet with lubricant.

The cone and the plate are two test specimens. Only a single material, AISI 1045 medium carbon steel, was selected for the plate. Dimensions of the plate are shown in Fig. 46. Hardness of the plate is

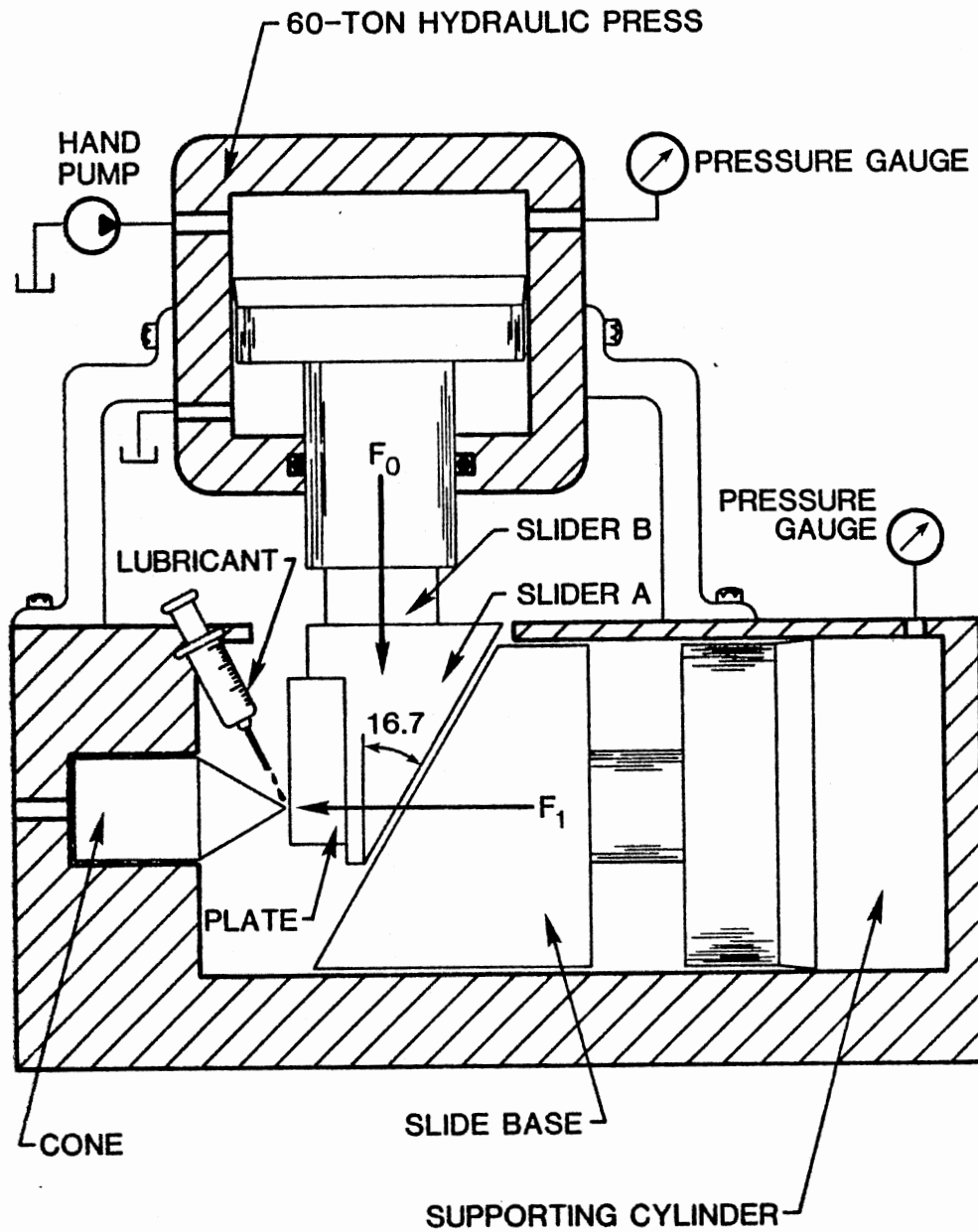


Fig. 45. Test Equipment for Static Asperity Deformation

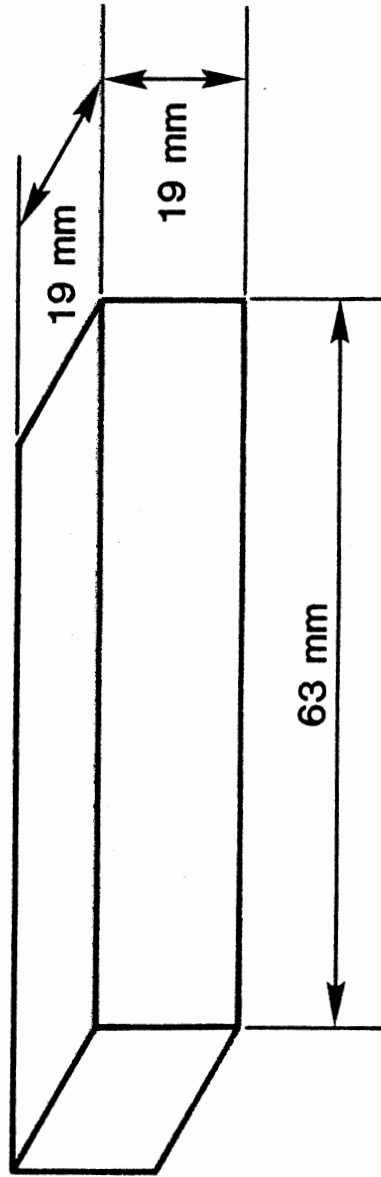


Fig. 46. Plate Dimensions

HR 98 on the B-scale, and its yield strength is 91 kpsi.

Two materials were selected for the cone--one is AISI 1020 low carbon steel with a hardness of HR 78 on the B-scale and a yield strength of 39 kpsi. The other is AISI 4340 medium carbon steel with a hardness of HR 90 on the B-scale and a yield strength of 66 kpsi. The cone made of AISI 1020 steel is designated the "soft" cone; whereas, the cone made of AISI 4340 steel is designated the "hard" cone. Dimensions of the cone are shown in Fig. 47.

For each test, a new pair of the cone and the plate was selected and installed on the test equipment. The sliding surfaces of slider A, slider B, and the slide base were lubricated by grease and assembled. Before the cone and the plate were installed, they were cleaned and their weights were measured. The length of the cone was also recorded. After installation, both surfaces of the cone and the plate were washed by ether and dried. Then, a sufficient amount of the specified lubricant was applied on the plate surface, and the test was initiated. Since this was a static test, the hydraulic press was pressurized slowly by a hand pump. As pressure of the hydraulic press built up, slider A moved down along the surface of the slide base, the plate compressed the top of the cone, and plastic deformation of the cone was observed. Lubricant was applied to the plate surface periodically to ensure a wet surface.

The applied force on top of slider A was monitored by the pressure gauge of the hydraulic press. The force acting on the cone parallel to the cone axis was monitored by the pressure gauge installed on the supporting cylinder.

After the test was completed, the cone and the plate were carefully removed from the test equipment, cleaned, and weighed. The length of

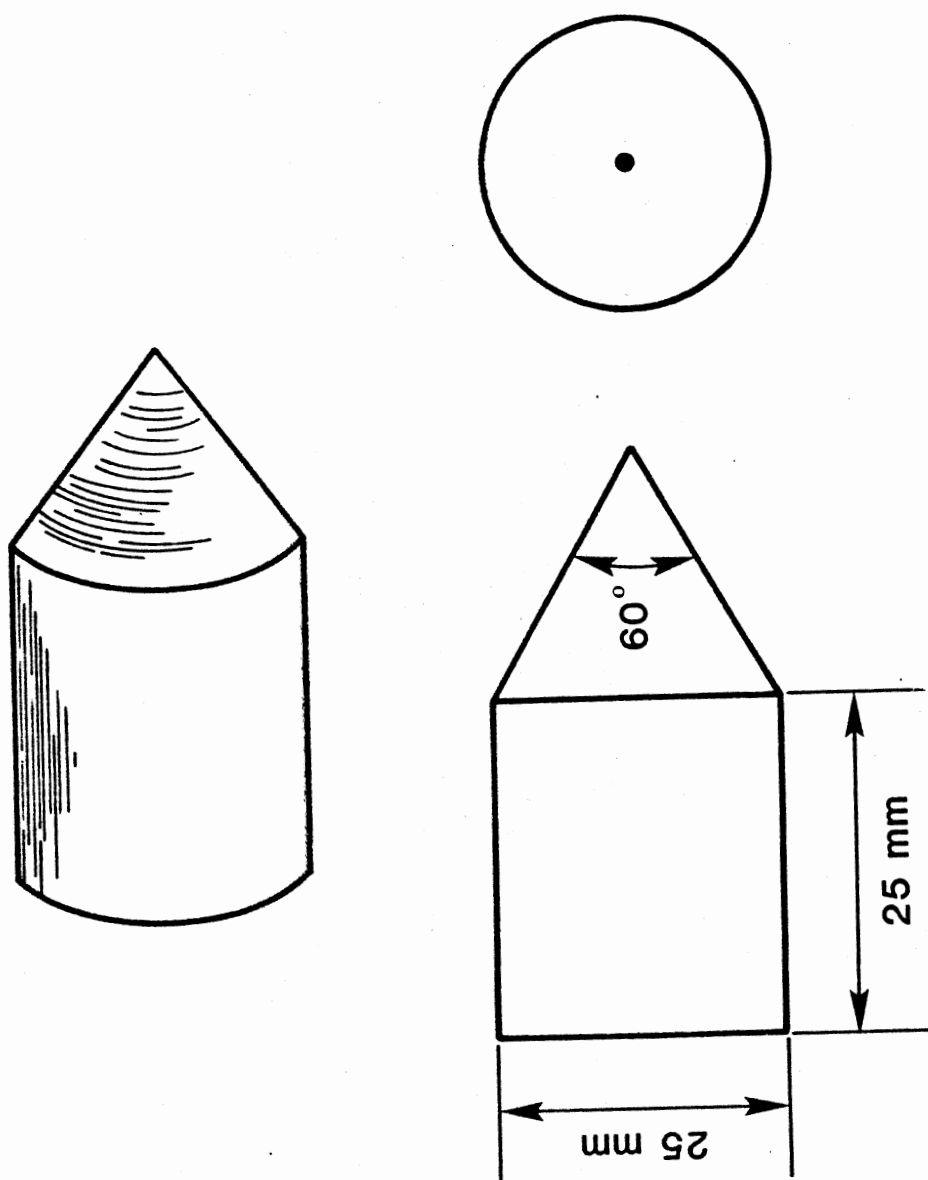


Fig. 47. Cone Dimensions

the cone was measured. The amount of wear fragments was weighted if there were any.

Six fluids were used in this series of tests. Test numbers and the materials tested with the different fluids are summarized in Table IX. The base stock oil is a mineral oil containing no antiwear additives. Zinc dithiophosphate, which is a typical antiwear additive, was added to the base stock oil and used for the tests in amounts of 0.1 and 1 percent by volume. Commercially available re-refined motor oil, a synthetic fluid (Skydrol), and a 95-5 high water base fluid (emulsion type) were also used for the tests.

It was intended that both soft and hard cones be tested with all the test fluids. But the hard cone was used instead of the soft cone in test 8 and the soft cone was used instead of the hard cone in test 15 by mistake. In test 4, slider B touched the housing of the test equipment, and the force measurements were faulty. These test failures were found during data analysis after the tests were completed.

The test results showed that the soft cone was deformed more than the hard cone because of its lower yield strength. A typical shape of the deformed soft cone is illustrated in Fig. 48. The deformed surface of the cone has a tear-dropped shape. On the surface of some of the tested soft cones, a slight delamination was observed; however, a smooth surface was observed on most of the soft cones. As a result of compression and sliding of the cone, a teardrop-shaped imprint was made on the plate surface. Fig. 49 shows an imprint on the plate surface made by the soft cone. A slight delamination was partially observed. The imprint is just a smooth image on the surface with no indentation, as shown in the cross section of the plate, Fig. 49.

The hard cone was deformed less than the soft cone; however, the

TABLE IX
TEST FLUIDS AND TEST MATERIALS

| TEST FLUID | TEST NUMBER | |
|-------------------------------|-------------|-----------|
| | SOFT CONE | HARD CONE |
| BASE STOCK OIL | #4* | #5 |
| BASE STOCK OIL + 0.1% ZINC | #6 | #7 |
| BASE STOCK OIL + 1.0% ZINC | | #8 #9 |
| RE-REFINED MOTOR OIL | #10 | #11 |
| SKYDROL (synthetic fluid) | #12 | #13 |
| 95-5 HWBF EMULSION TYPE | #14 #15 | |

* TEST FAILED

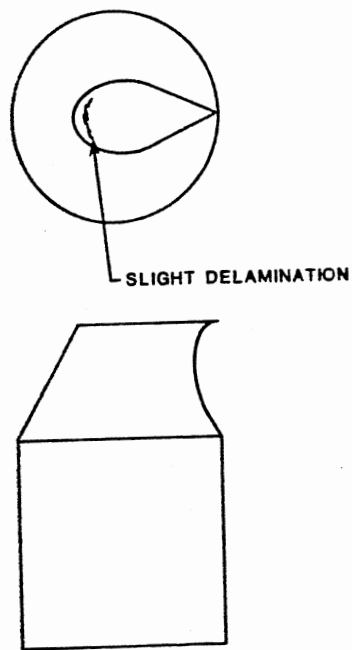


Fig. 48. Deformed
Soft
Cone

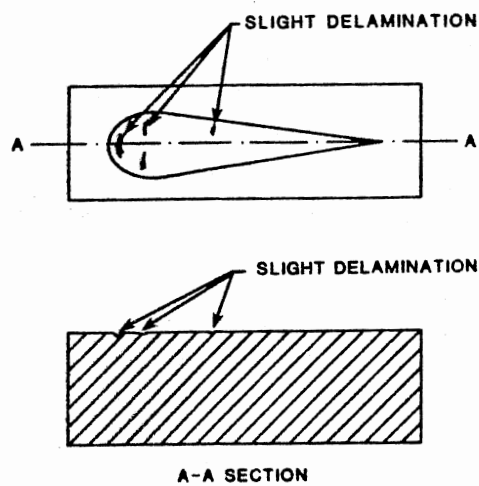


Fig. 49. Plate Surface Slided
with Soft Cone

deformed surface was undulated due to severe delamination. Since the material of the hard cone is brittle, cracks were formed as a result of plastic deformation, Fig. 50, and sometimes parts of the deformed material broke off from the cone, as shown in Fig. 50. Fig. 51 shows the surface condition of a plate mating with the hard cone. As the result of severe delamination, a series of ripple waveforms were engraved on the surface.

Although extensive deformation was observed for all the soft cones tested, none of them formed wear fragments because of their high ductility. All the hard cones had cracks on the deformed parts; and during test 8, 9, and 13, wear fragments formed. These wear particles were all collected and weighed.

Figs. 52 and 53 show the pressure of the hydraulic press versus pressure of the supporting cylinder during static deformation tests. The pressure of the hydraulic cylinder multiplied by its piston area, 18 in², indicates the vertical force F_0 applied to slider A in Fig. 45. The pressure of the supporting cylinder multiplied by its piston area, 10.16 in², indicates the horizontal force F_1 acting on top of the cone to deform it.

Fig. 52 shows the data from test 10, and Fig. 53 shows the data from test 11. The figures also show the deformed length and the size of deformed area of the cone at the final measurement. The deformed area was calculated assuming the elliptical shape shown in the figures. Note that, in Figs. 52 and 53, the pressure of the supporting cylinder at the final measurement was different in each test. To obtain the area at the same normal load for comparison, the reference pressure of the supporting cylinder must be specified and the calculated area corrected. A

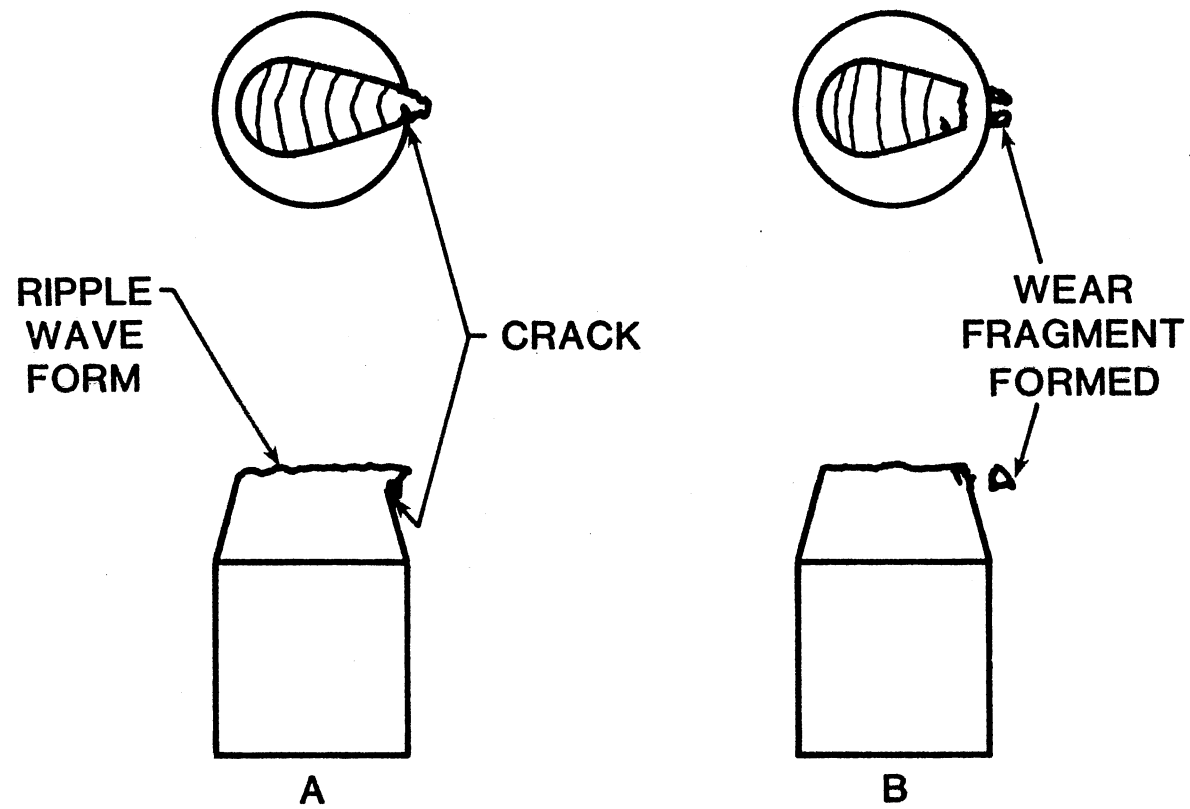


Fig. 50. Deformed Hard Cone

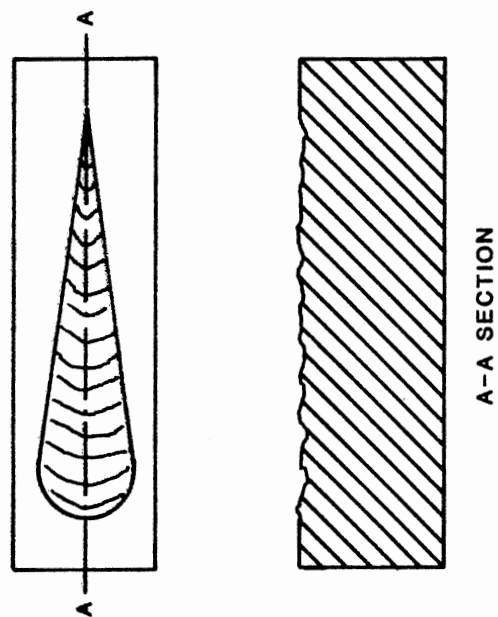


Fig. 51. Plate Surface Slided
with Hard Cone

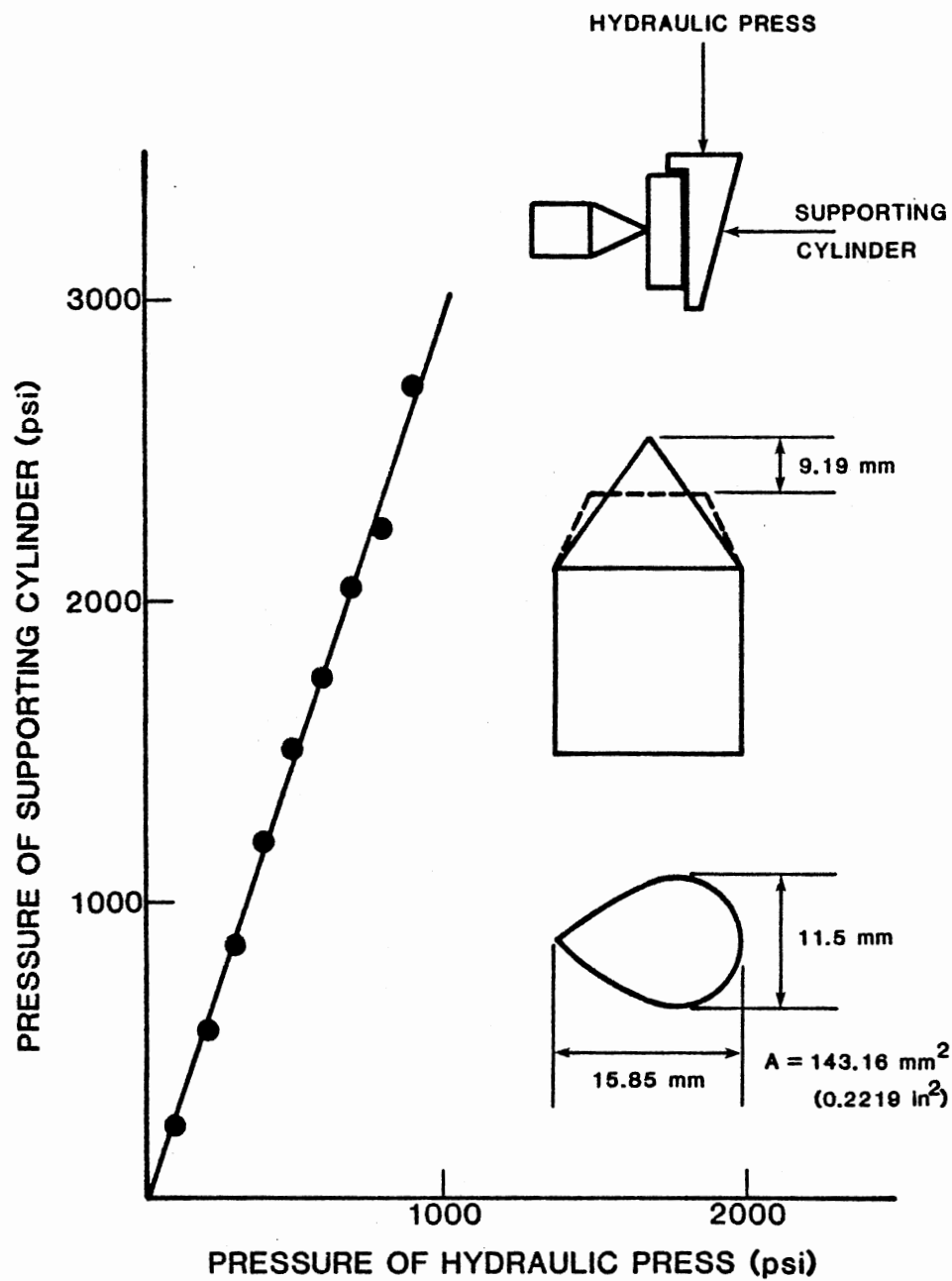


Fig. 52. Measured Data of Test No. 10, Soft Cone with Re-refined Motor Oil

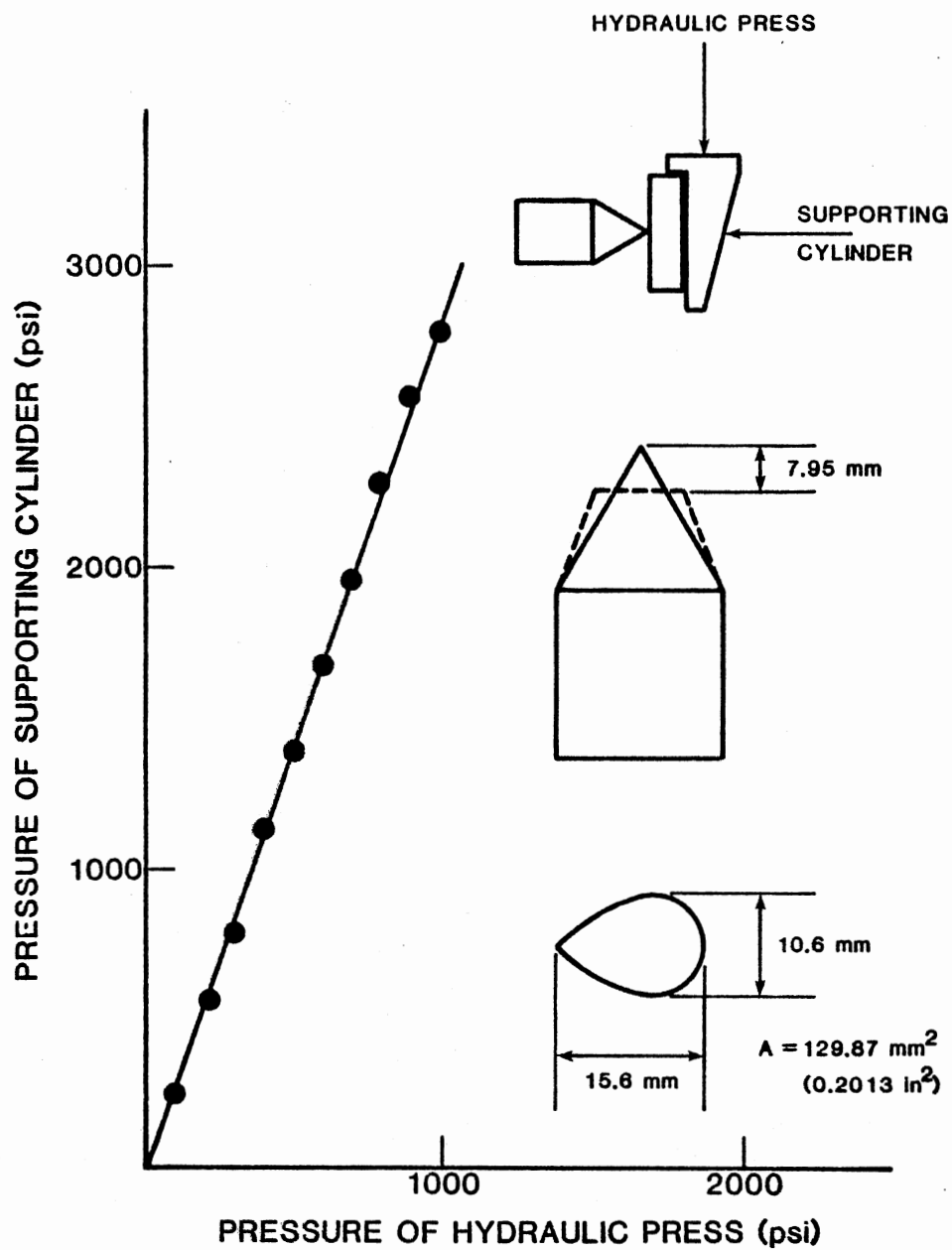


Fig. 53. Measured Data of Test No. 11, Hard Cone with Re-refined Motor Oil

pressure of 3000 psi is selected as the reference pressure of the supporting cylinder. Since the deformed area is proportional to the applied normal load correction of the area is made by simply dividing the calculated area by the final supporting cylinder pressure and multiplying it by a reference pressure of 3000 psi. Table X lists the corrected areas for the reference pressure.

From the lost length of the cone due to deformation, the deformed area of the conical top can be also calculated. With the same correction of the area for a reference pressure of 3000 psi, Table XI lists the areas calculated from the lost length of the cone.

Fig. 54 plots the results both in Tables X and XI. The deformed area calculated from the lost length of the cone is less than that calculated from the area size measurement for all the tests because of the ductility of the material. When the conical part was compressed by the flat plate and plastically deformed, the conical shape expanded due to the ductility of the material. The original slant did not remain around the deformed surface. The surface area calculated from the lost length of the cone did not consider the ductile expansion of the conical shape. Therefore, the surface area calculated from the area size measurement is a true estimate of the deformed surface that is proportional to the applied loads, but the deformed volume of the cone should be calculated from the lost length.

The above consideration leads to an important observation about the wear theory. When a conical shape is assumed for the wear surface asperity that is deformed by the other surface, actual deformation of the asperity is less than the theoretically calculated deformation because the theory does not incorporate the expansion of the conical

TABLE X

DEFORMED AREA CORRECTED FOR 3000 psi
BASED ON THE AREA SIZE MEASUREMENT

| MATERIAL | TEST NO. | TEST FLUID | CALCULATED AREA FROM MEAS. (in. ²) | FINAL PRESSURE OF SUPPORTING CYLINDER (psi) | CORRECTED AREA FOR 3000 psi (in. ²) |
|-----------|----------|-------------------------------|--|--|--|
| SOFT CONE | 6 | BASE STOCK OIL + 0.1% ZINC | 0.2354 | 3000 | 0.2354 |
| | 10 | RE-REFINED MOTOR OIL | 0.2219 | 2710 | 0.2456 |
| | 12 | SKYDROL (synthetic fluid) | 0.2151 | 2700 | 0.2390 |
| | 14 | 95-5 HWBF EMULSION TYPE | 0.2275 | 2760 | 0.2473 |
| | 15 | 95-5 HWBF EMULSION TYPE | 0.2323 | 2760 | 0.2525 |
| HARD CONE | 5 | BASE STOCK OIL | 0.0991 | 1350 | 0.2202 |
| | 7 | BASE STOCK OIL + 0.1% ZINC | 0.2094 | 2900 | 0.2166 |
| | 8 | BASE STOCK OIL + 1.0% ZINC | 0.1585 | 2830 | 0.1680 |
| | 9 | BASE STOCK OIL + 1.0% ZINC | 0.1709 | 2830 | 0.1812 |
| | 11 | RE-REFINED MOTOR OIL | 0.2013 | 2790 | 0.2165 |
| | 13 | SKYDROL (synthetic fluid) | 0.1878 | 2910 | 0.1936 |

TABLE XI

DEFORMED AREA CORRECTED FOR 3000 psi BASED
ON THE LOST LENGTH OF THE CONE

| MATERIAL | TEST NO. | TEST FLUID | LOST LENGTH (mm) | CALC. AREA (in. ²) | FINAL PRESSURE OF SUPPORTING CYLINDER (psi) | CORRECTED AREA FOR 3000 psi (in. ²) |
|-----------|----------|-------------------------------|---------------------|--------------------------------------|--|--|
| SOFT CONE | 6 | BASE STOCK OIL + 0.1% ZINC | 9.68 | 0.1521 | 3000 | 0.1521 |
| | 10 | RE-REFINED MOTOR OIL | 9.19 | 0.1371 | 2710 | 0.1517 |
| | 12 | SKYDROL (synthetic fluid) | 9.45 | 0.1449 | 2700 | 0.1610 |
| | 14 | 95-5 HWBF EMULSION TYPE | 9.60 | 0.1496 | 2760 | 0.1626 |
| | 15 | 95-5 HWBF EMULSION TYPE | 9.80 | 0.1559 | 2760 | 0.1694 |
| HARD CONE | 5 | BASE STOCK OIL | 4 | 0.0260 | 1350 | 0.0577 |
| | 7 | BASE STOCK OIL + 0.1% ZINC | 8.86 | 0.1274 | 2900 | 0.1318 |
| | 8 | BASE STOCK OIL + 1.0% ZINC | 7.57 | 0.0930 | 2830 | 0.0986 |
| | 9 | BASE STOCK OIL + 1.0% ZINC | 8.33 | 0.1126 | 2830 | 0.1194 |
| | 11 | RE-REFINED MOTOR OIL | 7.95 | 0.1026 | 2790 | 0.1103 |
| | 13 | SKYDROL (synthetic fluid) | 8.76 | 0.1245 | 2910 | 0.1284 |

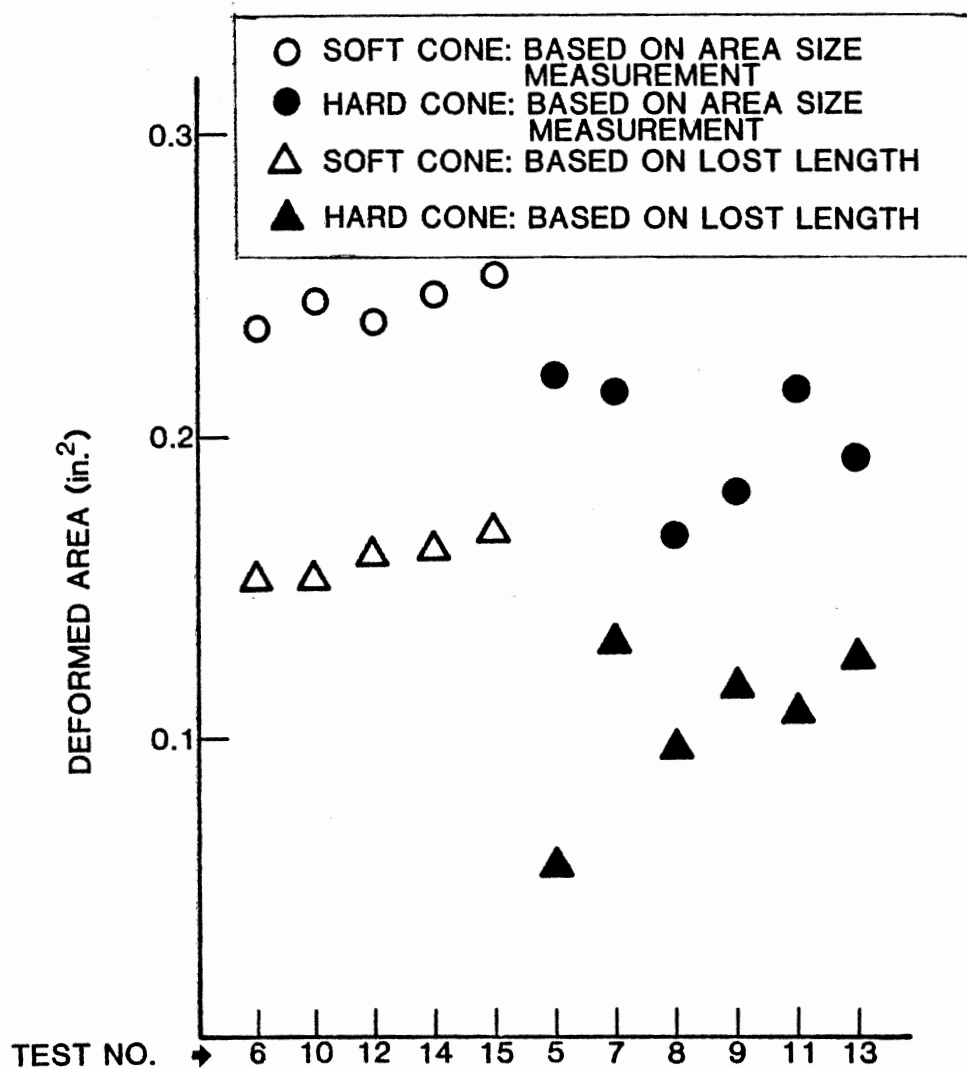


Fig. 54. Deformed Areas of Soft Cones and Hard Cones

shape due to the deformation. The degree of expansion depends on the ductility of the material. The difference between the actual and theoretical calculations is illustrated in Fig. 54.

For the same pressure (3000 psi) of the supporting cylinder, the soft cone always had a larger deformed area than the hard cone. This verifies the theory that the deformed volume is inversely proportional to the material yield strength. The theory also states that the volume of wear is proportional to the coefficient of wear fragment formation due to deformation, Eq. (15). Wear of the soft cone did not generate any wear fragments in spite of its large deformation. On the other hand, the wear of the hard cone generated some wear fragments, which implies that the coefficient of wear fragment formation is a strong function of material ductility, i.e., the more ductile material, the smaller the coefficient of wear fragment formation.

An overall analysis of the test results has been presented. However, the effect of each test fluid on the static deformation was not clearly shown, in the foregoing analysis.

The theory, Eq. (15) states that the volume of wear is a function of the coefficient of friction, which is determined by the applied lubricant. To derive the coefficient of friction associated with the test fluids, a force analysis of the test equipment is necessary. Fig. 55 shows the force distribution with no friction between slider A and the slide base and between slider A and the cone. An arrow, designated by F_0 , represents the force applied vertically to slider A. The force F_0 is divided into force F_1 , which is acting on top of the cone to compress it, and force F_2 , which pushes the slide base.

In reality, there is friction between slider A and the slide base

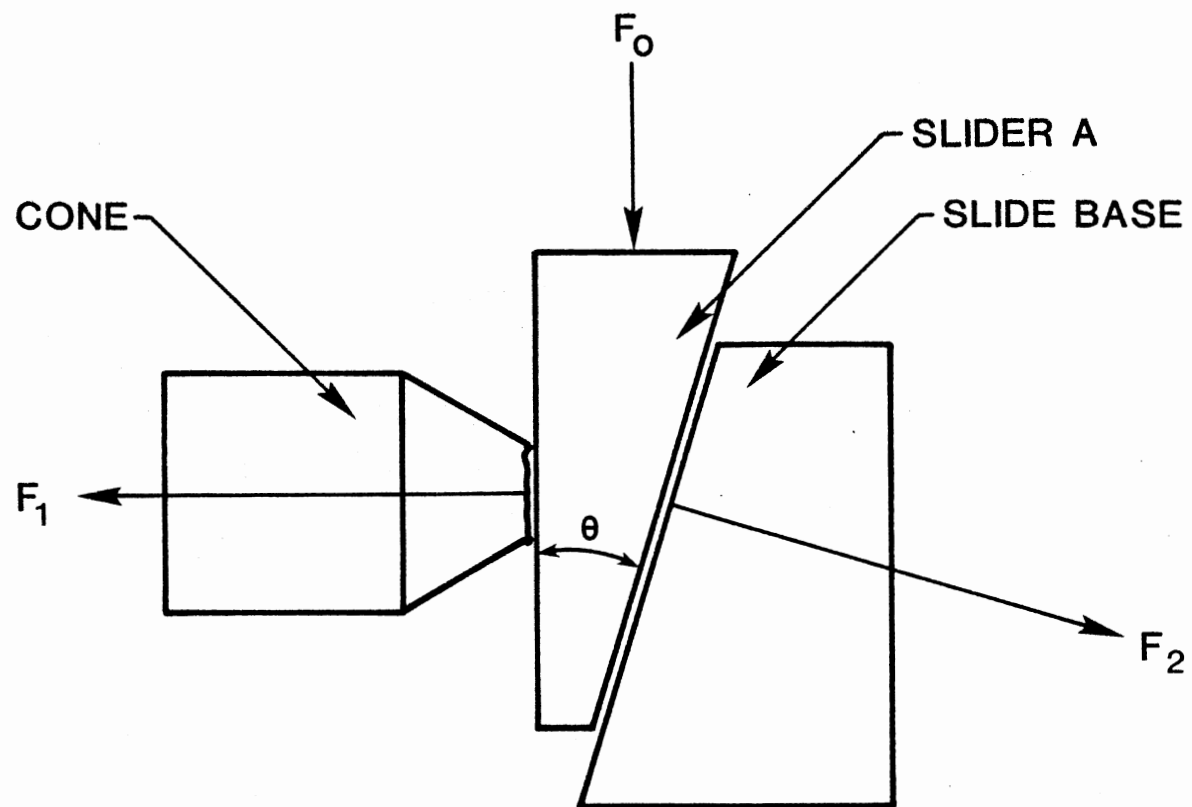


Fig. 55. Force Elements without Frictions

and between slider A and the cone, since slider A moves down along the sliding surface of the slide base. Fig. 56 illustrates the force distribution with friction included. Force F_3 is the force necessary to overcome the friction that is determined by the applied lubricant. Force F_4 is the force required to overcome the friction between slider A and the slide base. A sufficient amount of grease is applied between slider A and the slide base so that its coefficient of friction is estimated to be 0.1 in the test condition (33). The coefficient of friction between slider A and the cone is of interest and must be derived from the test data coupled with force analysis. Considering the friction forces, the applied force F_0 is divided into force F_5 , which is a combination of forces F_1 and F_3 , and force F_6 , which is a combination of forces F_2 and F_4 .

Fig. 57 reconstructs the force distribution to show all vertical and horizontal force elements. In Fig. 57, it is clear that force F_0 , which is applied by the hydraulic press, is equal to the sum of forces F_3 and F_7 . Force F_1 which compresses the cone, is equivalent to the force measured by the supporting cylinder.

Since the coefficient of friction between slider A and the slide base μ_2 is given by F_4/F_2 , the angle between $-F_1$ and F_6 is given by:

$$\gamma = \theta + \arctan \mu_2 \quad (48)$$

where

γ = angle between $-F_1$ and F_6

θ = angle of slider A

Then force F_3 is given by:

$$F_3 = F_0 - F_1 \tan \gamma \quad (49)$$

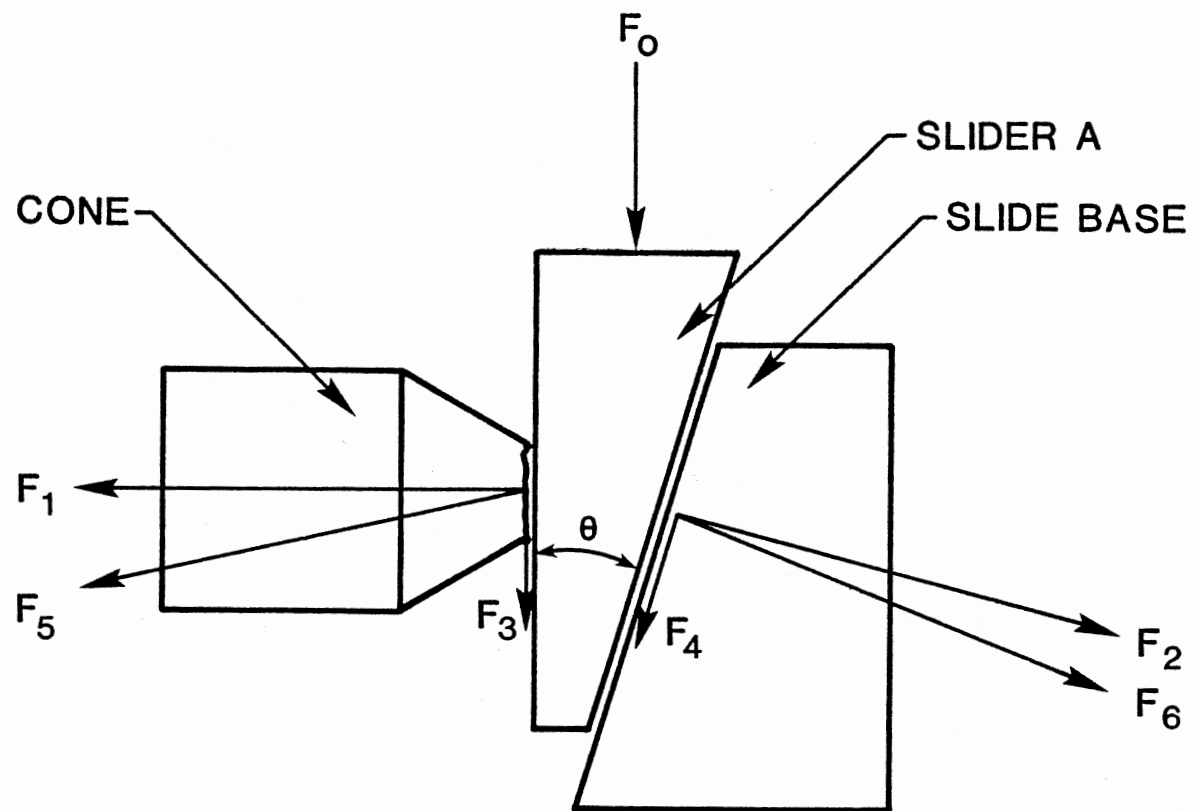


Fig. 56. Force Elements with Frictions

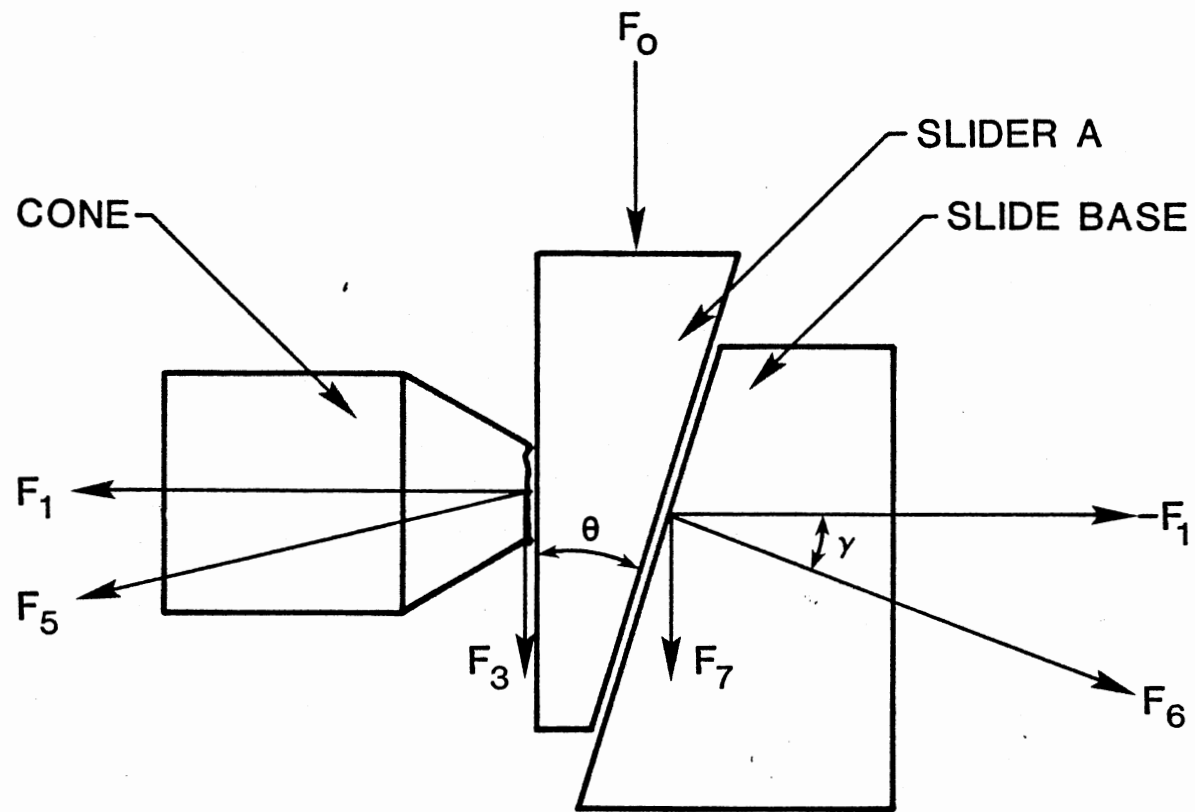


Fig. 57. Vertical and Horizontal Force Elements

The coefficient of friction between slider A and the cone μ_1 is given by F_3/F_1 ; and, therefore, it is expressed by:

$$\mu_1 = \frac{F_0}{F_1} - \tan (\theta + \arctan \mu_2) \quad (50)$$

Forces F_0 and F_1 were measured in the test. Angle θ is 16.7 degrees and the coefficient of friction μ_2 is 0.1.

Force F_1 is calculated to be 30,480 lb at a supporting cylinder pressure of 3000 psi. Force F_0 , required when force F_1 is 30,480 lb, is derived for each test from the test data and is tabulated in Table XII. The coefficient of friction μ_1 is calculated using Eq. (50) and is also tabulated in Table XII.

The derived coefficients of friction for the test fluids are plotted in Fig. 58. The effect of zinc dithiophosphate in reducing friction is apparent in Fig. 58. The fluids which produced less friction on the soft material also produced less friction on the hard material. Although the trend of fluid effects in reducing friction is the same on both test materials, the friction on the hard material is always higher than that on the soft material with the same fluid. This is considered because of severe delamination with the hard material. This observation reveals that the friction under static conditions, vary significantly for materials of different hardness even with the same lubricant.

Knowing the coefficient of friction with a specific fluid, the volume rate of plastic deformation with the fluid can be calculated by Eq. (14). The actual deformed volume of the test cone can be obtained

TABLE XII
COEFFICIENTS OF FRICTION WITH
DIFFERENT TEST FLUIDS

| MATERIAL | TEST NO. | TEST FLUID | F_0 AT $F_1 = 30480$ lbs. (lbs.) | COEFFICIENT OF FRICTION |
|-----------|----------|-------------------------------|---|----------------------------|
| SOFT CONE | 6 | BASE STOCK OIL + 0.1% ZINC | 19440 | 0.226 |
| | 10 | RE-REFINED MOTOR OIL | 18540 | 0.196 |
| | 12 | SKYDROL (synthetic fluid) | 18180 | 0.184 |
| | 14 | 95-5 HWBF EMULSION TYPE | 17820 | 0.173 |
| | 15 | 95-5 HWBF EMULSION TYPE | 17100 | 0.149 |
| HARD CONE | 5 | BASE STOCK OIL | 21960 | 0.308 |
| | 7 | BASE STOCK OIL + 0.1% ZINC | 20700 | 0.267 |
| | 8 | BASE STOCK OIL + 1.0% ZINC | 19440 | 0.226 |
| | 9 | BASE STOCK OIL + 1.0% ZINC | 20340 | 0.255 |
| | 11 | RE-REFINED MOTOR OIL | 19440 | 0.226 |
| | 13 | SKYDROL (synthetic fluid) | 19080 | 0.214 |

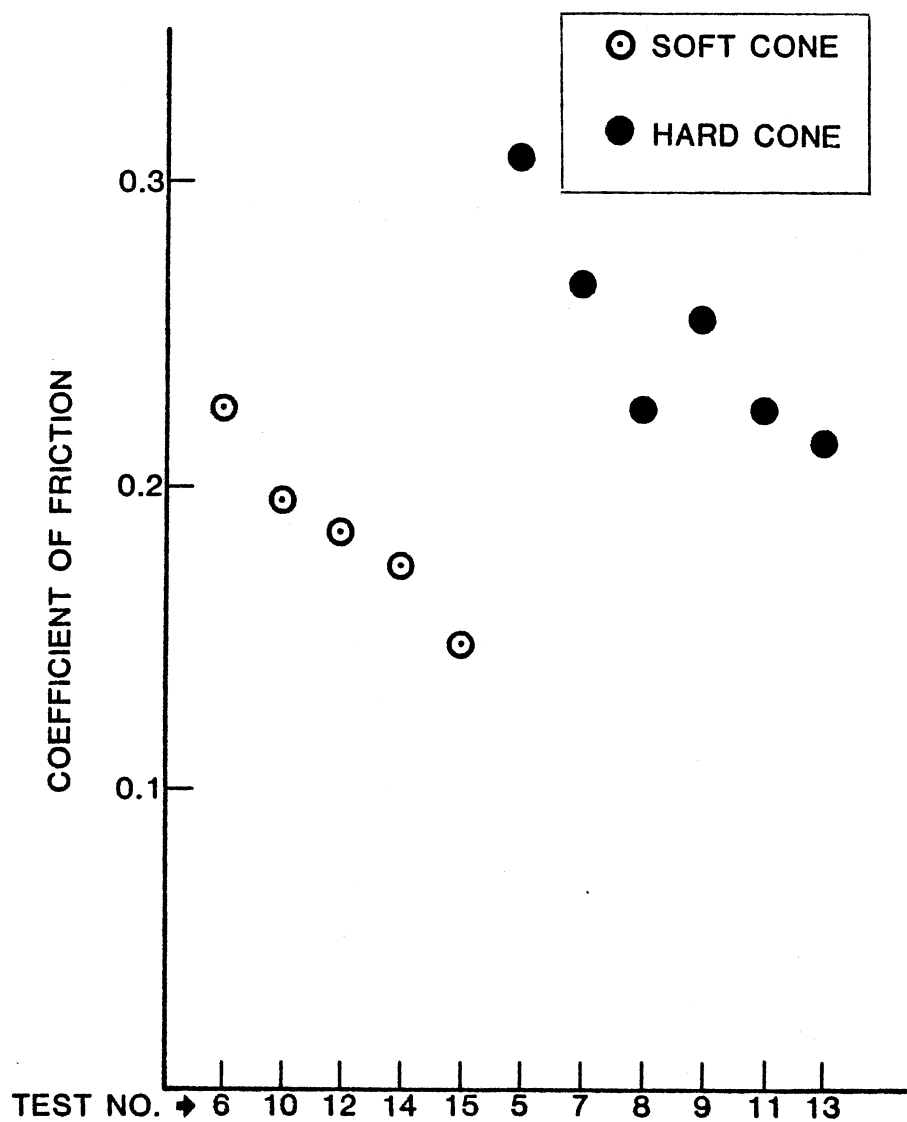


Fig. 58. Coefficients of Friction with Different Test Fluids

from the lost length of the cone. The actual volume rate of plastic deformation is then obtained by dividing the deformed volume by the effective sliding distance; i.e., the diameter of deformed surface. Table XIII tabulates the theoretical volume rate of plastic deformation calculated from the coefficient of friction using Eq. (14), and the actual volume rate of plastic deformation obtained from the lost length of the test cone for all the test fluids.

The theoretical and actual volume rates of plastic deformation are also plotted in Fig. 59. The theoretical values in Fig. 59 show that the volume rate of deformation on the soft material is much larger than that on the hard material despite the smaller coefficient of friction for the soft material. The same trend is observed on the actual volume rate of deformation.

There is a large difference between the theoretical and actual volume rates of deformation. The difference with the soft material is as large as three times the difference with the hard material. The difference between the theoretical and actual values is considered to be mainly due to the ductile expansion of the conical shape. The soft material is more ductile than the hard material; and, therefore, it has a larger expansion of the conical shape that results in a smaller volume rate of deformation.

This concept is illustrated in Fig. 60. As the flat surface compresses the top of the cone, the material deforms, and the conical shape expands. The expansion of the conical shape of a ductile material is larger than that of a brittle material, as shown in Fig. 60. With a given compressing force, the deformation stops when the equilibrium state is reached, where the given force equals the material yield

TABLE XIII

THEORETICAL AND ACTUAL VOLUME RATES
OF PLASTIC DEFORMATION

| MATERIAL | TEST NO. | TEST FLUID | COEFF. OF FRICTION | THEORETICAL VOLUME RATE OF DEFORMATION (in. ³ /in.) | ACTUAL VOLUME RATE OF DEFORMATION (in. ³ /in.) |
|-----------|----------|-------------------------------|--------------------------|--|---|
| SOFT CONE | 6 | BASE STOCK OIL + 0.1% ZINC | 0.226 | 0.242 | 0.0439 |
| | 10 | RE-REFINED MOTOR OIL | 0.196 | 0.238 | 0.0461 |
| | 12 | SKYDROL (synthetic fluid) | 0.184 | 0.237 | 0.0490 |
| | 14 | 95-5 HWBF EMULSION TYPE | 0.173 | 0.236 | 0.0489 |
| | 15 | 95-5 HWBF EMULSION TYPE | 0.149 | 0.233 | 0.0510 |
| HARD CONE | 5 | BASE STOCK OIL | 0.308 | 0.111 | 0.0248 |
| | 7 | BASE STOCK OIL + 0.1% ZINC | 0.267 | 0.108 | 0.0387 |
| | 8 | BASE STOCK OIL + 1.0% ZINC | 0.226 | 0.105 | 0.0293 |
| | 9 | BASE STOCK OIL + 1.0% ZINC | 0.255 | 0.107 | 0.0355 |
| | 11 | RE-REFINED MOTOR OIL | 0.226 | 0.105 | 0.0330 |
| | 13 | SKYDROL (synthetic fluid) | 0.214 | 0.104 | 0.0376 |

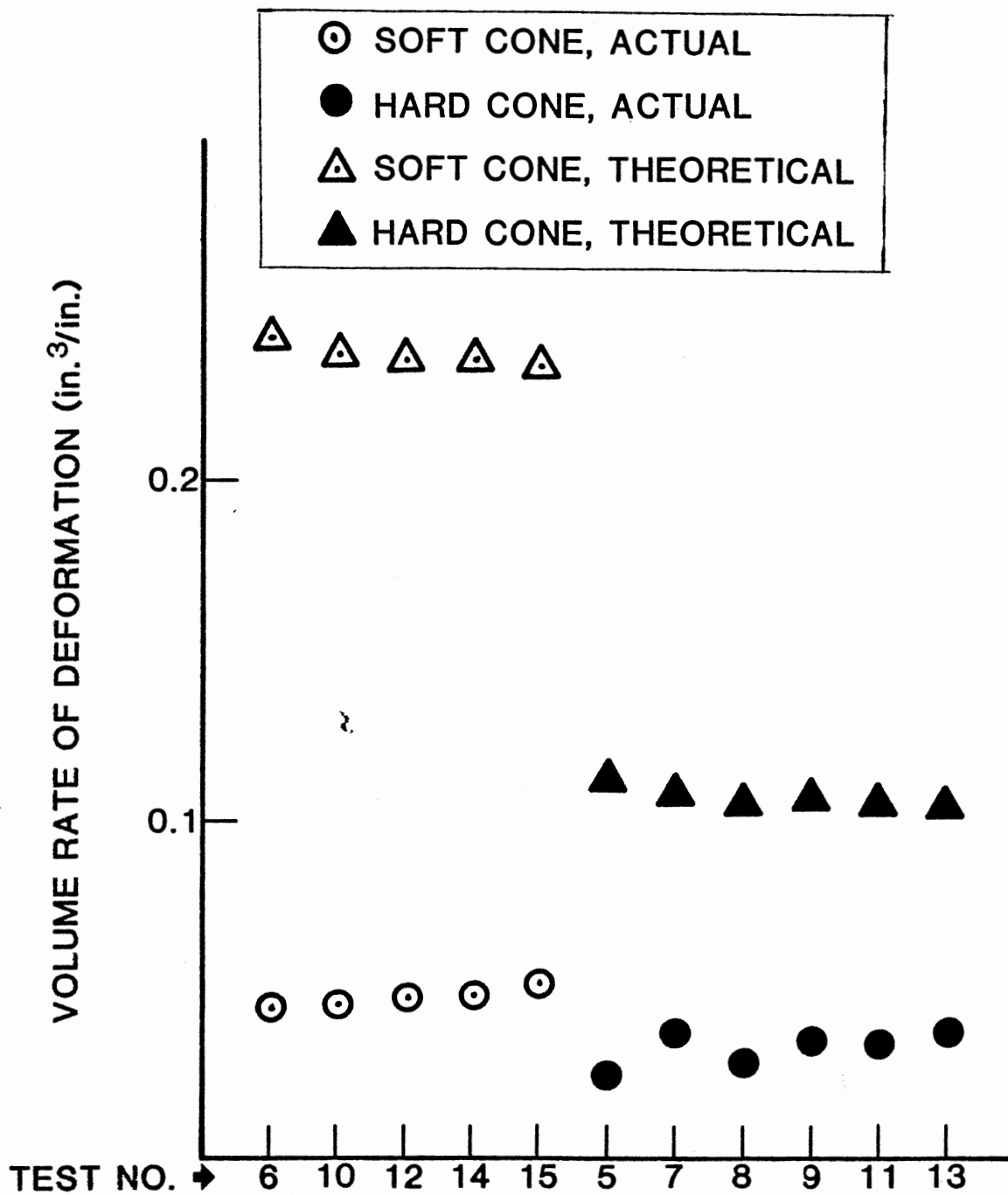
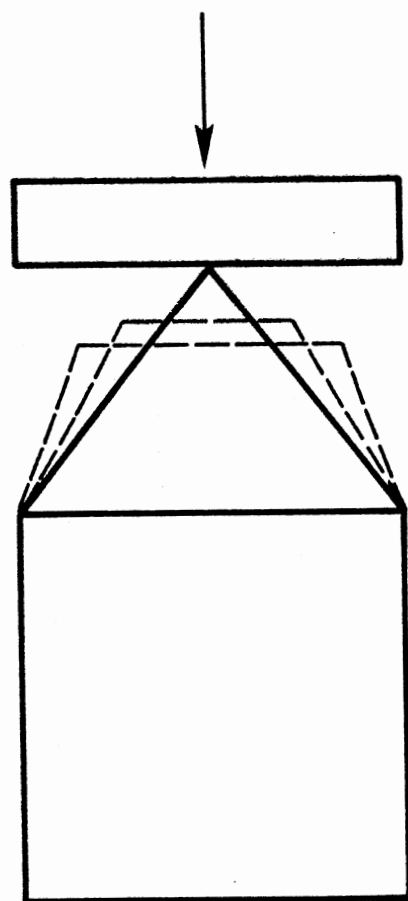
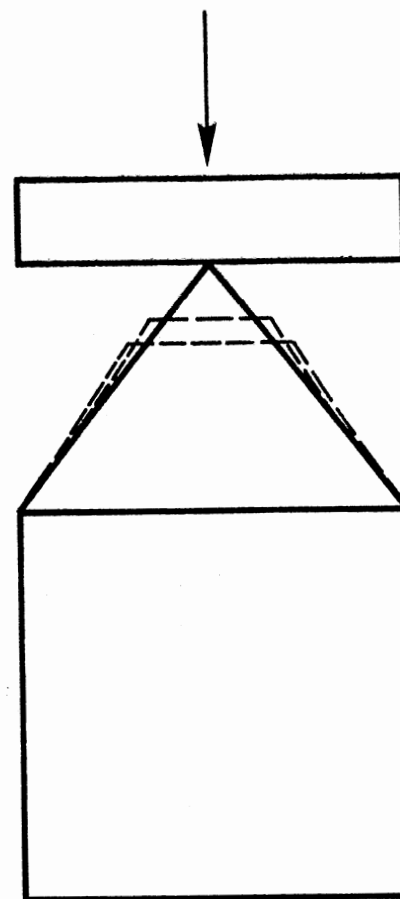


Fig. 59. Theoretical and Actual Volume Rates of Deformation



DUCTILE MATERIAL



BRITTLE MATERIAL

Fig. 60. Difference of Conical Shape Expansion Between Ductile and Brittle Materials

strength times the deformed area. The expansion of the ductile material is large, so that the actual equilibrium state is reached with much less deformation than that of the theoretical equilibrium state where no conical shape expansion is considered. The actual equilibrium state of the brittle material is still reached with less deformation than that of the theoretical state; however, a difference between the actual and theoretical deformations of the brittle material is not as large as that on the soft material because of the smaller expansion of the conical shape. This explains the differences observed in Fig. 59.

The volume of wear is obtained from Eq. (15) with a specific value for the coefficient of wear fragment formation. For all the soft cones, no wear fragments were observed; and, therefore, the coefficient of wear fragment formation is null. The hard cones in tests 8, 9, and 13 generated wear fragments of 0.4 grams, 0.45 grams, and 0.3 grams, respectively. Although all the other hard cones showed cracks which would lead to the formation of wear fragments, no particles broke off from the cones, and therefore, no wear formation is considered. Neglecting the small difference among the volume rates of deformation with respect to the various test fluids, the coefficient of wear fragment formation for the hard cone can be experimentally determined. The sum of the actual volume rates of deformation for all six hard cones is $0.1989 \text{ in}^3/\text{in}$. The volumes of wear fragments for test 8, 9, and 13 are calculated to be 0.00313 in^3 , 0.00352 in^3 , and 0.00235 in^3 , respectively, based on a density of 7.8 for the hard cone material. The volume rates of wear fragments are calculated by dividing the volume of wear fragments by the effective sliding distance. The calculated volume rates of wear fragments for test 8, 9, and 13 are $0.00910 \text{ in}^3/\text{in}$, $0.00930 \text{ in}^3/\text{in}$, and

0.00590 in³/in, respectively. The sum of the volume rates of wear fragments for these hard cones, 0.0243 in³/in, is divided by the sum of the volume rates of deformation for all the hard cones. The coefficient of wear fragment formation for the hard cone is obtained to be 0.122.

Dynamic Asperity Deformation Tests

And Analysis

In actual wear situations, wear generation is the dynamic process where the sliding velocity is one of the important parameters. The experimental test was conducted to study the effect of the sliding velocity on the plastic deformation of the surface asperity. This section presents the experimental test and analysis of the dynamic plastic deformation of the surface asperity.

Fig. 61 shows the test equipment developed to conduct the dynamic test for the plastic deformation process simulating a wear mechanism. Weight M_1 is dropped from the specific height L and falls straight down to hit the weight receiver. The impact given by weight M_1 moves weight M_1 itself, the weight receiver, slider B, slider A and the plate downward all together. Since slider A slides on the surface of a slide base in down and left direction, slider B slides against slider A to compensate for the lateral movement of slider A. As slider A slides down along with the surface of the slide base, the plate slides against the cone and also compresses it simultaneously. Slider A has an angle of 16.7 deg so that it moves down by one unit distance while it moves toward the left by three-tenths of the unit distance. Weight M_1 weighs 35 kg. The total weight of the weight receiver, slider B, slider A, and the plate which move together with weight M_1 is 13 kg and is designated M_2 .

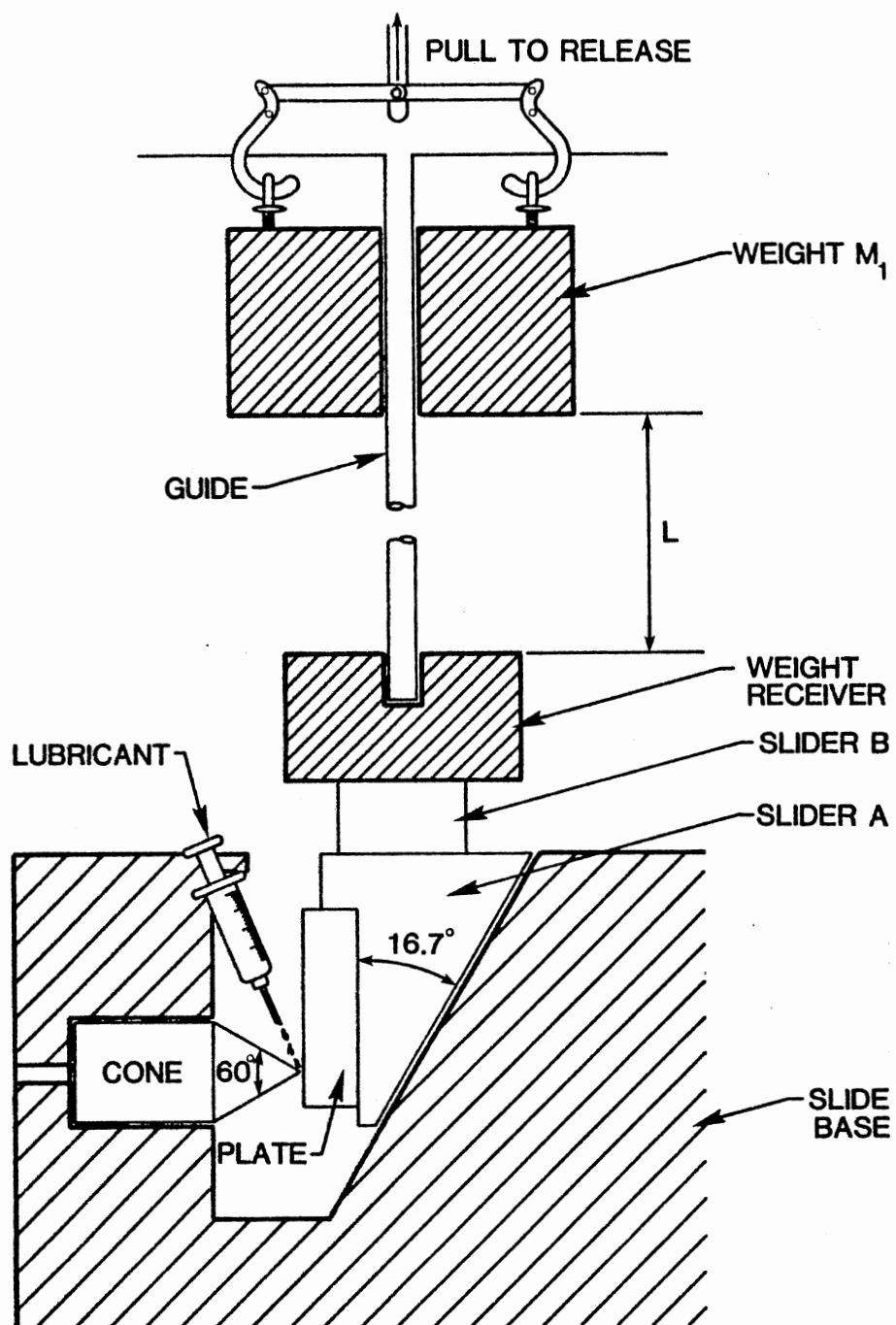


Fig. 61. Test Equipment for Dynamic Asperity Deformation

A sufficient amount of grease is applied between slider A and the slide base so that the friction between them is small. The materials and the shapes of the cone and the plate were the same as those used in the static asperity deformation test.

Before the test was started, the specimens were thoroughly cleaned by ether. Their weights and the length of the cone were measured. The plate and the cone were then installed in the test position. Both the cone and the plate were wet with a test fluid. Weight M_1 was raised up to a height of 226 cm from the weight receiver. Weight M_1 was released for its free fall. Weight M_1 reached the weight receiver after its free fall impacting the plate through the weight receiver, slider B, and slider A. Due to the impact, the plate slid against the cone and also compressed the top of the cone until it stopped.

After the test, the cone and the plate were removed from the test equipment and were washed by ether. Their weights and a length of the cone were measured. Special note was made if wear fragments were generated.

The test fluids were base stock oil, base stock oil with 0.1 percent zinc dithiophosphate, base stock oil with one percent zinc dithiophosphate, Skydrol (synthetic fluid), re-refined motor oil, and 95-5 high water base fluid (emulsion type). Both soft and hard cones were tested with each of these six test fluids.

Table XIV summarizes the test numbers, test fluids, test materials, lost lengths of the cones due to deformation, and wear fragments. Thin needle-shaped particles were observed for all the soft cones. But the amount of the particles was minute and could not be measured by weight loss of the cone or the plate. The total weight of the particles per

TABLE XIV
RESULTS OF DYNAMIC ASPERITY DEFORMATION TESTS

| TEST MATERIAL | | | SOFT CONE | | HARD CONE | |
|---------------|----|----------------------------|-------------------|------------------|-------------------|------------------|
| TEST NO. | | TEST FLUID | LOST LENGTH (in.) | WEAR PARTICLES ? | LOST LENGTH (in.) | WEAR PARTICLES ? |
| 4 | 5 | BASE STOCK OIL | 0.257 | YES | 0.249 | NO |
| 6 | 7 | BASE STOCK OIL + 0.1% ZINC | 0.239 | YES | 0.236 | YES |
| 8 | 9 | BASE STOCK OIL + 1.0% ZINC | 0.245 | YES | 0.239 | NO |
| 10 | 11 | SKYDROL (synthetic fluid) | 0.225 | YES | 0.226 | NO |
| 12 | 13 | RE-REFINED MOTOR OIL | 0.249 | YES | 0.230 | NO |
| 14 | 15 | 95-5 HWBF EMULSION TYPE | 0.240 | YES | 0.227 | NO |

test was estimated to be less than 0.1 grams.

With the hard cone, no wear particles were observed except for test 9. Some flake-type wear particles were observed in this test that were broken off of the material due to deformation. The other hard cones showed many cracks around the deformed surface but no wear particles actually broke off.

The lost length of the cones are plotted in Fig. 62. The trend for the soft cones exactly repeats the trend for the hard cones with slightly shorter lost lengths.

Fig. 63 shows the deformed surface of the soft cone in test 8. The surface burn is a spot where the material color changed to brown or black due to high temperature. Fig. 64 illustrates the surface of the plate which was rubbed by the deforming cone surface in test 8. Surface direct contact started first at 3 mm from the beginning of sliding. The initiation of the surface direct contact was evident because the surface was slightly scratched. Due to direct contact of the surfaces, much heat was generated and the surface was burnt. The burning started at 8.5 mm. With sufficient heat available and high contact pressure severe adhesion started at 16.5 mm; however, this severe adhesion stopped before the plate stopped. A mirror-smooth surface is observed in a region 4 mm from the end.

Fig. 65 shows the deformed surface of the hard cone in test 9. Fig. 66 illustrates the damaged surface of the plate in the same test. Direct surface contact started at 7 mm from the beginning, and burning started at 13 mm. Severe adhesion is observed from 20 mm to 1.5 mm before the end of the imprint. In the area of last 1.5 mm of the imprint, a mirror-smooth surface is observed.

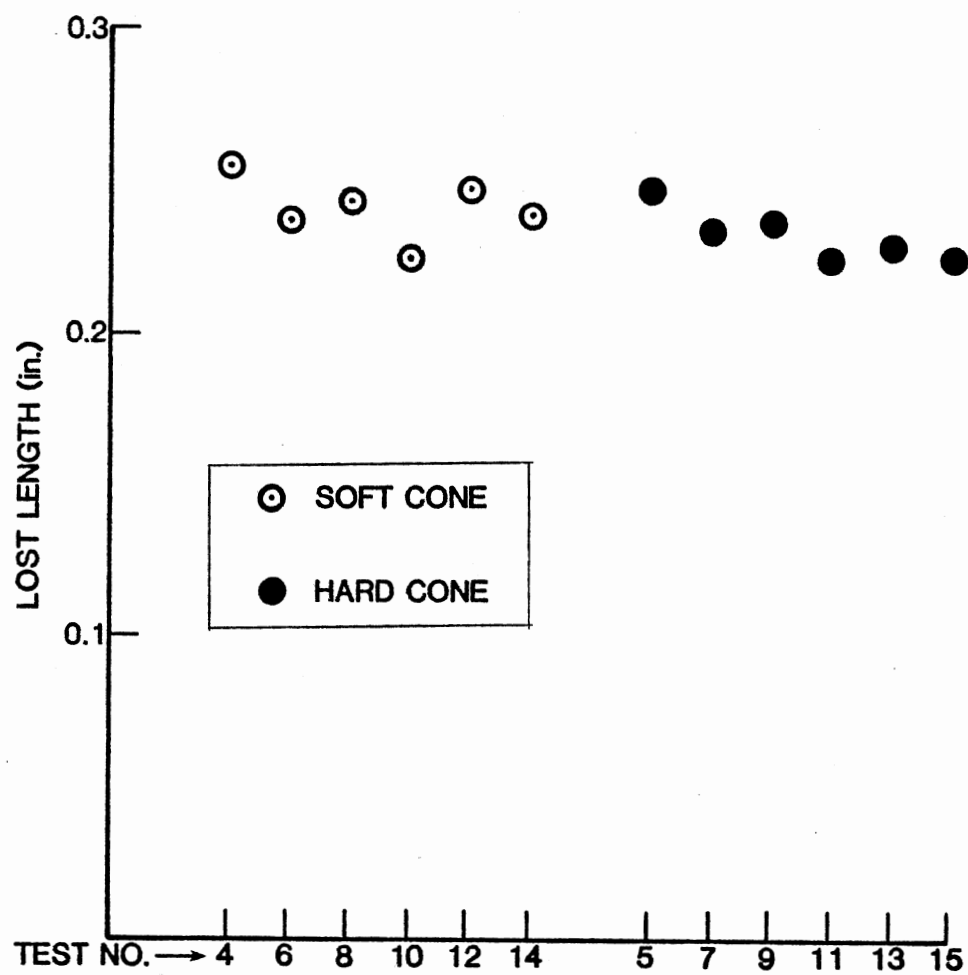


Fig. 62. Lost Lengths of Test Cones

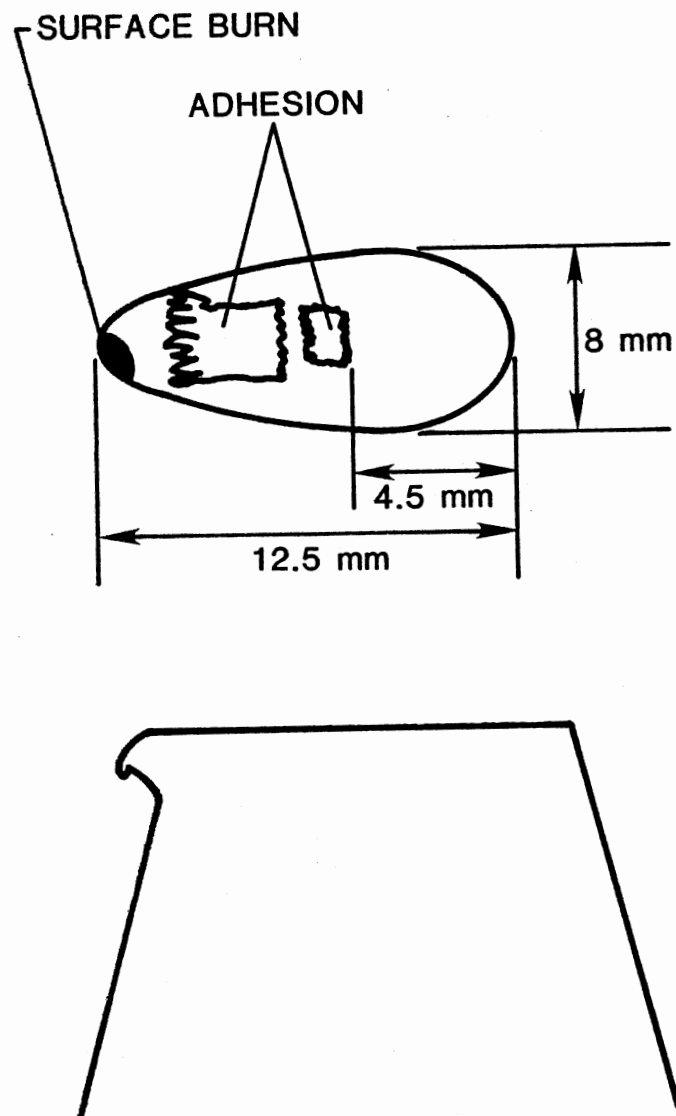


Fig. 63. Deformed Surface of Soft Cone

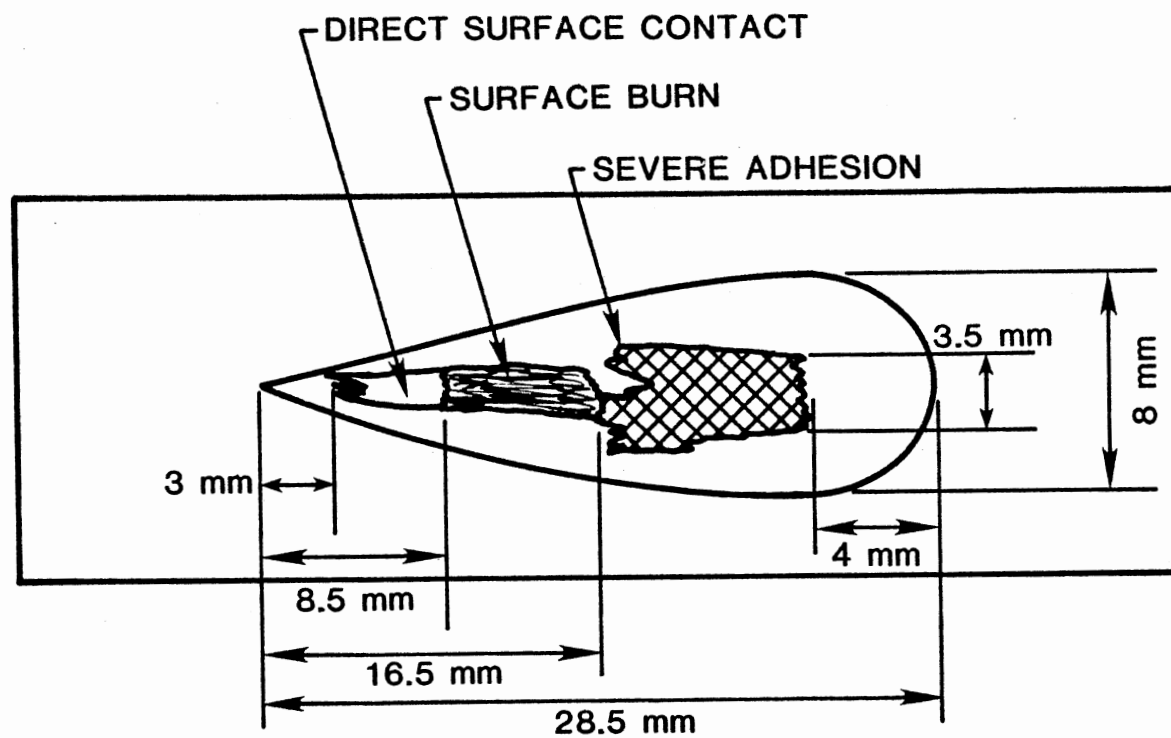


Fig. 64. Plate Surface Imprint Made by Soft Cone

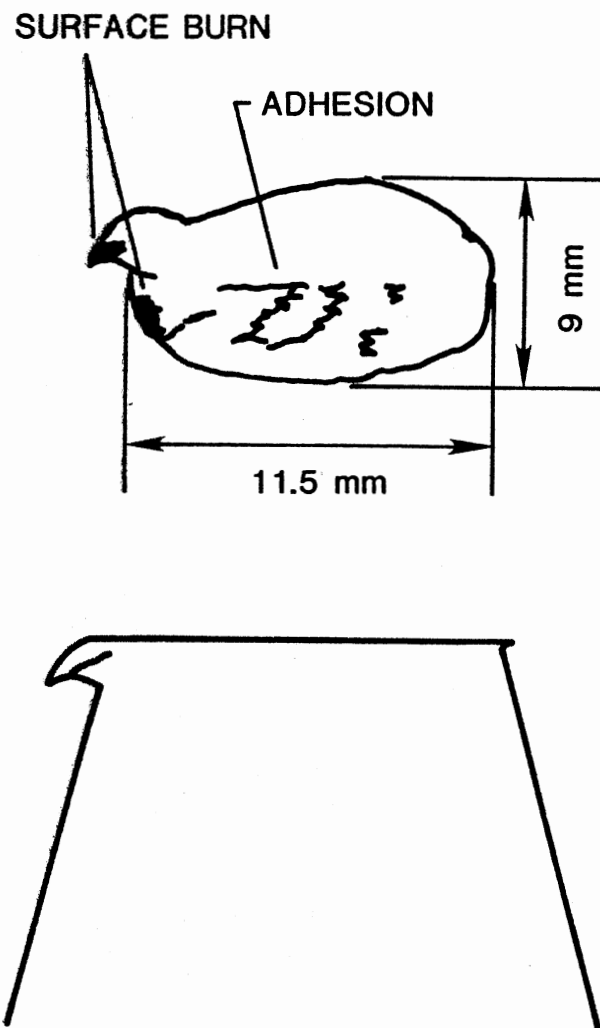


Fig. 65. Deformed Surface of Hard Cone

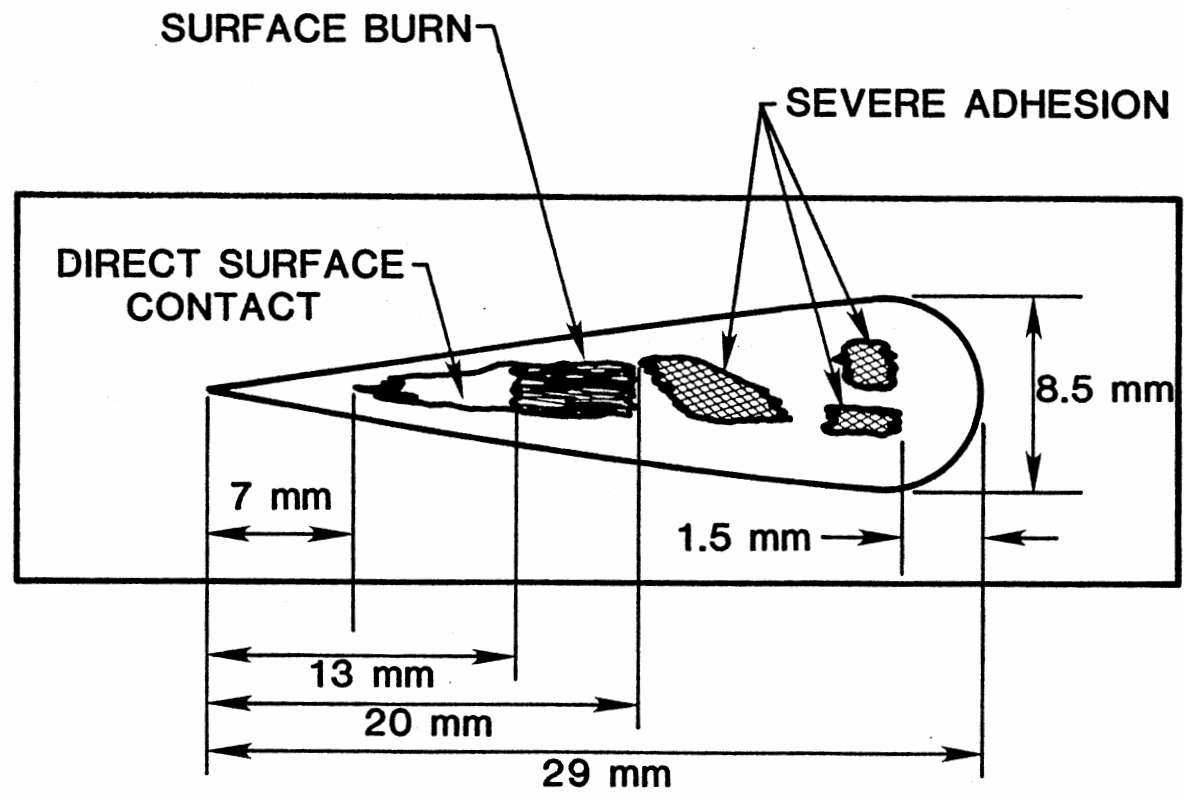


Fig. 66. Plate Surface Imprint Made by Hard Cone

For all other test plates, the same pattern of surface imprint was observed; i.e., no surface damage occurred in the initial region, direct surface contact started to cause a slight scratch, burning started due to high temperature, and severe adhesion occurred. The adhesion stopped before the plate stopped, and a mirror-smooth surface is observed in the last region of the imprint. Fig. 67 represents the general pattern of the imprint on the plate surface. In Fig. 67, average measurements for the different regions in the imprint are shown for both soft and hard cones.

An analysis of the experimental test is presented next. When weight M_1 reaches the weight receiver, its final velocity v_f is expressed by:

$$v_f = \sqrt{2gL} \quad (51)$$

where

g = acceleration

L = height of weight M_1 for free fall

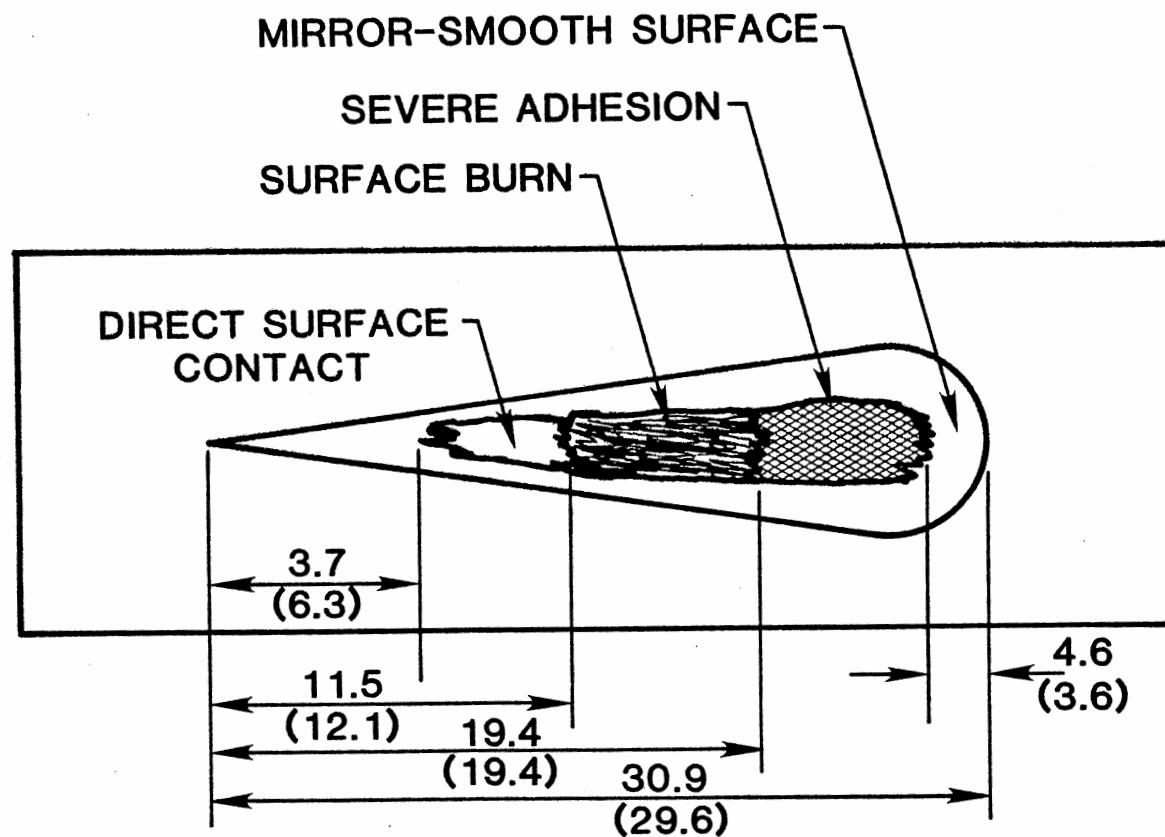
from the energy equation. Due to the impact from weight M_1 , weight M_1 by itself, the weight receiver, slider B, slider A, and the plate start to move together. The initial velocity of the total mass is expressed by:

$$v_0 = \frac{m_1}{m_1 + m_2} v_f \quad (52)$$

where

v_0 = initial velocity of combined mass M_1 and M_2

m_1 = mass of weight M_1



UNIT: mm

30.9 = IMPRINT TOTAL LENGTH BY SOFT CONE

(29.6) = IMPRINT TOTAL LENGTH BY HARD CONE

Fig. 67. General Pattern of Plate Surface Imprint

m_2 = mass of weight receiver, slider B, slider A, and plate (M_2)
from the momentum equation.

From the geometries of the test equipment and the test specimens,
the deformed surface area of the cone is expressed as a function of
sliding distance X ,

$$A = 0.09 \pi X^2 \left(\tan \frac{\theta_s}{2} \right)^2 \quad (53)$$

where

A = deformed surface area of cone

θ_s = base angle of asperity (cone angle)

Considering that the force acting on top of the cone is always in balance
with the material yield strength times deformed area, an energy equation
is derived for the deforming process of the cone,

$$\begin{aligned} \frac{1}{2} (m_1 + m_2) v_0^2 &= \frac{1}{2} (m_1 + m_2) v^2 \\ &+ \int_0^X 0.09 \pi X^2 \left(\tan \frac{\theta_s}{2} \right)^2 T_y dX \end{aligned} \quad (54)$$

where

T_y = yield strength of material

Eq. (54) is modified to calculate a velocity at the distance X .

$$v = \sqrt{v_0^2 - \frac{0.06 \pi X^3 \left(\tan \frac{\theta_s}{2} \right)^2 T_y}{(m_1 + m_2)}} \quad (55)$$

Eq. (54) also gives an equation to calculate the maximum sliding distance.

$$X_{\max} = \left[\frac{(m_1 + m_2) v_0^2}{0.06\pi \left(\tan \frac{\theta}{2}\right)^2 T_y} \right]^{1/3} \quad (56)$$

where

X_{\max} = maximum sliding distance

The final velocity of weight M_1 is calculated to be 666 cm/sec from Eq. (51) with $g = 980 \text{ cm/sec}^2$ and $L = 226 \text{ cm}$. Then the initial velocity of the combined mass of M_1 and M_2 is 486 cm/sec from Eq. (52) with $m_1 = 35 \text{ kg}$ and $m_2 = 13 \text{ kg}$. With a yield strength of 39 kpsi for the soft cone, the maximum sliding distance is calculated to be 4.07 cm. For the hard cone, a maximum sliding distance is 3.08 cm with a yield strength of 66 kpsi.

The actual sliding distance for the soft cone was 3.09 cm, which is 76 percent of the theoretical distance. The actual sliding distance for the hard cone was 2.96 cm, which is 96 percent of the theoretical distance. A larger discrepancy between the actual and theoretical distances on the soft cone is considered to be due to the larger ductile expansion of the conical shape.

By knowing the boundary conditions (an initial velocity of 486 cm/sec at $X = 0$ and a final velocity of 0 at $X = 3.09 \text{ cm}$ for the soft cone), the velocity at the distance X can be calculated from Eq. (55). The velocity versus sliding distance for the soft cone is shown in Fig. 68.

With the boundary conditions (an initial velocity of 486 cm/sec at $X = 0$ and a final velocity of 0 at $X = 2.96 \text{ cm}$), the velocity versus

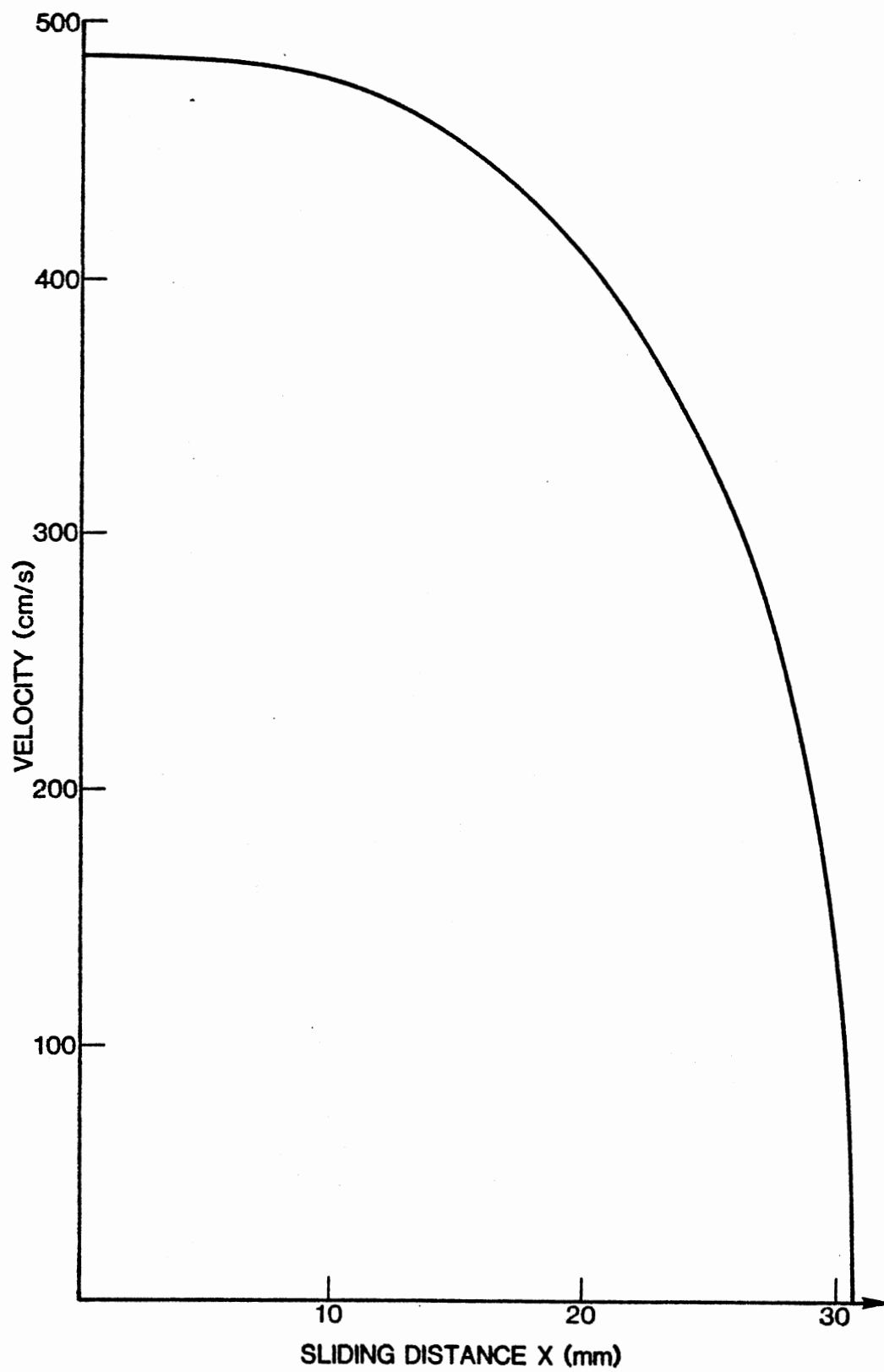


Fig. 68. Velocity Profile with Soft Cone

sliding distance is obtained for the hard cone and is depicted in Fig. 69.

Since the average sizes of the different regions in the imprint on the plate surface (direct surface contact region, burning region, severe adhesion region, and mirror-smooth surface region) are known for both soft and hard cones, the sliding velocities where these regions started can be obtained. Table XV lists the velocities for the different regions. From this table, note that the initial sliding velocities of the regions are quite similar for both soft and hard cones. This reveals that the sequence and the pattern with which these different sliding surface modes occur are similar regardless of the hardness of the materials in the given test condition.

The analysis verifies that direct contact of the sliding surfaces occurs at a sliding velocity of more than 480 cm/sec even with the presence of a lubricant. This is important because it implies that hydrodynamic lubrication cannot be assured only with high sliding velocity.

Another remarkable finding is that severe adhesion stopped at a sliding velocity of around 290 cm/sec. Then a mirror-smooth surface was maintained afterward despite high contact pressure. A sliding velocity of 290 cm/sec is still a high velocity; nonetheless, the severe adhesion was discontinued. This leads to a few important remarks for the study of surface contact wear.

The test wear condition was a single mode. The sliding surface was rubbed by the other surface only once. Heat was generated due to sliding friction; however, it immediately dissipated. In the burning region, there is no doubt that the temperature was high enough to burn the surface, but heat generation was not sufficient enough to maintain the adhesion when the velocity decreased to 290 cm/sec in the single sliding mode.

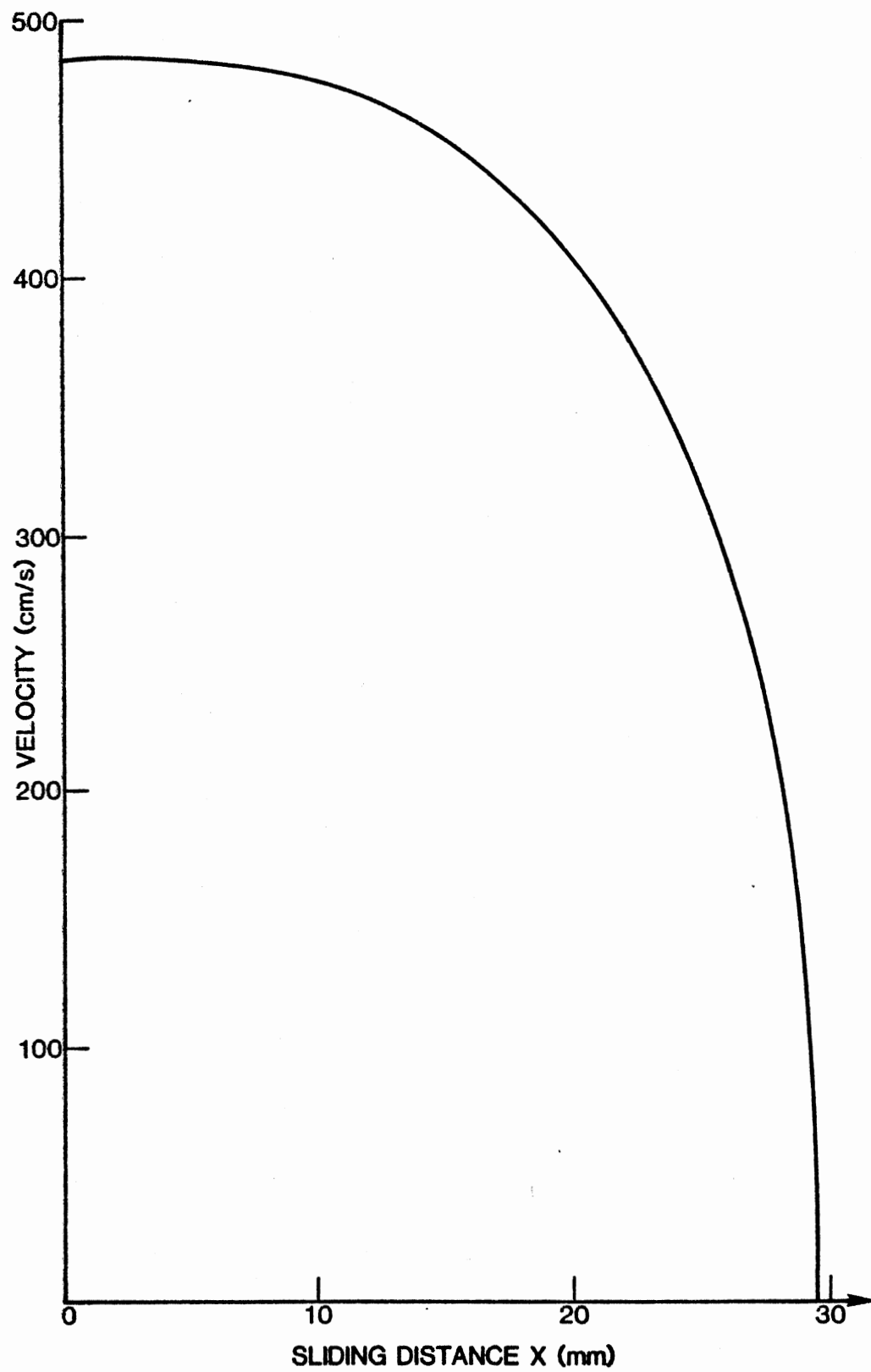


Fig. 69. Velocity Profile with Hard Cone

TABLE XV

IMPRINT REGIONS AND CORRESPONDING SLIDING VELOCITIES

| REGION | SOFT CONE | | HARD CONE | |
|---------------------------|------------------|--------------------|------------------|--------------------|
| | DISTANCE (mm) | VELOCITY (cm/s) | DISTANCE (mm) | VELOCITY (cm/s) |
| DIRECT SURFACE CONTACT | 3.7 | 486 | 6.3 | 482 |
| BURNING | 11.5 | 475 | 12.1 | 470 |
| SEVERE ADHESION | 19.4 | 418 | 19.4 | 416 |
| MIRROR-SMOOTH SURFACE | 26.3 | 295 | 26.0 | 286 |

In a multiple sliding mode, where the sliding surface is rubbed by the other surface repeatedly, a large amount of heat is accumulated near the sliding surface region to raise the temperature until heat generation and heat dissipation reach an equilibrium state, and adhesion occurs at a relatively low sliding velocity.

The above considerations imply the possibility that the sliding materials, lubricant, and operating conditions are carefully interrelated. Thus, the heat generation and the heat dissipation reach a state of equilibrium where no further accumulation of heat occurs near the sliding region and no adhesion is experienced even with a multiple sliding mode at a sliding velocity as high as 290 cm/sec.

The heat generated due to friction raises the temperature of the contacting surfaces instantaneously. Since the heat immediately dissipates, the neighboring material does not experience the high temperature, but the contacting surface continues to experience the high temperature as long as sliding contact is maintained. This high temperature associated with the contacting surface is referred to as the "flash temperature."

Rabinowicz (18) developed the equation with which the flash temperature can be calculated:

$$T_f = \frac{9400\mu Ev}{J(k_1 + k_2)} \quad (57)$$

where

T_f = flash temperature

μ = coefficient of friction

E = surface energy

v = sliding velocity

J = mechanical equivalent of heat

k_1, k_2 = thermal conductivities of two contacting materials

He also gave typical values for the parameters in Eq. (57) in the case of a steel-on-steel sliding condition. A typical value for the coefficient of friction is 0.5, surface energy is 1500 dyne/cm, and thermal conductivities of the two contacting materials are both 0.11 cal/°C cm sec. He gave a value of 0.75 °C/cm/sec for T_f/v for a steel-on-steel sliding condition.

Using Eq. (57) with the given parameters, a flash temperature chart is developed for the given test conditions. Fig. 70 is the flash temperature chart for the soft cone. The flash temperature with friction coefficients of 0.1, 0.2, 0.3, 0.4, 0.5, and 0.6 is plotted. It is apparent in Fig. 70 that a higher flash temperature is obtained when the coefficient of friction is large.

Rabinowicz assumed that the coefficient of friction was always 0.5 for steel-on-steel sliding; however, the coefficient of friction may change according to the sliding condition and surface conditions. From the static deformation test of surface asperity presented in the previous section, the average coefficient of friction of the soft cone on the plate is 0.19. For sliding that occurs under direct surface contact conditions, one of the experimental data showed that the friction coefficient for steel-on-steel contact was 0.42 and it increased as high as 0.57 [33]. Based on the above knowledge, the coefficient of friction is considered to be 0.42 at the beginning of the direct surface contact region, 0.57 after the direct surface contact region, and the flash temperature is estimated. The dotted curve in Fig. 70 shows the estimated flash temperature with a varying coefficient of friction. The

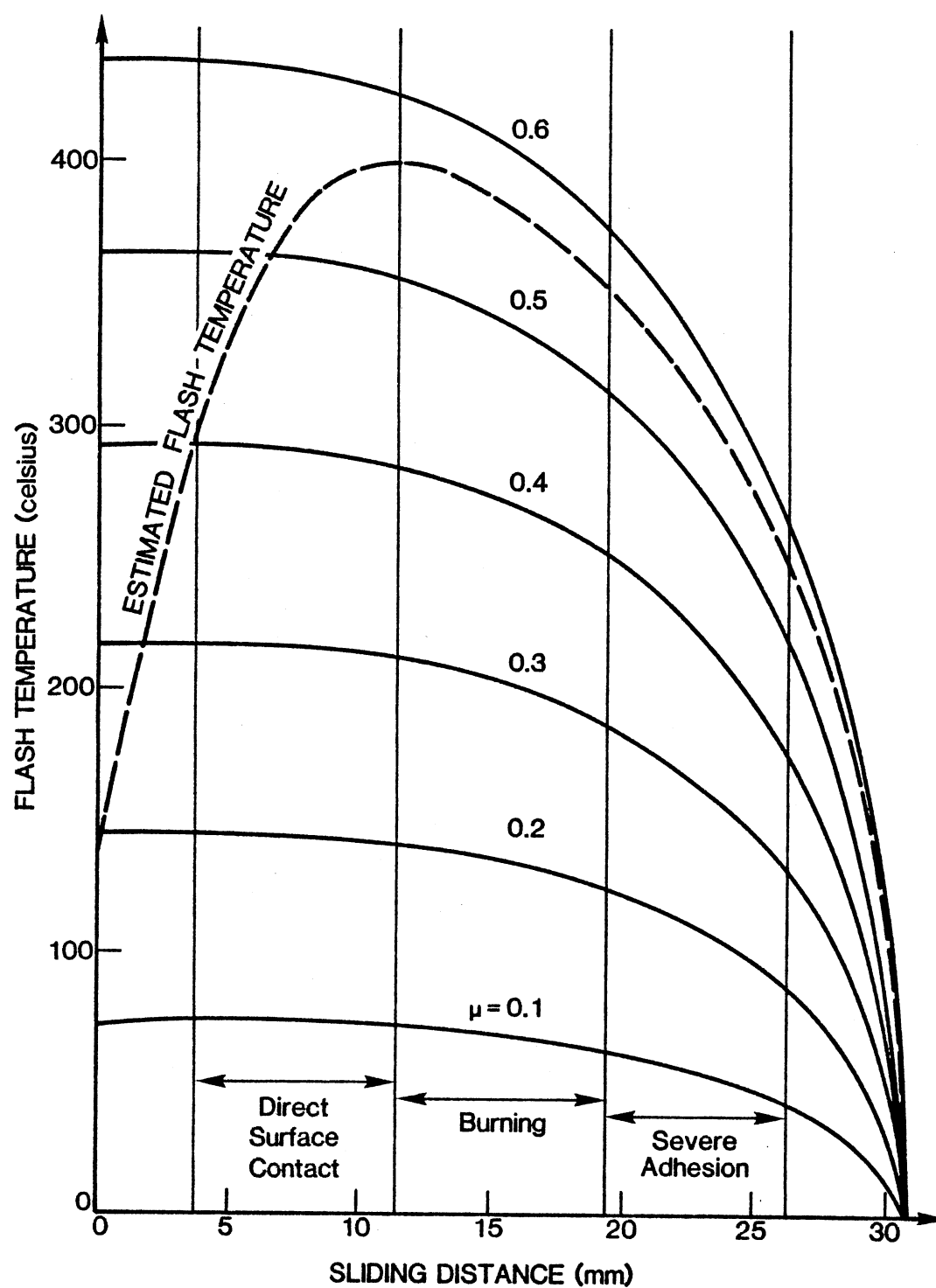


Fig. 70. Flash Temperature Chart for Soft Cone

estimated curve indicates that a maximum temperature of 400°C is reached at the beginning of the burning region.

Fig. 71 is the flash temperature chart for the hard cone. The static deformation test of the surface asperity determined the average coefficient of friction for the hard cone of the plate to be 0.25. The estimated flash temperature is derived for the hard cone like the soft cone. The dotted curve in Fig. 71 shows the estimated flash temperature for the hard cone with a varying coefficient of friction. At the beginning of the burning region, the flash temperature reaches 400°C .

Table XVI summarizes estimated flash temperatures for different regions with a varying coefficient of friction for both soft and hard cones. The estimated flash temperatures are similar for the soft and the hard cones in spite of their difference in material hardness.

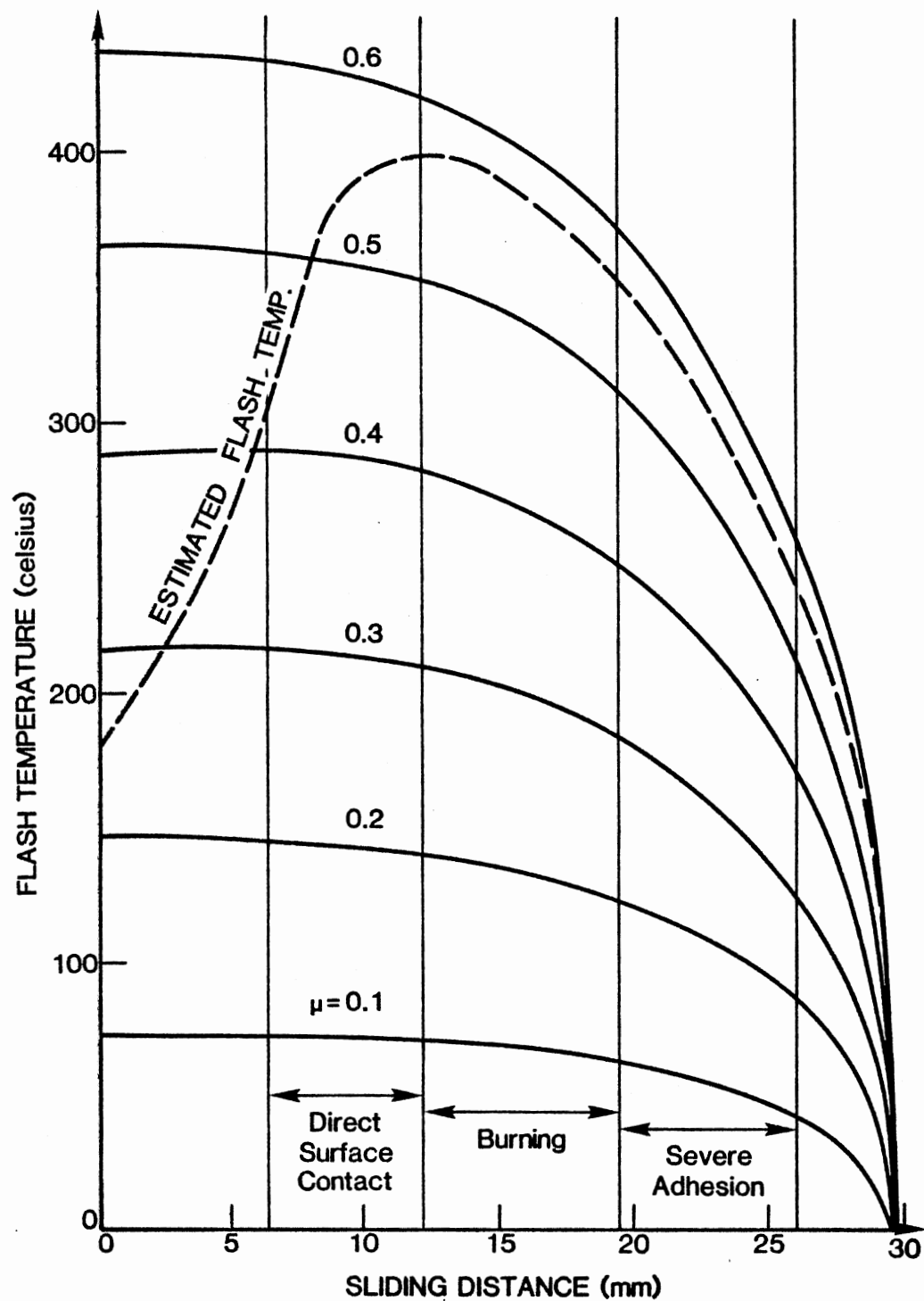


Fig. 71. Flash Temperature Chart for Hard Cone

TABLE XVI

ESTIMATED FLASH TEMPERATURES FOR SOFT AND HARD MATERIALS

| REGION | SOFT CONE | | HARD CONE | |
|------------------------|-------------------------|------------------|-------------------------|------------------|
| | COEFFICIENT OF FRICTION | FLASH TEMP. (°C) | COEFFICIENT OF FRICTION | FLASH TEMP. (°C) |
| INITIAL | 0.19 ~ 0.42 | 140 ~ 300 | 0.25 ~ 0.42 | 180 ~ 300 |
| DIRECT SURFACE CONTACT | 0.42 ~ 0.57 | 300 ~ 400 | 0.42 ~ 0.57 | 300 ~ 400 |
| BURNING | 0.57 | 400 ~ 350 | 0.57 | 400 ~ 350 |
| SEVERE ADHESION | 0.57 | 350 ~ 250 | 0.57 | 350 ~ 240 |
| MIRROR-SMOOTH SURFACE | 0.19 | LESS THAN 250 | LESS THAN 0.25 | LESS THAN 240 |

CHAPTER V

VERIFICATION OF ABRASIVE WEAR MODEL

Experimental Considerations

The developed abrasive wear model enables us to calculate the volume rate of abrasive wear with given parameters of abrasive conditions. The cutting depth of the surface material by the abrasive particle is first calculated by Eq. (28). The volume rate of abrasive wear is given by Eq. (17). The model clearly shows the effects of lubricating fluid lubricity, surface hardness, abrasive particle hardness, and lubricating fluid film thickness on abrasive wear.

To prepare for the experimental verification of the developed model, appropriate values are assigned for these parameters. The effects of the parameters on abrasive wear are discussed in this section.

Three materials, soft steel, medium steel, and hard steel, are considered with their shear yield strengths of 39 kpsi, 66 kpsi and 91 kpsi, respectively. The angle of the particle with respect to the sliding surface is assumed to be 45, 60, and 75 deg. Calculation of the cutting depth and the indentation depth is achieved for four values of the coefficient of friction -- 0, 0.1, 0.2, and 0.3.

To begin the calculation, combinations of the sliding surfaces should be first determined. Three combinations are considered:

1. Both surfaces are medium steel.

2. One surface is soft steel and the other is medium steel.
3. One surface is medium steel and the other is hard steel.

For the last two combinations, two different situations can be considered for each of them:

- 2a. The soft steel surface is cut, and the medium steel surface is indented by abrasive particles.
- 2b. The medium steel surface is cut, and the soft steel surface is indented by abrasive particles.
- 3a. The medium steel surface is cut, and the hard steel surface is indented by abrasive particles.
- 3b. The hard steel surface is cut, and the medium steel surface is indented by abrasive particles.

One of the two situations actually occurs for both combinations. The situation which requires less energy actually occurs. For three different particle angles, 45, 60 and 75 degs, the equilibrium force levels are calculated from Eq. (28) for each of the above situations assuming a null coefficient of friction. Results of the calculation are summarized in Table XVII. Since the situation with less energy required actually happens, the soft steel is cut, and the medium steel is indented at particle angles of 45 and 60 degs. However, the medium steel is cut, and the soft steel is indented at a particle angle of 75 deg. Similarly, the medium steel is cut, and the hard steel is indented at particle angles of 45 and 60 degs; however, the hard steel is cut, and the medium steel is indented at a particle angle of 75 degs.

In Table XVII, note that the equilibrium force at a particle angle of 60 deg is about 3.5 times the force at a particle angle of 45 deg. The force at a particle angle of 75 deg is about 7 times the force at a

TABLE XVII
EQUILIBRIUM FORCES FOR CUTTING AND INDENTATION

| EQUILIBRIUM FORCE LEVEL (LBS) | | | |
|---|----------------|--------|---------|
| SITUATION | PARTICLE ANGLE | | |
| | 45° | 60° | 75° |
| SOFT STEEL CUT MEDIUM STEEL INDENTED | 13.35d | 46.49d | 95.84d |
| MEDIUM STEEL CUT SOFT STEEL INDENTED | 19.79d | 55.44d | 91.30d |
| MEDIUM STEEL CUT HARD STEEL INDENTED | 22.21d | 74.98d | 148.42d |
| HARD STEEL CUT MEDIUM STEEL INDENTED | 28.31d | 83.36d | 143.46d |

d=PARTICLE SIZE IN INCH,

particle angle of 45 deg. This leads to the observation that any disturbances acting on the particle to break the equilibrium state tend to reduce the particle angle and decrease the energy state. The particle angle is considered to be determined by the roughness of the surfaces that trap the particle. Hence, reducing surface roughness helps to decrease the particle angle and, consequently, decreases abrasive wear.

Further examination of the equilibrium force levels with friction coefficients of 0.1, 0.2, and 0.3 reveals that the cutting and indenting conditions are about the same as that with a null coefficient of friction.

With the knowledge of the above findings, the cutting depth and the indentation depth are calculated and summarized in Table XVIII. The particle hardness required to cut the surface as well as to indent the surface is also tabulated. With a coefficient of friction of 0.1, the particle hardness should be more than 2.21 times the hardness of the cut surface and 3.53 times the hardness of the indented surface. If the particle hardness is less than that, the particle is sheared off, and no abrasive wear occurs.

When the coefficient of friction increases to 0.3, the particle hardness should be more than 2.69 times the hardness of the cut surface and 3.91 times the hardness of the indented surface. Thus, a fluid with better lubricity allows the abrasive particles to be less hard to cause abrasive wear. In other words, the worse lubricity of lubricant, the harder the abrasive particles ought to be to cause abrasive wear.

In Table XVIII, note that the cutting depth is maximum at a particle angle of 60 deg for all three combinations. It is interesting to see

TABLE XVIII

CUTTING DEPTH AND INDENTATION DEPTH IN ABRASIVE WEAR

| PARTICLE ANGLE | COEFFICIENT OF FRICTION | PARTICLE HARDNESS FOR CUTTING | PARTICLE HARDNESS FOR INDENTATION | MEDIUM STEEL CUT MEDIUM STEEL INDENTED | | SOFT STEEL CUT MEDIUM STEEL INDENTED | | MEDIUM STEEL CUT SOFT STEEL INDENTED | | MEDIUM STEEL CUT HARD STEEL INDENTED | | HARD STEEL CUT MEDIUM STEEL INDENTED | |
|----------------|-------------------------|-------------------------------|-----------------------------------|---|-------------------|---|-------------------|---|-------------------|---|-------------------|---|-------------------|
| | | | | CUTTING DEPTH | INDENTATION DEPTH | CUTTING DEPTH | INDENTATION DEPTH | CUTTING DEPTH | INDENTATION DEPTH | CUTTING DEPTH | INDENTATION DEPTH | CUTTING DEPTH | INDENTATION DEPTH |
| 45° | 0 | 2.0 | 3.15 | 0.115d | 0.016d | 0.121d | 0.010d | | | 0.119d | 0.012d | | |
| | 0.1 | 2.21 | 3.53 | 0.116 | 0.016 | 0.122 | 0.010 | | | 0.120 | 0.012 | | |
| | 0.2 | 2.44 | 3.81 | 0.115 | 0.016 | 0.121 | 0.010 | | | 0.119 | 0.012 | | |
| | 0.3 | 2.69 | 3.91 | 0.114 | 0.017 | 0.121 | 0.011 | | | 0.118 | 0.013 | | |
| 60° | 0 | 2.0 | 3.15 | 0.258 | 0.128 | 0.298 | 0.087 | | | 0.284 | 0.102 | | |
| | 0.1 | 2.21 | 3.53 | 0.259 | 0.127 | 0.299 | 0.086 | | | 0.285 | 0.101 | | |
| | 0.2 | 2.44 | 3.81 | 0.257 | 0.129 | 0.298 | 0.088 | | | 0.283 | 0.103 | | |
| | 0.3 | 2.69 | 3.91 | 0.251 | 0.135 | 0.293 | 0.093 | | | 0.278 | 0.108 | | |
| 75° | 0 | 2.0 | 3.15 | 0.247 | 0.299 | | | 0.179d | 0.367d | | | 0.204d | 0.341d |
| | 0.1 | 2.21 | 3.53 | 0.249 | 0.297 | | | 0.181 | 0.365 | | | 0.206 | 0.339 |
| | 0.2 | 2.44 | 3.81 | 0.245 | 0.300 | | | 0.178 | 0.368 | | | 0.203 | 0.342 |
| | 0.3 | 2.69 | 3.91 | 0.236 | 0.310 | | | 0.169 | 0.376 | | | 0.194 | 0.351 |

d = PARTICLE SIZE

that the cutting depth is maximum at a coefficient of friction at 0.1 instead of zero for all the cases. As the coefficient of friction increases from 0.1, the cutting depth decreases and the indentation depth increases in all the situations tabulated in Table XVIII.

An increase of the cutting depth due to a change of the coefficient of friction from 0.1 to 0.3 at a particle angle of 45 deg is an average of 1.4 percent. At a particle angle of 60 deg, it is an average of 2.5 percent; and, at a particle angle of 75 deg, it is an average of 5.9 percent. Thus, the larger the particle angle, the larger the increase of the cutting depth due to the increasing coefficient of friction.

Development of Experimental Facility

The Gamma Falex system was developed to investigate wear of sliding surfaces under boundary lubrication conditions. The sliding velocity of the Gamma Falex system is as low as 9.6 cm/sec to ensure boundary lubrication. The fluid film thickness under boundary lubrication is considered null so that the sliding surfaces contact each other, and all the surface load is supported by contacting surface asperities.

The abrasive wear theory developed here reveals that the clearance between the sliding surfaces is one of the major factors affecting abrasive wear generation. If the clearance is null and no abrasive particles get into the clearance, no abrasive wear occurs although surface contact wear takes place. Hence, ensuring a certain clearance between the sliding surfaces is important for the experimental equipment to verify the abrasive wear theory.

A variable speed hydraulic motor was installed on the Gamma Falex system so that the system could produce rotating speeds of the journal

up to 3200 rpm. To inject abrasive particles and maintain a specific concentration of the abrasive particles in the test system, a peristaltic pump was installed with a fluid circulation circuit. The variable speed Gamma Falex system used for the abrasive wear test is illustrated in Fig. 72.

Experimental Tests

The first experimental test was conducted with MIL-L-2104 mineral base fluid. The experiment was initiated under clean conditions where no abrasive particles were injected in the test system. Fig. 73 shows test results under clean conditions.

The test was started with a rotating journal speed of 580 rpm and test load of 100 lbs. The test load of 100 lbs was maintained for most of the test unless otherwise specially noted. The test at 580 rpm was continued for 10 minutes and the wear reading versus test time in that test condition is depicted in Fig. 73. The wear rate is 0.5, which is the wear reading divided by the test time at 580 rpm. Thus, a unit of the wear rate in this test is wear reading divided by minutes. After a 10-min operation at 580 rpm the rotating speed of the journal was doubled to 1160 rpm, and the test was continued for 20 min at the same test load of 100 lb. When the rotating speed was increased from 580 rpm to 1160 rpm, there was a sudden drop in the wear reading as seen in Fig. 73. This is due to an increase of the fluid film, and the amount of decrease in the wear reading corresponds to the increased fluid film thickness. A wear reading of one is equivalent to 1.625 micrometers of scar depth on the test specimens; and, therefore, a decrease of the wear reading by three indicates an increase in the fluid film of 4.875 micrometres. The

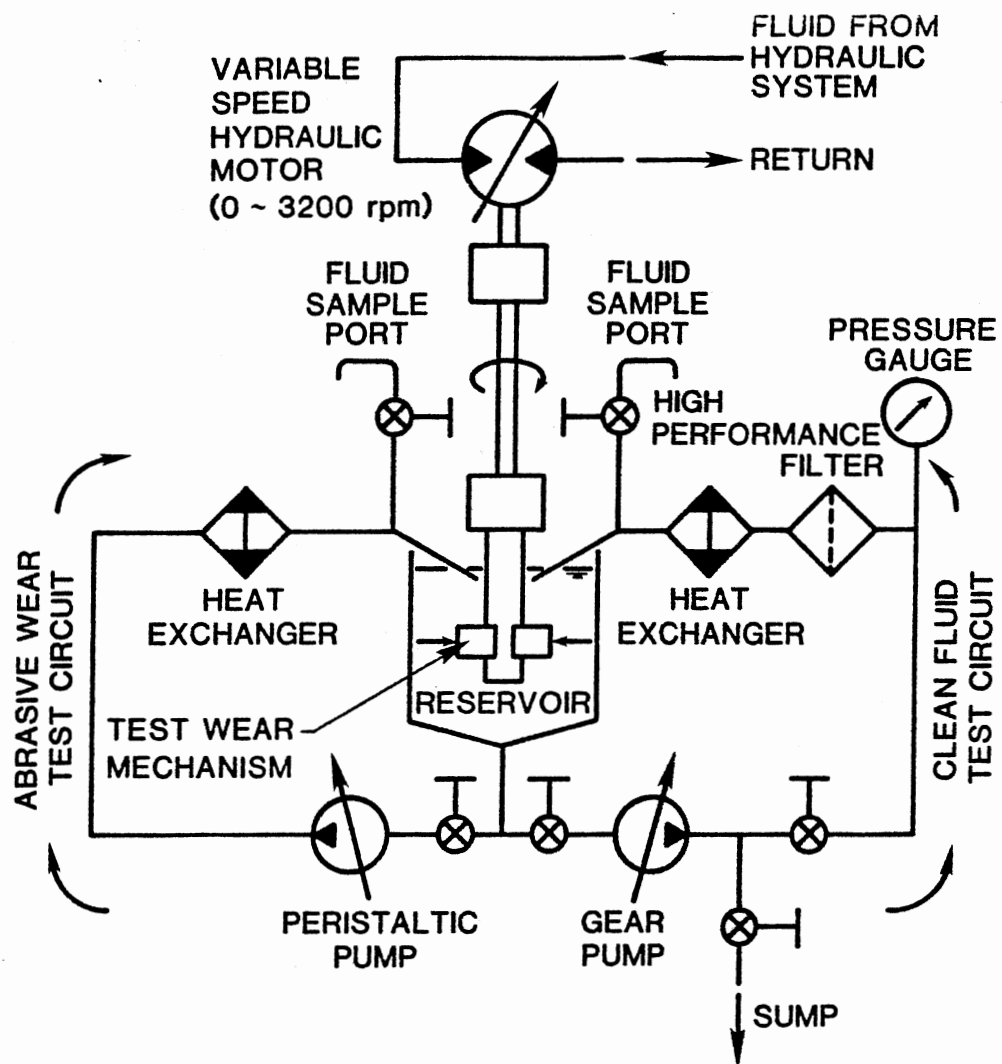


Fig. 72. Variable Speed Gamma Falex System

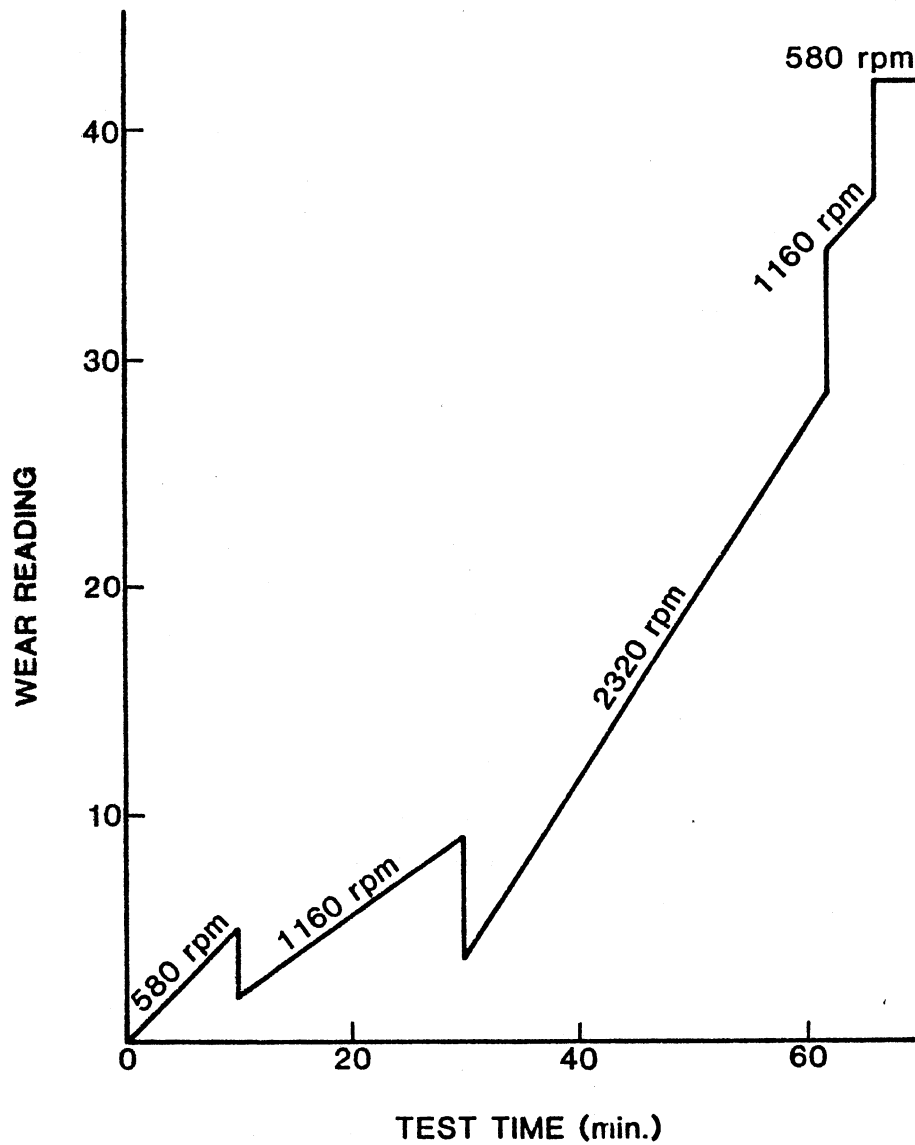


Fig. 73. Initial Clean Test with MIL-L-2104

wear rate at 1160 rpm decreased to 0.35 as observed in the figure. This is considered to be due to an increase of the fluid film. The increased fluid film reduces surface asperity contact.

The rotating speed of the journal was then increased up to 2320 rpm. A decrease of the wear reading by five was observed, which indicates an increase in the fluid film of 8.125 micrometres. The test at 2320 rpm was continued for 32 min, and the wear rate was observed to be 0.77, as can be seen in the figure. The reason for the high wear rate in spite of the increased fluid film is considered to be due to a high sliding velocity. Although the increased fluid film significantly decreased the surface asperity contact, there were still asperity junctions. This condition is often referred as a mixed lubrication condition.

After the test at 2320 rpm, the rotating speed was decreased to 1160 rpm, and there was an increase in the wear reading. An increase in the wear reading by 6.5 corresponds to a decrease of the fluid film by 10.563 micrometres. The rotating speed was further reduced to 580 rpm, and an increase in the wear reading by 5 was observed, which indicates a decrease of the fluid film by 8.125 micrometres.

From the geometry of the test specimens, the rotating speed can be interpreted in relation to the sliding velocity of the contacting surfaces. Table XIX tabulates the rotating speeds with the corresponding sliding velocities.

The test in the clean condition was terminated after 70 min. After completion of the clean test, the same test specimens and the same fluid were used to conduct the test with abrasive particles. Classified AC Fine Test Dust, 0-5 micrometres in size with a concentration of 300 mg/L, was injected into the test fluid. Abrasive particles of this size

TABLE XIX

ROTATING SPEEDS OF THE JOURNAL AND
CORRESPONDING SLIDING VELOCITIES

| ROTATING SPEED (rpm) | SLIDING VELOCITY (cm/sec) |
|-------------------------|------------------------------|
| 290 | 9.6 |
| 580 | 19.3 |
| 1160 | 38.6 |
| 2320 | 77.1 |

include particles less than and equal to 5 micrometres.

The filter circuit of the test system was isolated, and only a peristaltic pump was activated to circulate the contaminated fluid without changing the abrasive concentration. The test was conducted at 580 rpm, 1160 rpm, and 2320 rpm. The test continued at each rotating speed for 10 min. The abrasive test with 0-5 micrometres of ACFTD was completed after 30 min. The peristaltic pump was turned off, the filter circuit was connected to the test system, and the abrasive particles were eliminated by the filter. After 10 min of filtration, the clean test was conducted with the same test specimens and the same test fluid at 580 rpm, 1160 rpm and 2320 rpm. The test was continued at each rotating speed for 10 min. Test results of the 30-min, 0-5 micrometre abrasive test followed by 10-min filtration and 30-min clean test are illustrated in Fig. 74.

During the abrasive test at 580 rpm, the wear rate was 0.6, which is not much different from the clean test in Fig. 73. This implies that the effect of the abrasive particles is not significant at 580 rpm. In other words, abrasive particles do not cause severe abrasive wear under boundary lubrication. At 1160 rpm, the wear rate increased to 0.9, which indicates a slight effect of the abrasive particles, but it is not yet significant.

When the rotating speed was increased to 2320 rpm, a drastic increase in the wear rate was observed, Fig. 74. The wear rate was 3.5, which is much higher than the wear rate at 2320 rpm in the clean fluid. This extremely high wear rate is considered to be due to severe abrasive wear. The rotating speed increased the fluid film thickness, and the clearance was increased. The increased clearance was the right

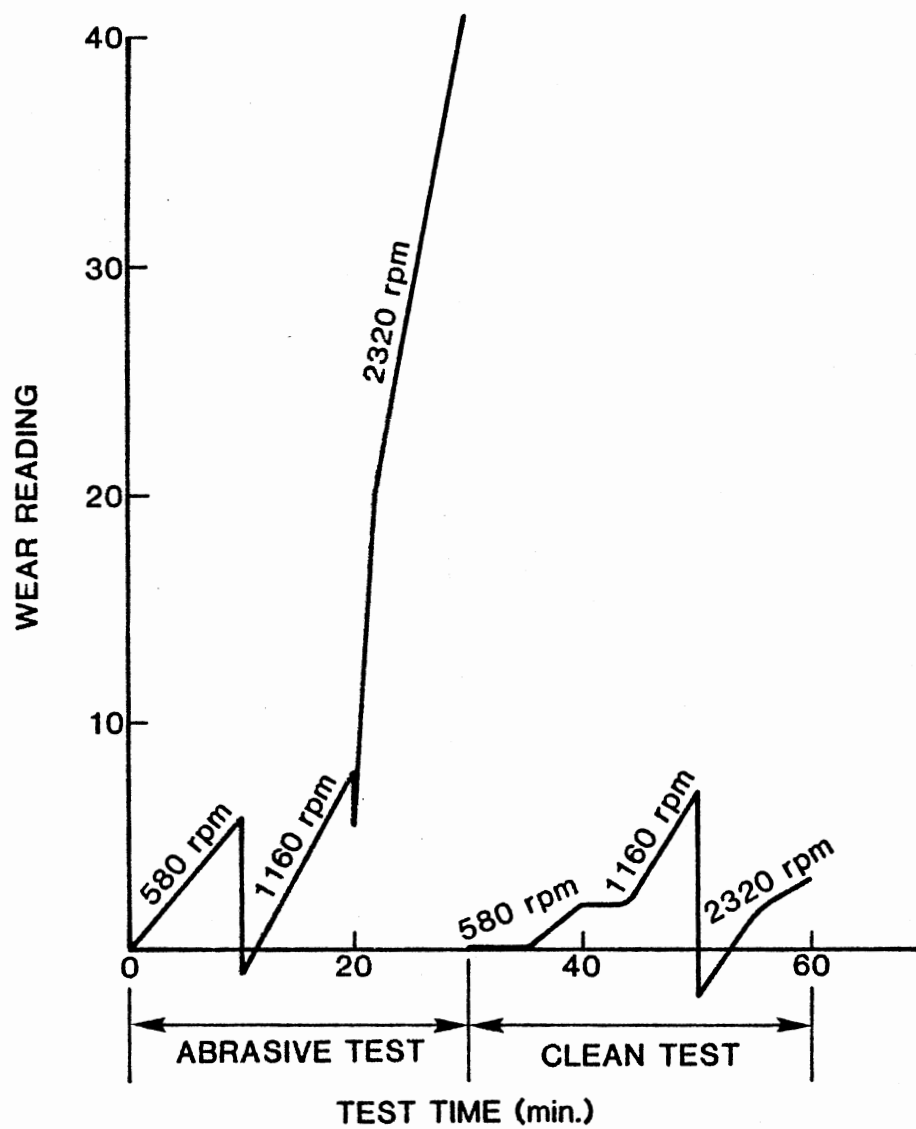


Fig. 74. 0-5 Micrometres Abrasive Test and Clean Test with MIL-L-2104

size for most of the abrasive particles to migrate into the clearance and cause severe abrasive wear.

At the end of the abrasive test, a fluid sample was extracted from the test system, and ferrographic analysis was conducted. Wear particles from both surface contact wear and abrasive wear were observed, which revealed that both surface contact wear and abrasive wear occurred during the abrasive wear test. Particles from surface contact wear have a flake or needle-shape; whereas, particles from abrasive wear have a curly string shape [26].

After filtering the abrasive particles, the wear rates observed were 0.2, 0.5, and 0.5 at 580 rpm, 1160 rpm, and 2320 rpm, respectively. Two reasons are considered for these low wear rates. Since the surface contact area increased significantly, better hydrodynamic lubrication was maintained. Also, abrasive particles were eliminated by the filter, and only surface contact wear occurred.

After the 0-5 micrometre ACFTD test followed by filtration and a clean test, the 0-10 micrometre ACFTD test was conducted. The same specimens were used, and the 0-10 micrometre classified AC Fine Test Dust was injected into MIL-L-2104 mineral base fluid with a concentration of 300 mg/L. The test was conducted in the same manner as the 0-5 micrometre ACFTD test. The test results are shown in Fig. 75.

Notice in Fig. 75 that little wear was observed with the 0-10 micrometer ACFTD at any rotating speed. Wear rates were 0.3, 0.4, and 0.8 at 580 rpm, 1160 rpm, and 2320 rpm, respectively. The low wear rate with the larger size abrasive particles is explained by a change in the contact surface geometry. In the 0-5 micrometre abrasive test, the contact surface was abraded severely, and its area was significantly

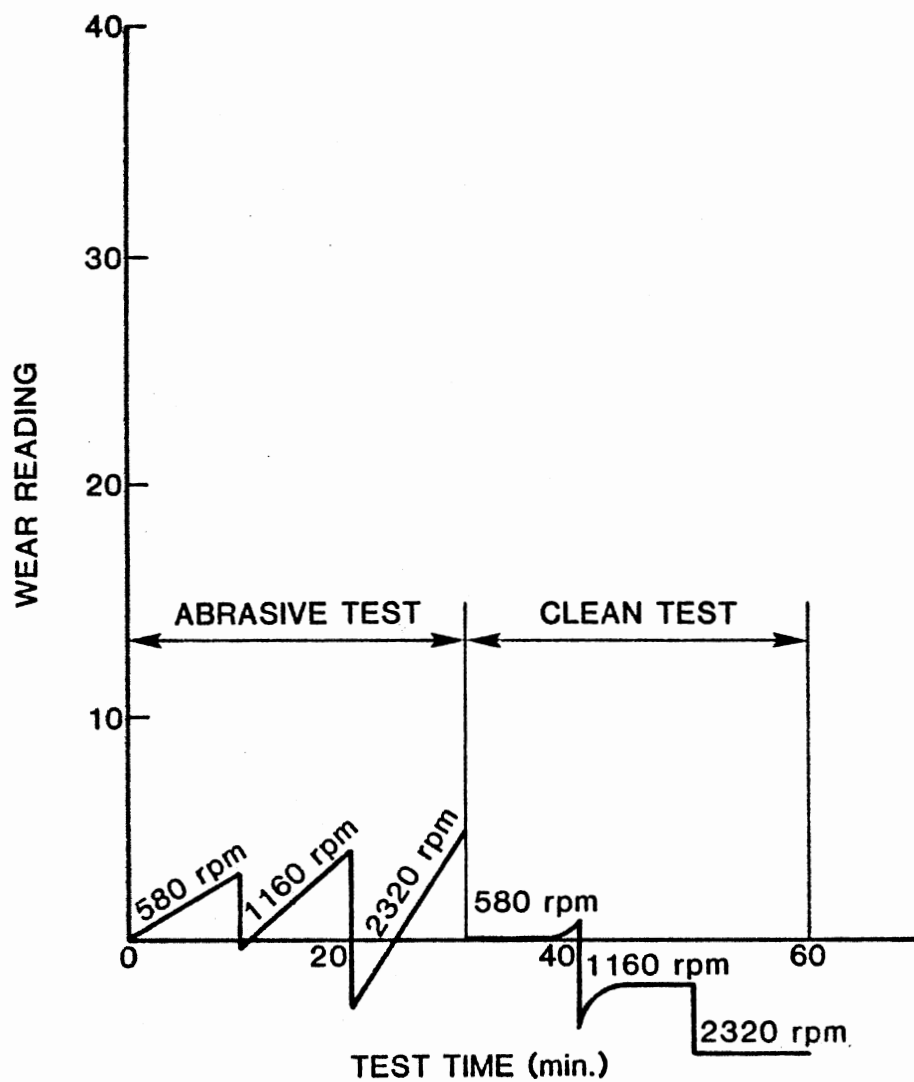


Fig. 75. 0-10 Micrometres Abrasive Test and Clean Test with MIL-L-2104

stretched. In the clean test following the 0-5 micrometre abrasive test, rough surface asperities were rubbed against each other and smooth surfaces were created. Due to the large, smooth contact surfaces, good hydrodynamic lubrication was maintained in the 0-10 micrometre abrasive test where the fluid film was thick enough to prevent the particles of 0-10 micrometres from severely abrading the surfaces.

The above explanation is reinforced by the result of the clean test following the 0-10 micrometres abrasive test, Fig. 75. The clean test showed wear rates of 0.1, 0.2, and zero at 580 rpm, 1160 rpm, and 2320 rpm, respectively. The null wear rate at 2320 rpm indicates perfect hydrodynamic lubrication where no surface asperity contact occurred.

After the 0-10 micrometre abrasive test followed by the clean test was completed, the 0-20 micrometre abrasive test was conducted. The 0-20 micrometre classified AC Fine Test Dust was injected into MIL-L-2104 mineral base fluid with a concentration of 300 mg/L, and the same test specimens were tested at 580 rpm, 1160 rpm, and 2320 rpm in the same manner as the 0-10 micrometre abrasive test. Wear rates were 0.2, zero, and 0.3 at 580 rpm, 1160 rpm, and 2320 rpm, respectively. It is evident that the widened sliding surfaces maintained such a thick hydrodynamic fluid film that even the 0-20 micrometre abrasive particles did not cause severe abrasive wear.

In a manner similar to the first experimental test, five other tests were conducted with various test fluids. The test results of these five tests were interpreted into wear rates of the test specimens and are summarized in Table XX. The second and third tests were conducted with MIL-L-2104 mineral base fluid. The fourth test was with a base stock oil that contains no antiwear additives. The fifth test

TABLE XX

ABRASIVE WEAR TEST RESULTS ON THE VARIABLE SPEED GAMMA FALEX SYSTEM

| TEST NO. | TEST FLUID | ROTATING SPEED | CLEAN TEST | 0-20 μ m TEST | CLEAN TEST | 0-40 μ m TEST | CLEAN TEST | 0-80 μ m TEST | CLEAN TEST | 0-80 μ m 200 lbs. TEST | 0-80 μ m 100 lbs. TEST |
|----------|---------------------------|----------------|-----------------|-------------------|------------|-------------------|------------|-------------------|------------|----------------------------|----------------------------|
| 2 | MIL-L-2104 | 580 rpm | 0.5 | 1.1 | 0.2 | 0.4 | 0.5 | 0.6 | 0.8 | | |
| | | 1160 rpm | 0.33 | 3.5 | 0.25 | 1.1 | 0.5 | 1.2 | 1.9 | | |
| | | 2320 rpm | 4 | 3.2 | 0.5 | 3.8 | 0.65 | 1.7 | 0.6 | | |
| 3 | MIL-L-2104 (SOFT V-BLOCK) | 580 rpm | 0.25 | 0.2 | 0.4 | 0.4 | 0.2 | 0.2 | 0.1 | | |
| | | 1160 rpm | 0.5 | 1.1 | 1.0 | 0.9 | 0.5 | 0.4 | 0.1 | | |
| | | 2320 rpm | 0.75 | 1.4 | 2.5 | 2.1 | 2.0 | 0.7 | 0.4 | | |
| 4 | BASE STOCK OIL | 580 rpm | 0.6 | 0.1 | 0.4 | 0.2 | 0 | 0.4 | | | |
| | | 1160 rpm | 0.25 | 0.3 | 0 | 0 | 0 | 0 | | 2.1 | |
| | | 2320 rpm | 0 | 0 | 0 | 0 | 0 | 0 | | 5.13 | 0.1 |
| 5 | BASE STOCK OIL + 1% ZINC | 580 rpm | 0.3 200 lbs. | | | | | | | | |
| | | 1160 rpm | | | | | | | | 7.5 | |
| | | 2320 rpm | | | | | | | | 4.83 | 2.0 |
| 6 | 95-5 HWBF | 580 rpm | 0.75 | 1.4 | 0.4 | 0.5 | 0.9 | 1.3 | 1.2 | | |
| | | 1160 rpm | 0.5 | 0.9 | 0.3 | 1.2 | 0.6 | 1.0 | 1.0 | | |
| | | 2320 rpm | 0.55 | 0.8 | 0.5 | 4.5 | 0.7 | 1.3 | 0.6 | | |

was with the same base stock oil to which was added one percent by volume of zinc dithiophosphate. Zinc dithiophosphate is one of the most commonly used antiwear additives. The sixth test was conducted with an emulsion type 95-5 high water base fluid that contains 95 percent water and 5 percent concentrate by volume.

A test load of 100 lb was used unless otherwise specified. For each test except test 5, the test was initiated with a 60-min clean test. Then the 0-20 micrometres classified AC Fine Test Dust was injected with a concentration of 300 mg/L, and the 30-min abrasive test was conducted, which was followed by the 10-min filtration and the 30-min clean test. In the same manner, the 0-40 micrometre abrasive test and the 0-80 micrometre abrasive test were conducted.

In test 4, almost no wear was observed in the 0-20, 0-40, and 0-80 micrometre abrasive tests at 100 lb. After the 0-80 micrometre abrasive test at 100 lb, the test load was doubled to 200 lb at a rotating speed of 1160 rpm, and the wear rate was observed. The wear rate at 200 lb was also observed at 2320 rpm. Then, the test load was reduced to 100 lb, and the wear rate was again observed.

Test 5 was conducted to investigate the effect of the antiwear additive on abrasive wear in comparison with test 4. In test 4, high wear rates were observed at a test load of 200 lb after the first 100 lb 0-80 micrometre abrasive test was completed. To investigate the effect of the antiwear additive on abrasive wear in test 5, the clean test was continued at 580 rpm until the test specimens has a contact area which was the same at the completion of the first 100 lb 0-80 micrometre abrasive test in test 4. In this way, the sliding surface condition in test 5 was adjusted to be the same as that at the end of

the first 100 lb 0-80 micrometre abrasive test in test 4.

Then, the 0-80 micrometre test was conducted in test 5 at 1160 rpm and 2320 rpm with a test load of 200 lb. After the 200 lb test at 2320 rpm was completed, the test load was reduced to 100 lb, and the wear rate was observed at 2320 rpm.

For all the tests except test 3, standard test specimens were used. The standard test specimens consist of two V-blocks made of AISI 1137 steel with a yield strength of 91 kpsi and one journal made of AISI 3135 steel with a yield strength of 66 kpsi. For test 3 only, a "soft" V-block was used which is made of AISI 1020 steel with a yield strength of 39 kpsi; however, the journal in test 3 was standard AISI 3135 steel.

The test fluid temperature was 65°C for all the tests except for test 6. For the 95-5 HWBF in test 6, the test temperature was 50°C. The viscosity of MIL-L-2104 at 65°C is 15.2 cP. The viscosity of the base stock oil at 65°C is 22.5 cP. Zinc dithiophosphate added to the base stock oil does not change the viscosity of the base stock. The viscosity of the 95-5 HWBF at 50°C is approximately 1 cP.

Analysis of Test Results

The test results are discussed and analyzed to verify the abrasive wear theory in this section. In test 2 with MIL-L-2104 mineral base fluid, it is obvious that abrasive wear occurred when the abrasive particles were injected. In the 0-20 micrometre abrasive test, the wear rate at 580 rpm was 1.1; however, the wear rate at 1160 rpm was 3.5. This large increase in the wear rate is considered to be due to the change of the clearance. At 580 rpm, the clearance was not large enough to have a majority of abrasive particles in the fluid. When the

rotating speed was increased to 1160 rpm, the hydrodynamic effect increased the clearance to the size which allowed most of abrasive particles to migrate into the clearance and generate abrasive wear. A similar phenomenon can be observed in the 0-40 micrometre abrasive test.

In test 3 with the "soft" V-blocks, abrasive wear was obvious; however, the wear rates in the abrasive tests were all less than those in test 2. This means that the soft V-block was associated with less abrasive wear than the hard V-block. The test specimens used in test 3 were the V-blocks made of AISI 1020 steel with a yield strength of 39 kpsi, and the journal was made of AISI 3135 steel with a yield strength of 66 kpsi. The standard test specimens used in test 2 were the V-blocks made of AISI 1137 steel with a yield strength of 91 kpsi, and the journal was made of AISI 3135 steel with a yield strength of 66 kpsi. Thus, the combination of the test specimens in test 2 is the "medium steel and hard steel." The combination of the test specimens in test 3 is the "soft steel and medium steel."

From the theoretical considerations of abrasive wear, it was already shown that a combination of "soft steel and medium steel" has less abrasive wear than a combination of "hard steel and medium steel" at a large particle angle, Table 18. The above consideration implies that the abrasive particle angle relative to the surfaces in both tests 2 and 3 was large.

In test 4, almost no abrasive wear was observed at a test load of 100 lb. This fact reveals the importance of fluid viscosity in preventing abrasive wear. The base stock oil has a viscosity of 22.5 cP at a test temperature of 65°C which is higher than a viscosity of 15.2 cP for MIL-L-2104. Hence, the hydrodynamic fluid film with the base

stock oil was thicker than that with MIL-L-2104. The hydrodynamic fluid film with the base stock oil at high rotating speeds tolerated the abrasive particles, and no abrasive wear was observed.

To verify this concept, the test load was doubled to squeeze the hydrodynamic fluid film. At 200 lb and 1160 rpm with 0-80 micrometre abrasive particles, a high wear rate was observed that indicated a decrease in the fluid film and consequent severe abrasive wear. When the rotating speed was increased to 2320 rpm, abrasive wear was even more severe. This illustrates the drastic effect of the fluid film on abrasive wear.

After the 200 lb test, the test load was decreased again to 100 lb, and the wear rate was observed at 2320 rpm. A wear rate of 0.1 instead of zero implies that the sliding surface was severely abraded at 200 lb and was roughened. Because of the high asperities on the rough sliding surfaces, wear was generated even at 100 lbs.

In test 5 the sliding surface area was widened to the same size as in test 4 before the 0-80 micrometre 200 lb abrasive test was initiated. The better lubricity of the base stock oil with 1 percent zinc dithiophosphate is evident because a wear rate at 580 rpm was 0.3 even at a test load of 200 lb. This is one-half the wear rate of the base stock oil alone at 580 rpm with 100 lb in test 4.

The wear rate in the 0-80 micrometre 200 lb abrasive test at 1160 rpm was 7.5, which is more than three times the wear rate with the base stock oil alone. Because of this high wear rate, the wear reading increased rapidly. In spite of the extremely widened sliding surface area, the wear rate at 2320 rpm was 4.83, which is still a very high wear rate. The severity of abrasive wear with the base stock oil

containing zinc dithiophosphate was also indicated by a high wear rate in the 0-80 micrometre 100 lb abrasive test at 2320 rpm after the 200 lb test. The sliding surfaces were abraded and extremely roughened during the 200 lb test. Hence, even after the test load was decreased down to 100 lb, the rough surfaces with high asperities caused the high wear rate of 2.0.

Test 6 was conducted with the emulsion type 95-5 high water base fluid (HWBF). Since the 95-5 HWBF has an extremely low viscosity (close to 1 cP) compared with the other mineral base fluids, its wear characteristic is different from the other fluids. Because of the low viscosity, the fluid film formed by high rotating speeds was thin. Therefore, no large differences were observed between the wear rates in the clean tests and the abrasive tests, except the 0-40 micrometre abrasive test at 2320 rpm. In the 0-40 micrometre abrasive test at 2320 rpm, it is considered that the clearance was maintained just right size for most of the effective abrasive particles to migrate into the clearance and generate severe wear.

Overall, the effect of abrasive particles was insignificant at a low rotating speed. Whereas, a drastic effect was observed at a high rotating speed. This observation leads to the following remarks:

- * The effect of abrasive particles under boundary lubrication is insignificant.

- * There is a specific clearance size where severe abrasive wear occurs.

Abrasive Tests on Fluid Power Pumps

To validate the feasibility of the abrasive wear theory in actual

applications, abrasive wear tests were conducted on fluid power pumps. A gear-type fluid power pump with a flow rate of 25 gpm at a rotating speed of 1800 rpm was selected as the test pump. Four identical pumps from the same manufacturer were prepared and used for the abrasive wear tests with four different fluids. The four test fluids were MIL-L-2104 mineral oil, base stock oil with no antiwear additives, base stock oil containing 1 percent zinc dithiophosphate, and micro-emulsion type 95-5 high water base fluid.

The test pressure for the test fluids except the 95-5 HWBF was 2500 psi. The test pressure for the 95-5 HWBF was 500 psi because it was considered that a life of the test pump with the 95-5 HWBF at 2500 psi might be drastically shortened due to its extremely low viscosity. The test temperature was 65°C for the first three fluids and 50°C for the 95-5 HWBF.

Fig. 76 shows a test circuit for the pump abrasive wear test. The pump abrasive wear test was conducted according to the standard procedure for evaluating performance degradation of a fluid power pump due to abrasive wear [34, 35]. The test procedure is briefly explained as follows:

1. The test pump is first operated under clean conditions with the filter in the circuit for 2 hr.
2. The initial flow rate of the test pump is established.
3. The filter is isolated from the test circuit, and 0-5 micrometers classified AC Fine Test Dust is injected into the test fluid with a concentration of 300 mg/L.
4. The test pump is operated with the abrasive particles for 30 min.

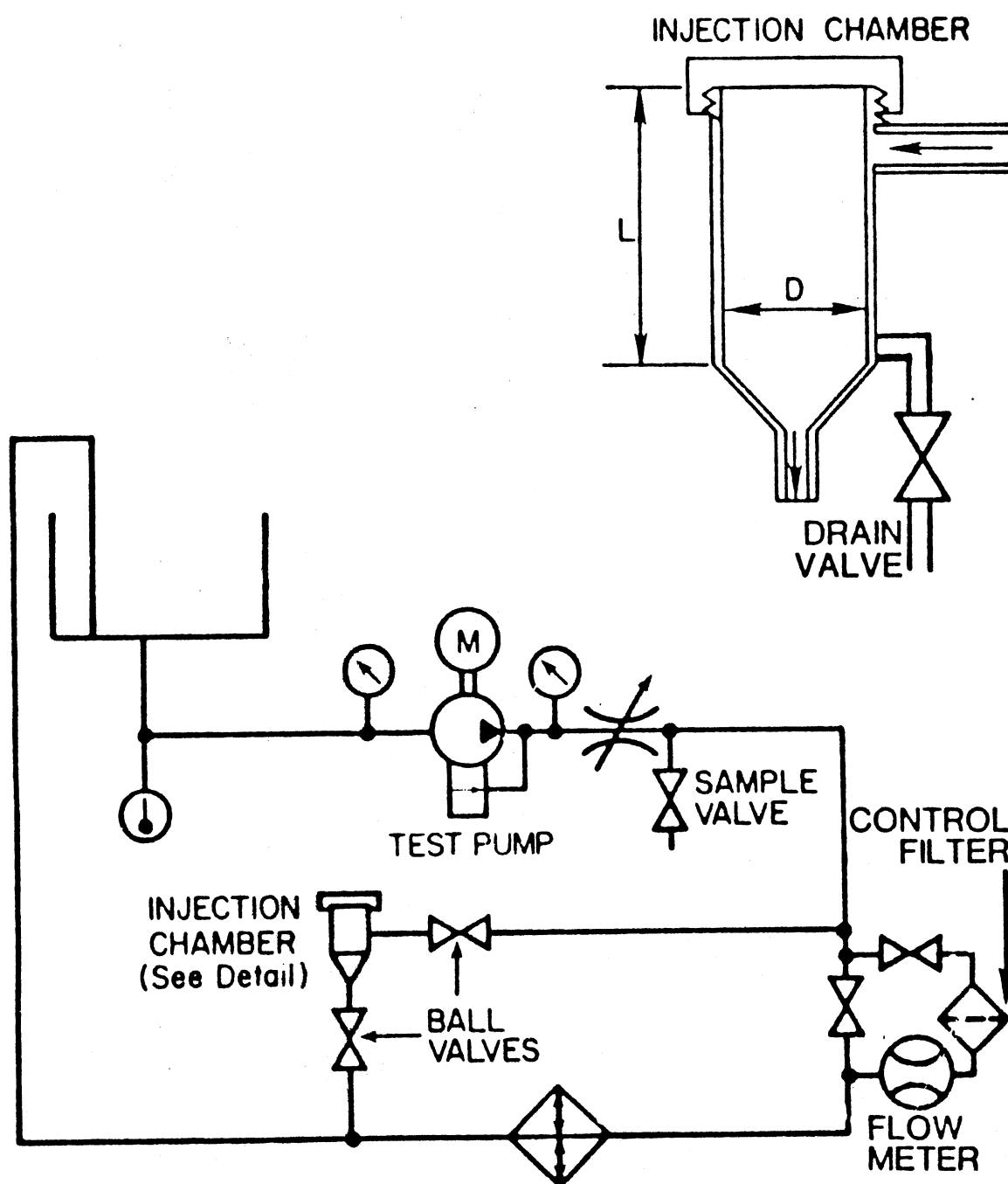


Fig. 76. Pump Abrasive Wear Test Circuit

5. After 30 min from the injection of the abrasive particles, the filter is connected to the circuit, and the fluid is filtered for 10 min.
6. After the fluid is cleaned by 10 min filtration, the degraded flow rate due to abrasive particles is recorded.
7. Steps 3 through 6 are repeated for abrasive particles (ACFTD) of the sizes, 0-10, 0-20, 0-30, 0-40, 0-50, 0-60, 0-70, and 0-80 micrometres unless the flow degradation ratio exceeds 30 percent of the initial flow rate when the test is terminated.

The degradation of the pump flow rate due to a certain size of abrasive particles is repeatable. This was verified by conducting multiple injections of the same size and quantity of abrasive particles (36).

The repeatability of the gear pump abrasive wear tests was investigated at the Fluid Power Research Center on 8 gear pumps. The result of the investigation revealed that the average deviation of the flow degradation data from one pump to the other was 1.88 percent and the maximum deviation observed in the tests was 8.0 percent. This indicates a good repeatability of the gear pump abrasive wear tests (37).

The above mentioned repeatability study on the gear pump abrasive wear tests validates the pump test results presented herewith. The differences of the data, which are referred to as evidence of the effects of fluid viscosity, fluid antiwear characteristic or operating pressure, are all much larger than 8.0 percent.

Pump Test Results and Analysis

Fig. 77 shows the pump test results with the four different test fluids. The flow degradation ratio, which is the degraded flow rate divided by the initial flow rate, is plotted as a function of the injected abrasive particle size.

Comparing the results from MIL-L-2104 and the base stock oil, it is obvious that the degradation with MIL-L-2104 started at a smaller abrasive particle size. The degradation with MIL-L-2104 was much larger than that with the base stock oil for the same size abrasive particles such as 0-30, 0-40, and 0-50 micrometres. This illustrates clearly the effect of fluid viscosity on abrasive wear. The viscosity of the base stock oil is higher than that of MIL-L-2104; and, therefore, a thicker hydrodynamic fluid film was formed that protected the pump better from abrasive wear. This agrees with the results of the previous tests on the variable speed Gamma Falex system.

Comparing the results from the base stock oil and the base stock oil containing 1 percent zinc dithiophosphate, little difference is observed up to 0-60 micrometres; however, a large difference is observed at 0-70 and 0-80 micrometres. The little difference at small abrasive sizes up to 0-60 micrometres is considered to be due to a mild abrasive condition. These two fluids are basically the same fluid except that the latter contains zinc dithiophosphate, a good antiwear agent. This antiwear agent is known to be activated under severe sliding contact condition, reduce friction, and protect sliding surfaces. Thus, under a mild abrasive condition, the antiwear agent is not activated, and the amounts of abrasive wear with these fluids are considered to be about the same.

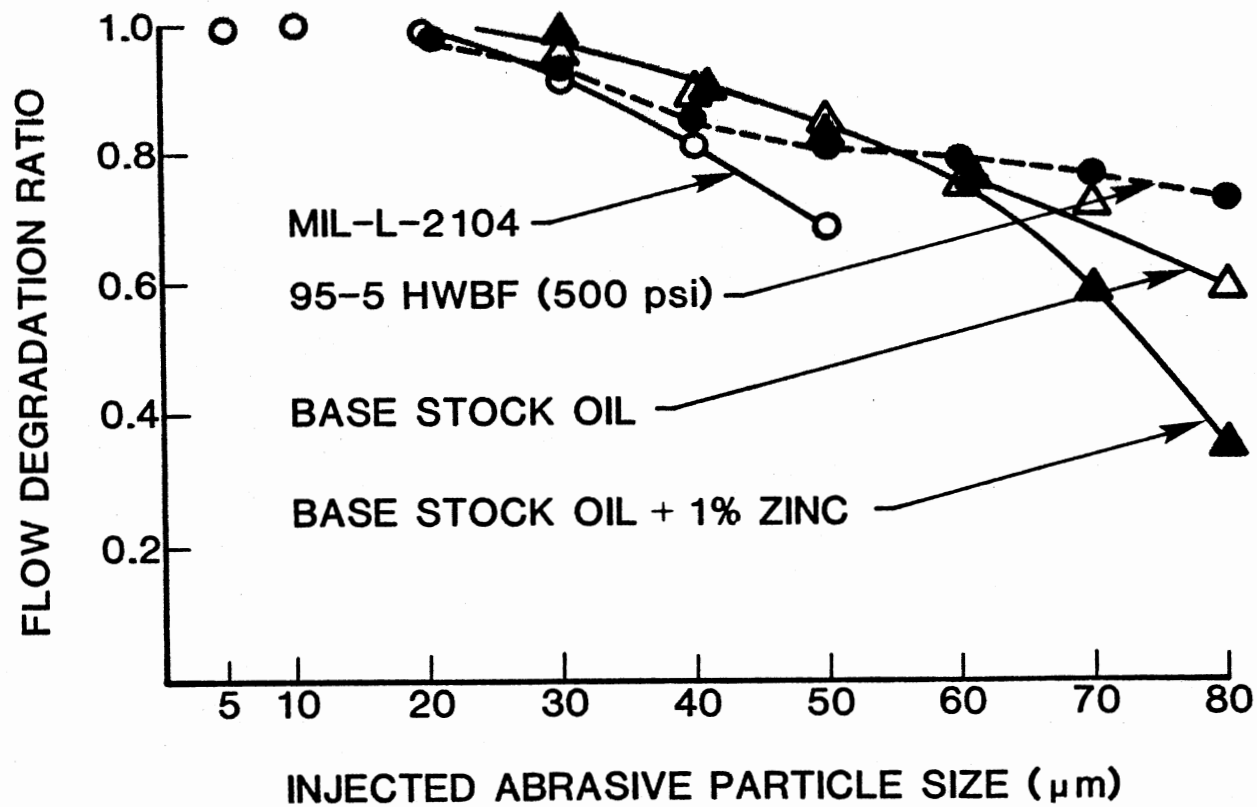


Fig. 77. Gear Pump Abrasive Wear Test Results

The large difference in flow degradation ratio between these two fluids at 0-70 and 0-80 micrometres is due to an extremely severe abrasive condition. Severe cutting and indentation by large abrasive particles activate the antiwear agent which reduces friction between the surface and the abrasive particle, and advance abrasive wear as explained by the abrasive wear theory.

This concept is reinforced by an observation made during the test. The color of the base stock oil containing 1 percent zinc dithiophosphate started to change to a greenish color immediately after injections of 0-70 and 0-80 micrometre abrasive particles. No color change was observed before the injection of 0-70 micrometre abrasive particles. The greenish color change of the fluid is evidence of a chemical reaction where the antiwear additive is activated.

The chemical behavior of the antiwear agent is beyond the scope of this thesis; however, it is considered appropriate to state the evidence of fluid color change due to the chemical reaction of the antiwear agent in order to support the verification of the abrasive wear theory.

With 95-5 HWBF, the flow degradation started at the abrasive size of 0-20 micrometres, which is the smallest size for the start of degradation among the four test fluids. However, the degradation did not proceed as much as with the other fluids and ended with the least degradation at 0-80 micrometres. The early degradation at a small abrasive size is considered to be due to the low viscosity of the 95-5 HWBF. The low viscosity forms a thin hydrodynamic fluid film that cannot protect the surfaces even from small abrasive particles. Because of the poor protection of the surfaces by the thin hydrodynamic fluid film, the flow degradation is expected to proceed more severely than

with the other fluids for larger sizes of abrasive particles. But the actual degradation proceeded less than with the other fluids for larger sizes of abrasive particles. This controversial result is considered to be due to the low operating pressure.

The test gear pump has a hydraulically balanced wear plate. The wear plate floats between the gear and the housing and is pushed against the gear face by hydraulic pressure. Since abrasive wear, which leads to flow degradation of the pump, occurs mainly in the clearance between the gear face and the wear plate, the pressure pushing the wear plate against the gear face is a factor affecting the abrasive wear condition. For the first three fluids, a pressure of 2500 psi was used; whereas, 500 psi was used for the 95-5 HWBF. A pressure of 500 psi for the 95-5 HWBF is one-fifth the pressure for the other three fluids; and, therefore, the severity of the abrasive wear with the 95-5 HWBF is considered to be much less when compared with the other fluids in the test gear pump structure. This consideration reveals that the operating pressure can be a significant factor affecting abrasive wear condition in actual applications. This gear pump test illustrates that lowering the operating pressure reduces abrasive wear.

As a result of the pump abrasive wear tests, three things were clarified. The first two verify the developed abrasive wear theory and the last one presents a factor affecting abrasive wear in actual applications:

1. Fluid viscosity is an important factor affecting abrasive wear condition.
2. A fluid with better lubricity causes more abrasive wear.
3. The operating pressure of the fluid power system can be a significant factor affecting abrasive wear conditions.

CHAPTER VI

SUMMARY AND CONCLUSIONS

Summary

There are two major modes of wear under sliding conditions -- surface contact wear and abrasive wear. A new surface contact wear theory was developed by considering the plastic deformation of sliding surface materials and the lubricity of the fluid existing between the sliding surfaces. A new abrasive wear theory was developed which considers the effects of fluid lubricity, sliding surface hardness, abrasive particle hardness, surface geometry, and fluid film thickness on wear generation.

The Gamma Falex system, which is the improved version of the wear tester specified by the ASTM procedure, was used to verify the developed surface contact wear model. Three conditions were hypothesized based on a theoretical surface contact wear model and were verified by experimental tests. To further validate the concept of surface asperity plastic deformation which is incorporated into the developed surface contact wear theory, static and dynamic asperity deformation tests were conducted. These tests clarified the effects of surface hardness and sliding velocity on surface contact wear.

The developed abrasive wear model was verified by the use of the variable speed Gamma Falex system which is capable of changing the lubricating condition of the sliding surfaces from boundary lubrication

to mixed lubrication and to hydrodynamic lubrication. To validate the feasibility of the developed abrasive wear model in actual applications, abrasive wear tests were conducted on fluid power pumps. The results of the pump test not only validated the model but also indicated that the operating pressure can be a significant factor affecting abrasive wear condition in actual applications.

Conclusions

From the research investigation described in the preceding chapters, a number of conclusions can be made. The following list summarizes the major accomplishments and conclusions:

1. A new theory for surface contact wear was developed based on the consideration of plastic deformation of surface materials and lubricity of a fluid existing between sliding surfaces.
2. The complete shape of the abrasive particle was defined to develop a feasible abrasive wear model.
3. A new abrasive wear theory was developed based on the consideration of surface cutting and indentation mechanisms by the abrasive particle.
4. The new abrasive wear theory states that the abrasive particle should be at least 3.15 times as hard as the surface material to cause abrasive wear; otherwise, the particle is sheared off by the surface, and no abrasive wear occurs.
5. The Gamma Falex system, which is an improved version of the wear tester specified by the ASTM procedure, was

developed to conduct the test for the verification of the developed surface contact wear model.

6. The repeatability of the Gamma Falex system was studied with a total of 47 tests. The results of the repeatability study provided significant guidance about the confidence levels of the Gamma Falex test data.
7. The test wear mechanism of the Gamma Falex system was analyzed. The analysis led to mathematical relationships about the wear reading, the wear scar depth, the wear scar width, the wear surface area, and the unit load on the wear surface.
8. The experimental test of the Gamma Falex system verified the developed surface contact wear model. the effects of the load, fluid lubricity, and material hardness were predicted by the model and were verified by the experimental test.
9. The static asperity deformation test showed that little delamination occurred with a soft material; whereas, severe delamination occurred with a hard material.
10. The soft material produced no wear fragments in spite of its large plastic deformation during the static deformation process. On the contrary, the hard material produced wear fragments. This reveals that the coefficient of wear fragment formation is a strong function of material ductility under static condition.
11. The conical shape of the asperity expanded as static plastic deformation progressed. The degree of the

expansion was dependent on material ductility. This leads to an important remark about the developed surface contact wear theory; i.e., the actual deformation of the asperity is less than the theoretical deformation because the theory does not incorporate expansion.

12. The results of static asperity deformation tests indicated that a fluid providing less friction on the soft material also provided less friction on the hard material and vice versa.
13. Friction on the hard material was always higher than that on the soft material for the same lubricant. This reveals that the friction under static conditions varies significantly due to the material hardness.
14. The results of the dynamic asperity deformation tests showed that the initiation of surface contact wear at high sliding velocity always follows the same pattern consisting of incubation region, direct contact region, burning region, and severe adhesion region.
15. The results of the dynamic asperity deformation tests also showed that the effect of material hardness on adhesion is insignificant at high sliding velocity.
16. The dynamic asperity deformation test revealed that hydrodynamic lubrication can be suspended even at a high sliding velocity of 480 cm/sec.
17. Severe adhesion stopped when the sliding velocity decreased to 290 cm/sec in the dynamic asperity deformation test. The suspension of severe adhesion at

this high sliding velocity is considered to be due to the reduction of heat generation and a high heat dissipation in the test condition. This observation reveals that adhesive wear can be reduced or eliminated even at a high sliding velocity by providing high heat dissipation in the region near the sliding surfaces and reducing heat generation.

18. A close examination of the developed abrasive wear model revealed that the effective size of abrasive particles for abrasive wear depends on the clearance between the sliding surfaces and surface roughness.
19. The angle of abrasive particles relative to the sliding surface depends on surface geometry.
20. The smaller the abrasive particle angle, the lower the energy state; therefore, any disturbances which alter the state of abrasion tend to reduce the particle angle and, consequently, reduce abrasive wear.
21. A particle angle of 60 deg gave a maximum abrasive wear among the angles of 45, 60, and 75 degs which were considered.
22. Examination of the model also revealed that the soft material is cut and the hard material is indented by the abrasive particle at particle angles of 45 and 60 degs; however, the opposite situation emerges with a particle angle of 75 degs.
23. The hardness of the abrasive particle required to cause abrasive wear should be higher as the coefficient of

friction between the particle and the surface increases.

24. As the coefficient of friction between the abrasive particle and the surface increases, the cutting depth decreases and the indentation depth increases. Consequently, the higher coefficient of friction causes less abrasive wear.
25. The larger particle angle gives a larger increase of the cutting depth due to the increasing coefficient of friction.
26. The variable Gamma Falex system was developed to verify an abrasive wear model, which is capable of changing the lubricating condition of the sliding surfaces from boundary lubrication to mixed lubrication and to hydrodynamic lubrication.
27. The variable speed Gamma Falex system precisely measures the thickness of the fluid film between the sliding surfaces.
28. The experimental test with the use of the variable Gamma Falex system showed that abrasive particles do not cause severe abrasive wear under boundary lubrication conditions.
29. The result of the experimental test on the variable Gamma Falex system revealed the importance of fluid viscosity in preventing abrasive wear. When the fluid viscosity was high enough to lift the surfaces and open the clearance larger than the abrasive particle size, no abrasive wear occurred.

30. The results of the experimental tests on the variable Gamma Falex system verified that a fluid with better lubricity causes more abrasive wear.
31. The abrasive wear test was conducted on fluid power pumps to validate the feasibility of the developed abrasive wear model, and the importance of fluid viscosity in reducing abrasive wear was verified. The higher the fluid viscosity, the lower the performance degradation of the pump was observed due to abrasive wear.
32. The pump abrasive test also verified that a fluid with better lubricity causes more abrasive wear.
33. The pump abrasive test revealed that the operating pressure of the fluid power system can be a significant factor affecting the abrasive wear condition. The gear pump used in the test indicated that lowering the operating pressure reduces abrasive wear.

BIBLIOGRAPHY

- (1) Holm, R. Electrical Contacts. Stockholm: H. Gerbers, 1946.
- (2) Burwell, J. T., and C. D. Strang. "On the Empirical Law of Adhesive Wear." Journal of Applied Physics, 23 (1952), 18.
- (3) Archard, J. F. "Contact and Rubbing of Flat Surfaces." Journal of Applied Physics, 24 (1954), 981.
- (4) Yoshimoto, G., and T. Tsukizoe. "On the Mechanism of Wear Between Metal Surfaces." Wear, 1 (1958), 472-490.
- (5) Suh, N. P. "The Delamination Theory of Wear." Wear, 46 (1978), 241-250.
- (6) Rigney, D. A., and W. A. Glaeser. "The Significance of Wear Surface Microstructure in The Wear Process." Wear, 46 (1978), 241-250.
- (7) Kuhlmann-Wilsdorf, Doris. Dislocation Concepts in Friction and Wear. University of Virginia, Technical Report Submitted to Office of Naval Research, Contract No. N00014-76-C-1009, 1980.
- (8) Suh, N. P., and H. C. Sin. On the Genesis of Friction and Its Effect on Wear. "Solid Contact and Lubrication, Winter Annual Meeting of the American Society of Mechanical Engineers," 1980.
- (9) Kruschov, M. M., and M. A. Babichev. "Resistance to Abrasive Wear and the Hardness of Metals." Dokl. Akad. (Nauk SSSR), 88 (1953), 445-448.
- (10) Avient, B. W. E., J. Goddard, and H. Wilman. "An Experimental Study of Friction and Wear During Abrasion of Metals." Proceedings of the Royal Society of London, Ser. A, 258 (1960), 159-180.
- (11) Mulhearn, T. W., and L. E. Samuels. "The Abrasion of Metals: a Model of the Process." Wear, 5 (1962), 478-498.
- (12) Toporov, G. V. "The Influence of Structure on the Abrasive Wear of Cast Iron." Friction and Wear in Machinery, 12 (1958), 39-59.
- (13) Rabinowicz, E., L. A. Dunn, and P. G. Russell. "A Study of Abrasive Wear under Three-Body Conditions." Wear, 4 (1961), 345-355.

- (14) Kruschov, M. N. "Resistance of Metals to Wear by Abrasion as Related to Hardness." Proceedings of the Conference on Laboratory Wear, sponsored by the Institution of Mechanical Engineers, 1 (1957), 181-188.
- (15) Richardson, R. C. "Wear of Metals by Relatively Soft Abrasives." Wear, 11 (1968), 245.
- (16) Rabinowicz, E., and A. Mutis. "Effect of Abrasive Particle Size on Wear." Wear, 8 (1965), 381-390.
- (17) Sarkar, A. D. Wear of Metals. New York: Pergamon International Library, 1976.
- (18) Rabinowicz, E. Friction and Wear of Materials. New York: John Wiley and Sons, 1966.
- (19) Nathan, G. K., and W. J. D. Jones. "Influence of the Hardness of Abrasives on the Abrasive Wear of Metals." Proceedings of the Institution of Mechanical Engineers, 181, Pt. 30 (1966-67), 215-221.
- (20) Sin, H., N. Saka, and N. P. Suh. "Abrasive Wear Mechanisms and the Grit Size Effect." Wear, 55 (1979), 163-190.
- (21) Roach, A. E. "Performance of Oil-Film Bearings with Abrasive-Containing Lubricant." Transactions of the American Society of Mechanical Engineers (July, 1951), 677-686.
- (22) Scott, W. "Relationship Between Solid Particle Contaminant Size and Thickness of Oil Films in Hydraulic Systems." Institution of Mechanical Engineers, C99 (1976), 93-99.
- (23) Tao, F. F., and J. K. Appeldoorn. "An Experimental Study of Wear Caused by Loose Abrasive Particles in Oil." Lubrication Conference, American Society of Lubrication Engineers/American Society of Mechanical Engineers, Houston, Texas, October 14-16, 1969.
- (24) Johnson, W., and P. B. Mellor. Engineering Plasticity. London: Van Nostrand Reinhold Company, 1973.
- (25) Inoue, R. "Sliding Surface Wear Under Lubricating and Abrasive Conditions." Research proposal, Oklahoma State University, Stillwater, Oklahoma, January, 1982.
- (26) Bowen, E. R., and V. C. Westcott. Wear Particle Atlas. Burlington, Massachusetts: Foxboro/Trans-Sonics, Inc., 1976.
- (27) McCrone, W. C., and J. G. Delly. The Particle Atlas. 2nd Edition. Ann Arbor, Michigan: Ann Arbor Science Publishers, Inc., 1973.

- (28) Fitch, E. C. An Encyclopedia of Fluid Contamination Control. Washington D.C.: Hemisphere Publishing Corporation, 1980.
- (29) Dobson, J., and J. S. Steckl. "Failure Prediction Using Ferrographic Oil Analysis Techniques." The BFPR Journal, 15 (1982), 179-187.
- (30) Kroeker, B. A. "Air Cleaner Fine Test Dust, Kirnbauer's Concepts vs. Weight Distribution." Presented at the 1980 SAE A-6 Fall Meeting, Los Angeles, Oct. 17-18, 1980.
- (31) Stovall, D., and R. Inoue. "Analyzing Surface Roughness Profiles for Fluid Antiwear Assessment." The FRH Journal, 3 (1983), 107-110.
- (32) Grunzweig, J., et. al. "Calculations and Measurements on Wedge-Indentation." Journal of the Mechanics and Physics of Solids, 2 (1954), 81-86.
- (33) Swedeen, R., K. Izawa, and K. S. Nair. "Frictional Forces Created in Hydraulic Components By Fluid Contamination--A Case Study." The BFPR Journal, 14 (1981), 357-365.
- (34) "Method of Establishing the Flow Degradation of Hydraulic Fluid Power Pumps When Exposed to Particulate Contaminant. NFPA Recommended Standard T3.9.18-1976. Thiensville, Wisconsin: National Fluid Power Association, Inc., 1976.
- (35) "Hydraulic Fluid Power - Fixed Displacement Pumps - Flow Degradation Due to Classified AC Fine Test Dust Contaminant." ISO/TC 131/n SC6/WG6. Geneva, Switzerland: International Organization for Standardization, June 1980.
- (36) McBurnett, J. R. "Contaminant Sensitivity of Fluid Power Pumps." Fifth Annual Basic Fluid Power Research Conference, Oklahoma State University, Stillwater, Oklahoma 1971.
- (37) Fitch, E. C. "Component Contaminant Sensitivity--A Status Report on Pumps." Paper 74-42, Eighth Annual Fluid Power Research Conference, Oklahoma State University, Stillwater, Oklahoma 1974.
- (38) Samans, C. H. Metallic Materials in Engineering. New York: McMillian Company, 1963.
- (39) Inoue, R., and E. C. Fitch. "Antiwear Characteristics of Hydraulic Fluids and Contaminant Abrasivity." National Conference on Fluid Power, Chicago, 1981.

APPENDIX

LIMITATIONS OF PRESENT WORK AND SUGGESTIONS
FOR APPLICATIONS

Limitations of Present Work

The following limitations are stated for the work presented in this dissertation:

1. The surface contact wear theory was developed based on the surface asperity deformation concept. When wear fragments are formed as a result of the material plastic deformation, fracture of the material occurs. The fracture mechanism which is quite different from the plastic deformation mechanism was not included in the development of the theoretical model.
2. Application of the surface contact wear theory developed in this research is limited to the coefficient of friction less than 0.577 due to the Von Mises yield criterion.
3. A large size of simulated surface asperity was utilized to verify the asperity plastic deformation concept. Such verification method designated as the macro approach has a limitation of application in size of surface asperities. If the size of surface asperities is smaller than the grain size of the surface material, the theory verified by the macro approach is not valid. The test materials used in this research are annealed carbon steels which have the grain size of less than one micrometre (38). Since the size of surface asperities on the test

materials is at least more than several micrometres, the theory verified by the macro approach is valid for the test materials.

4. In the abrasive wear tests on gear pumps, only a single pump was tested for each type of the test fluids. Hence, the validity of the pump abrasive tests presented in this dissertation relies on the repeatability tests reported in Reference 37.

Wear Life Prediction of Sliding Mechanisms

The technology and knowledge obtained from the research can be used to assess the wear life of a lubricated sliding mechanism. The application includes two different sliding conditions; boundary lubrication and hydrodynamic lubrication.

In boundary lubrication condition, two sliding surfaces are in contact and protection of the surfaces from wear relies on the lubricity of the applied lubricant. Lubricity is defined as a capability of reducing friction and wear in sliding mechanisms. The lubricity of lubricants under boundary lubrication condition is not associated with fluid viscosity. The lubricity of lubricants under boundary lubrication can be accurately evaluated by running the 30-min Gamma Falex test under the standard test conditions (rotating speed of 290 rpm and test load of 300 lb). The Gamma slope which is the slope of the wear reading versus test time data line represents the lubricity of the test fluid under boundary lubrication condition.

Eq's. (32), (38), and (47) give an equation showing the relationship between the volume rate of surface contact wear and the Gamma slope:

$$V_r = cs^{1.5} \quad (58)$$

where,

$c = \text{constant}$

When the amount of total wear volume, which can be lost for the entire life of the sliding mechanism is V_{\max} , the life of the sliding mechanism with the test fluid in boundary lubrication condition is obtained by

$$T = \frac{V_{\max}}{V_r} = \frac{V_{\max}}{cs^{1.5}} \quad (59)$$

Note in Eq. (59) that the larger the Gamma slope the shorter life that results.

With a reference fluid selected for the purpose of rating other fluids, the lubricity of the test fluid can be estimated relative to the reference field. The life of the sliding mechanism with the test fluid can be also calculated relative to the life with the reference fluid. Using MIL-L-2104 mineral base fluid as the reference fluid, the life achieved with MIL-L-2104 is

$$T_m = \frac{V_{\max}}{cs_m^{1.5}} \quad (60)$$

where,

$T_m = \text{life with MIL-L-2104}$

$s_m = \text{Gamma slope of MIL-L-2104}$

If a Gamma slope of MIL-L-2104 and a life of the mechanism achieved with MIL-L-2104 are known, a life with the test fluid can be calculated by simply measuring the Gamma slope of the test fluid:

$$T_t = T_m \left(\frac{s_m}{s_t} \right)^{1.5} \quad (61)$$

where,

T_t = life with test fluid

s_t = Gamma slope of test fluid

The quantity $(s_m/s_t)^{1.5}$ in Eq. (61) is a life factor which is multiplied to the life achieved with MIL-L-2104 mineral base fluid to obtain the life with the test fluid in boundary lubrication condition. This factor is designated as the "contact Gamma" and used as a lubricity rating value. The larger the contact Gamma, the better the lubricity and vice versa.

A Gamma slope of MIL-L-2104 is 0.109. Consider five fluids with the Gamma slope of 0.98, 0.3, 0.12 and 0.07. Assuming a life of the sliding mechanism to be 1000 hr with the use of MIL-L-2104, lives of the same mechanisms with the five fluids are estimated to be 37 hr, 219 hr, 402 hr, 866 hr and 1943 hr, respectively.

In hydrodynamic lubrication condition, no surface contact wear occurs because there is no surface asperity contact existing. However, abrasive wear occurs when abrasive particles exist. The lubricity of fluids under hydrodynamic lubrication includes the viscosity of the fluid. A higher viscosity creates a thicker fluid film between the sliding surfaces that provides better protection of the surfaces from both surface contact wear and abrasive wear.

To evaluate the capability of a fluid to protect a sliding mechanism from abrasive wear under hydrodynamic lubrication, the variable speed Gamma Falex system can be used. Hydrodynamic lubrication

condition is maintained and the evaluation is achieved by injecting classified AC Fine Test Dust into the test fluid. Using MIL-L-2104 mineral base fluid as a reference fluid, a rating system can be developed.

From analyzing the wear mechanism of the Gamma Falex system, it was verified that the wear surface area increases as the wear reading advances. With MIL-L-2104 at a load of 100 lb a perfect hydrodynamic lubrication condition is obtained when the wear reading is advanced to 120.

Under these conditions, 300 mg/L of 0-5 micrometres classified AC Fine Test Dust is injected into the test system filled with MIL-L-2104 fluid. Immediately abrasive wear is observed as the injected abrasive particles abrade the surfaces. But abrasion will stop because the surface area increases due to abrasion and the fluid film thickness exceeds the size of abrasive particles. At this time, the fluid is cleaned by a filter and 300 mg/L of 0-10 micrometres classified AC Fine Test Dust is injected. Just like the 0-5 micrometres ACFTD test, abrasive wear is observed for a while but abrasive wear will stop in a short time due to the increase of the fluid film. This procedure is repeated for 0-20 micrometres ACFTD and the amount of abrasive wear is observed.

From the test results, abrasive wear produced on the standard Gamma Falex test wear mechanism protected by MIL-L-2104 is evaluated with respect to 0-5, 0-10 and 0-20 micrometres ACFTD. Particle distributions of these test contaminants have been measured and are shown in Fig. 78. Number of particles greater than five micrometres in 300 mg/L of 0-5 micrometres ACFTD is 3.7×10^4 . Number of particles greater than 10 micrometres in 300 mg/L of 0-10 micrometres ACFTD is 8.3×10^3 . Number

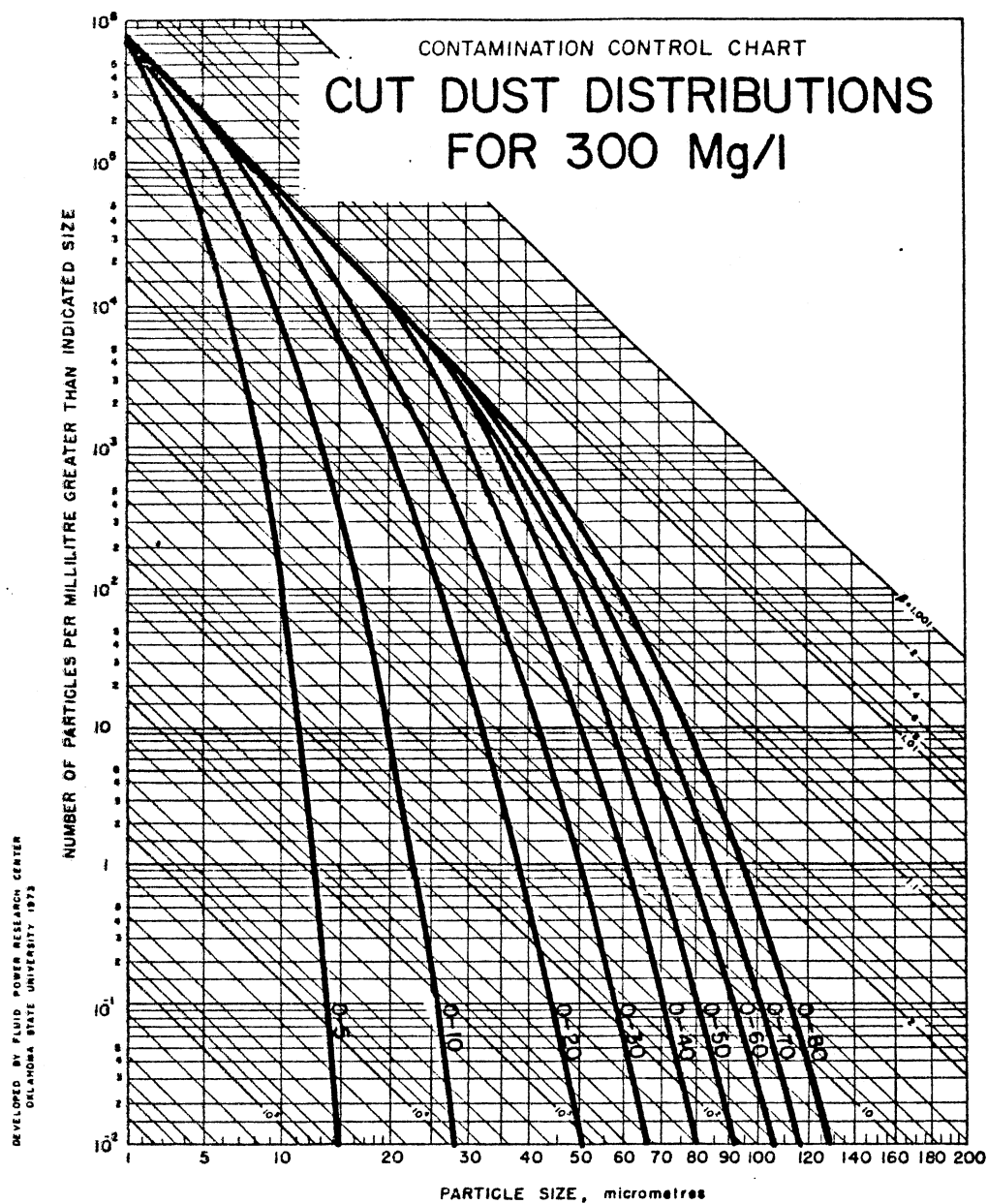


Fig. 78. Particle Distributions of Classified AC Fine Test Dust

of particles greater than 20 micrometres in 300 mg/L of 0-20 micrometres ACFTD is 10^3 .

Consider a sliding mechanism which is hydrodynamically lubricated with MIL-L-2104. The mechanism is protected by a Beta Ten of 2 filter (28) and a controlled particle distribution is shown in Fig. 79.

Particle numbers greater than 5, 10 and 20 micrometres of the Beta Ten of 2 filter distribution in Fig. 79 are 4×10^4 , 1.2×10^3 and 1.5×10 , respectively.

The protection capability of MIL-L-2104 in the variable speed Gamma Falex system was evaluated with 300 mg/L of 0-5, 0-10 and 0-20 micrometres classified ACFTD's. Let the measured Gamma slope be s_{m5} , s_{m10} and s_{m20} for 0-5, 0-10 and 0-20 micrometres classified ACFTD's, respectively. Since the volume rate of abrasive wear on the variable speed Gamma Falex system is proportional to the Gamma slope to the power of 1.5, Eq. (58), volume rates of abrasive wear produced by the test abrasive particles are as follows:

| <u>Abrasive Particles</u> | <u>Volume Rate of Abrasive Wear</u> |
|---------------------------|-------------------------------------|
| 0-5 micrometres | $cs_{m5}^{1.5}$ |
| 0-10 micrometres | $cs_{m10}^{1.5}$ |
| 0-20 micrometres | $cs_{m20}^{1.5}$ |

Using the above data, volume rates of abrasive wear on the sliding mechanism protected by the Beta Ten of 2 filter are estimated as follows:

| <u>Abrasive Particle Size</u> | <u>Volume Rate of Abrasive Wear</u> |
|-------------------------------|--|
| 5 micrometres | $\frac{4 \times 10^4}{3.7 \times 10^4} cs_{m5}^{1.5}$ |
| 10 micrometres | $\frac{1.2 \times 10^3}{8.3 \times 10^3} cs_{m10}^{1.5}$ |

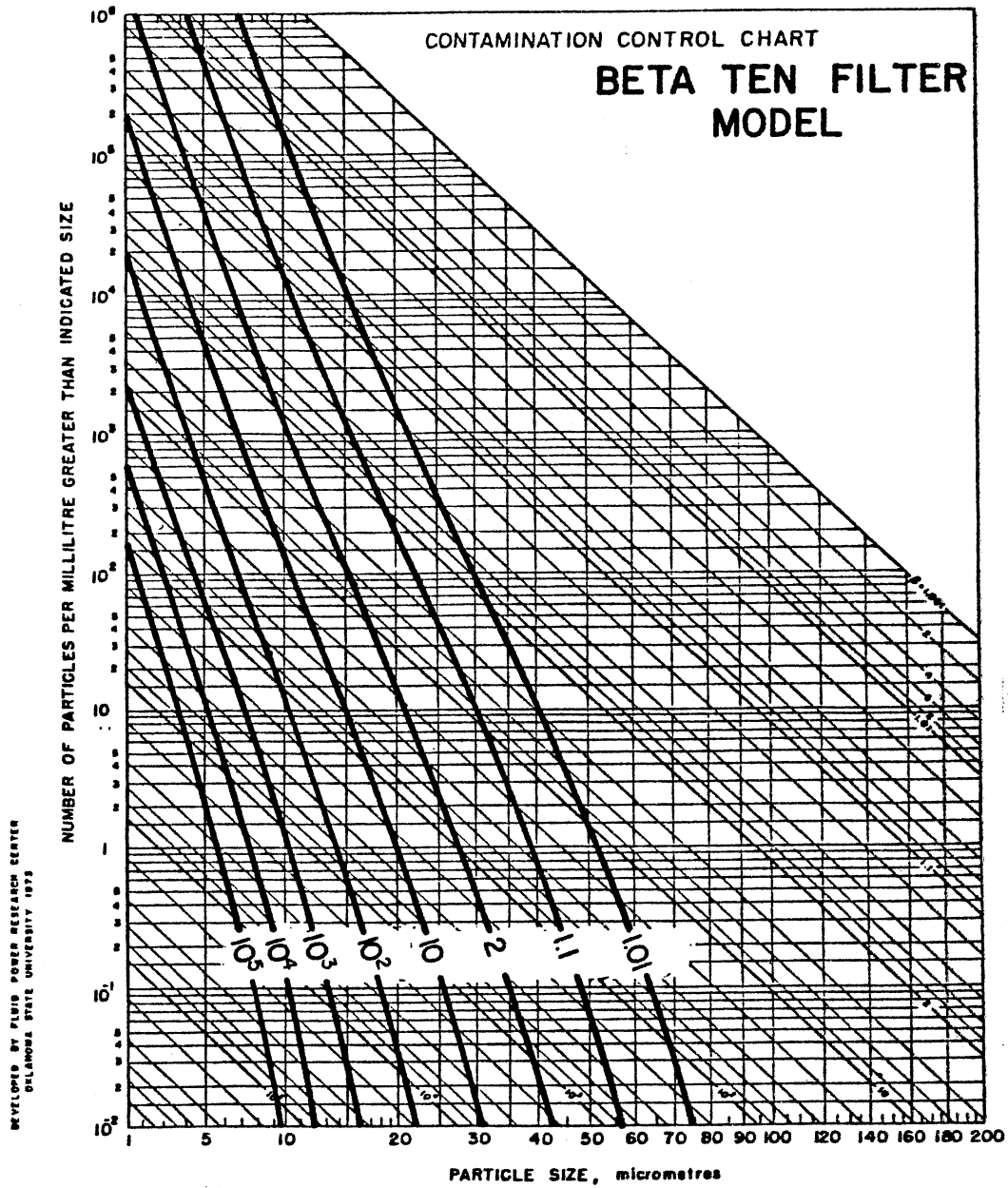


Fig. 79. Particle Distributions Controlled by Beta Ten Filters

$$20 \text{ micrometres} \quad \frac{1.5 \times 10}{10^3} \quad cs_{m20}^{1.5}$$

Conduct the variable speed Gamma Falex test with test fluid A, a fluid other than MIL-L-2104, and let the measured Gamma slope be s_{a5} , s_{a10} and s_{a20} for 300 mg/L of 0-5, 0-10 and 0-20 micrometres ACFTD's, respectively. Volume rates of abrasive wear on the sliding mechanism protected by a Beta Ten of 2 filter are:

| <u>Abrasive Particle Size</u> | <u>Volume Rate of Abrasive Wear</u> |
|-------------------------------|--|
| 5 micrometres | $\frac{4 \times 10^4}{3.7 \times 10^4} cs_{a5}^{1.5}$ |
| 10 micrometres | $\frac{1.2 \times 10^3}{8.3 \times 10^3} cs_{a10}^{1.5}$ |
| 20 micrometres | $\frac{1.5 \times 10}{10^3} cs_{a20}^{1.5}$ |

Assuming the amount of total wear volume allowed to be lost for the entire life of the sliding mechanism to be V_{max} , a life of the mechanism with MIL-L-2104 by the abrasive particles greater than five micrometres can be calculated.

$$T_m = \frac{V_{max}}{\frac{4 \times 10^4}{3.7 \times 10^4} cs_{m5}^{1.5}} \quad (62)$$

In the same manner, the life of the sliding mechanism with test fluid A by the abrasive particles greater than five micrometres is

$$T_a = \frac{\frac{V_{\max}}{4 \times 10^4}}{\frac{V_{\max}}{3.7 \times 10^4}} c s_{a5}^{1.5} \quad (63)$$

where,

T_a = life of the mechanism with test fluid A.

When a life with test fluid A is required to be the same as that with MIL-L-2104, it can be done by changing the number of particles because abrasive wear is proportional to the number of particles. The change of the number of particles can be effectively achieved by selecting different Beta Ten filter as illustrated in Fig. 79.

Suppose that the number of particles greater than five micrometres with the test fluid should be changed by a factor of m in order to maintain the same life as with MIL-L-2104, the factor m is expressed by

$$m = \left(\frac{s_{m5}}{s_{a5}} \right)^{1.5} \quad (64)$$

If the factor m is 0.1 for the particle size greater than five micrometres, it is multiplied by the number of particles at five micrometres of the Beta Ten equal to 2 filter in Fig. 79 (4×10^4) to give 4×10^3 which corresponds to a Beta Ten of 10 filter, one order of magnitude better filter than a Beta Ten of 2 filter. Thus, the numbers of particles greater than 5, 10 and 20 micrometres needed to maintain the same life as with MIL-L-2104 are calculated as follows:

| <u>Abrasive Particle Size</u> | <u>Particle Number</u> |
|-------------------------------|--|
| 5 micrometres | $4 \times 10^4 \left(\frac{s_{m5}}{s_{a5}} \right)^{1.5}$ |

$$10 \text{ micrometres} \qquad 1.2 \times 10^3 \left(\frac{s_{m10}}{s_{a10}} \right)^{1.5}$$

$$20 \text{ micrometres} \qquad 1.5 \times 10 \left(\frac{s_{m20}}{s_{a20}} \right)^{1.5}$$

The corresponding Beta Ten filter can be obtained for each of the particle sizes in Fig. 79. The best Beta Ten filter among the filters obtained for the size of 5, 10 and 20 micrometres is assigned as the filter necessary with the test fluid to maintain the same life with MIL-L-2104.

The capability of a fluid to protect a sliding mechanism from abrasive wear can be expressed by a given Beta Ten value using Beta Ten of 2 for MIL-L-2104 as a reference. The necessary Beta Ten filter value obtained in the above procedure is designated as the "contaminant Gamma" of the fluid and used as a rating value to express the capability of the test fluid to protect the sliding mechanism from abrasive wear. A contaminant Gamma of MIL-L-2104 is, therefore, 2 by definition.

Since the lubricity under hydrodynamic lubrication includes the fluid viscosity, no wear should occur when the viscosity is high enough to cause the clearance to be larger than the abrasive particle size. Under these conditions, if the load can be increased to squeeze the fluid film, then abrasive wear with a given abrasive particle size will occur. From the hydrodynamic lubrication theory, the load is inversely proportional to the square of the fluid film thickness. Hence, when the load is doubled, the fluid film is squeezed down to 0.7 times the original thickness.

If no wear is observed after 0-5 micrometres classified ACFTD is injected at a load of 100 lb, then the load is increased to 200 lb and

abrasive wear for 0-5, 0-10 and 0-20 micrometres classified ACFTD is observed. Calculated numbers of particles at 5, 10 and 20 micrometres are then plotted at 7, 14 and 28 micrometres in Fig. 79 to obtain the necessary Beta Ten filters. In the same manner, if the test is conducted at a load of 400 lb, the calculated numbers of particles are plotted at 10, 20 and 40 micrometres in Fig. 79. This incorporates the viscosity effect on abrasive wear protection into the Gamma rating system.

When the fluid viscosity is so low that a perfect hydrodynamic lubrication can not be maintained in the test condition, the load is decreased to half the original level. Then, calculated numbers of particles are plotted at 3.5, 7 and 14 micrometres.

A test procedure to obtain the contaminant Gamma rating of a fluid is presented:

1. Install the standard test specimens on the variable speed Gamma Falex system.
2. Fill the test circuit with test fluid.
3. Achieve a specified test temperature while circulating the test fluid through the abrasive test circuit.
4. Inject 300 mg/L of 0-5 micrometres classified AC Fine Test Dust into the test system.
5. Rotate the journal and load the test specimens to 100 lb.
6. Advance the wear reading up to 120 at any rotating speed.
7. When the wear reading reaches 120, stop the rotation of the journal.
8. Filter the test fluid for 10 min.
9. Rotate the journal at 2320 rpm.

10. Observe the wear rate for 10 min.
11. If the wear rate does not stabilize to zero at the end of a 10-min period, decrease the load by half and repeat Step 10.
12. Isolate the filter circuit from the test system and circulate the test fluid only through the abrasive test circuit.
13. Inject 300 mg/L of 0-5 micrometres classified ACFTD into the test system.
14. Record the wear reading at every 2-min interval for 30 min, or for 10 min if no wear is observed.
15. If no wear occurs for the 10-min period, double the load and repeat Step 14.
16. Filter the test fluid for 10 min.
17. Isolate the filter circuit from the test system.
18. Repeat Steps 13 through 17 for 0-10 and 0-20 micrometres classified ACFTD's with a concentration of 300 mg/L.

To demonstrate the derivation of the contaminant Gamma rating of a fluid, an example is presented. Assume that the Gamma slopes obtained from the test with MIL-L-2104 are 2.3, 2.8 and 3.2 for 0-5, 0-10 and 0-20 micrometres classified ACFTD's, respectively. Gamma slopes of the test fluid are 3.5, 5 and 4.7 for 0-5, 0-10 and 0-20 micrometres classified ACFTD's, respectively. Calculated numbers of particles at 5, 10 and 20 micrometres are 2.1×10^4 , 5×10^2 and 8.4, respectively. Plotting these numbers in Fig. 79, the corresponding filters at 5, 10 and 20 micrometres are found to be Beta Ten of 3, 4 and 3, respectively. The best Beta Ten value should be taken as a rating value and, therefore, the contaminant Gamma rating of the test fluid is 4.

If a fluid with a contaminant Gamma of 10 is used in the sliding mechanism protected by Beta Ten of 2 filter, the life is decreased by one order of magnitude. On the other hand, the life is increased by one order of magnitude if a fluid with a contaminant Gamma of 1.1 is used in the sliding mechanism protected by Beta Ten of 2 filter.

The abrasivity of a field contaminant is often different from that of AC Fine Test Dust. Field contaminant such as coal dust is known to be much less abrasive than ACFTD; whereas, "gold mine dust" has been found to be more abrasive than ACFTD (39). When the abrasive life of the sliding mechanism is experimentally evaluated with the use of ACFTD and it is actually exposed to field abrasive particles other than ACFTD, field life prediction should be made with consideration of the abrasivity of field particles.

The abrasivity of particles can be evaluated with the use of the variable speed Gamma Falex system. This is done by first passing AC Fine Test Dust through a 44 micrometres sieve to eliminate large particles. Advance the wear reading of the standard test specimens up to 120 and ensure a perfect hydrodynamic lubrication. The test fluid should be MIL-L-2104 mineral base fluid. Inject 300 mg/L of classified ACFTD into the test system and continue the test until the wear reading stabilizes to zero. The steepest Gamma slope obtained from the test indicates the most severe abrasion caused by the classified ACFTD.

In the same manner, pass field abrasive particles through a 44 micrometres sieve to obtain test particles. Conduct the same test for the test particles until wear reading stabilizes to zero.

The abrasivity ratio should be obtained by dividing the steepest Gamma slope with the classified ACFTD by the steepest Gamma slope with

the test particles. From the foregoing presentation of the relationship between the Gamma slope and the volume rate of abrasive wear, it is obvious that the abrasivity ratio to the power of 1.5 is a factor which when multiplied by the life achieved with ACFTD gives the life associated with the test particles. This factor is designated as the "Zeta rating" of the abrasive particles. Thus, the Zeta rating is a measure of the abrasivity of field abrasive particles relative to the abrasivity of AC Fine Test Dust.

With the use of contact Gamma rating, the contaminant Gamma rating and the Zeta rating, a field life for a sliding mechanism exposed to an operating condition different from the laboratory condition can be properly predicted.

Recommendation for Further Study

This investigation has resulted in the development of useful wear test facilities and valuable information associated with surface contact wear and abrasive wear. To further advance the technology in this field, the following investigations are recommended for future study:

1. As a result of the asperity deformation tests, ductile expansion of the surface asperity has been found to be a significant factor affecting the volume rate of asperity deformation. Further investigation coupled with experimentation should be conducted to incorporate the ductile expansion of the surface asperity into theoretical equations.
2. The dynamic asperity deformation test has verified that surface adhesion is a strong function of the sliding

velocity. An experimental method should be developed to investigate effects of sliding velocity, load and heat dissipation rate on adhesion. This investigation will lead to a design methodology for sliding mechanisms that are free from adhesive wear.

3. With the use of the Gamma Falex system, the wear susceptibility of various surface materials under boundary lubrication should be studied. This study would lead to the development of selection criteria for the materials of sliding mechanisms in boundary lubrication condition.
4. With the use of the variable speed Gamma Falex system, the contaminant Gamma test proposed in this dissertation should be conducted with at least several different fluids to verify the feasibility and applicability of the Gamma rating system.
5. The contaminant abrasivity test should be conducted on the variable speed Gamma Falex system to study the variation of field contaminant abrasivity.
6. Under hydrodynamic lubrication conditions, higher fluid viscosity helps decrease abrasive wear; whereas, a better fluid antiwear characteristic promotes abrasive wear. Both viscosity and antiwear characteristic are lubricity properties of the fluid. Further experimentation should be conducted on the variable speed Gamma Falex system to investigate the optimization of fluid lubricity properties for minimizing abrasive wear under hydrodynamic lubrication conditions.

7. With the use of the variable speed Gamma Falex system, transition from surface contact wear to abrasive wear in presence of abrasive particles should be studied by changing the rotating speed of the journal. This study will clarify critical roles of the surface roughness, the size of abrasive particles and the clearance between two sliding surfaces in conjunction with the transition. Information obtained as a result of this study will serve as criteria necessary to determine design parameters and operating conditions for optimal wear life of a sliding mechanism.
8. The Rolling mechanisms are as important as sliding mechanisms in mechanical systems. Rolling contact wear and abrasive wear under elasto-hydrodynamic lubrication conditions that are not covered in this dissertation should be investigated. Wear produced from rolling contact is considered due to fatigue of the surface materials and, therefore, the surface contact wear theory presented in this investigation can not be applied.

Abrasive wear under elasto-hydrodynamic lubrication conditions is affected by the clearance between two rolling surfaces. Furthermore, there is some amount of sliding existing between two rolling surfaces. Hence, a part of the abrasive wear theory developed in this investigation may be applicable for the study of abrasive wear under elasto-hydrodynamic lubrication conditions.

VITA²

Riichi Inoue

Candidate for the Degree of

Doctor of Philosophy

Thesis: SURFACE CONTACT WEAR AND ABRASIVE WEAR IN LUBRICATED SLIDING MECHANISMS

MAJOR FIELD: Mechanical Engineering

Biographical:

Personal Data: Born in Kobe, Japan, August 10, 1948, the son of Mr. and Mrs. Yoshio Inoue. Married in Kobe, October 14, 1973, to Nobuko Hakka. Beget Takashi Inoue, October 14, 1974, and Rick Inoue, August 29, 1981.

Education: Graduated from Mikage High School, Kobe, Japan, in March 1967; received the Bachelor of Agriculture degree from Kobe University in 1971; received the Master of Science degree from Oklahoma State University in 1978, with a major in Mechanical Engineering; completed requirements for the Doctor of Philosophy degree at Oklahoma State University in December, 1982.

Professional Experience: Design Engineer, Unic Corporation, 1971-1976; Project Engineer, Fluid Power Research Center, 1976-1978; Staff Engineer, Fluid Power Research Center, 1978-1979; Research Engineer, Fluid Power Research Center, 1979-1981; Technical Director, Fluid Power Research Center, 1981-Present; Expert Witness in a Patent Infringement Suit, 1978; Industrial Consultant, 1978-Present.

Professional and Academic Affiliations: Japan Society of Mechanical Engineers, Society of Automotive Engineers, American Society of Lubricating Engineers, Phi Kappa Phi, Oklahoma Chapter of Registered Professional Engineers.